SEDIMENTATION DURING LIQUID PROCESSING OF METAL MATRIX COMPOSITES

SEDIMENTATION DURING LIQUID PROCESSING OF METAL MATRIX COMPOSITES

by

S. Lafrenière, B.Eng

A Thesis

Submitted to the School of Graduate Studies

in Partial Fulfillment of the Requirements

for the Degree

Master of Engineering

McMaster University

October 1990

Master of Engineering (1990) McMaster University

Hamilton, Ontario

TITLE: Sedimentation during Liquid Processing of Metal Matrix Composites.

AUTHOR: Serge Lafrenière

B.Eng. Ecole Polytechnique de Montréal

Québec, Canada

SUPERVISORS: Professor G.A. Irons

NUMBER OF PAGES: xv, 118

ABSTRACT

During the incorporation of ceramic particles into metallic alloy melts for the production of metal matrix composites, the particles tend to float or sink, depending on their density. In order to study the sedimentation patterns, a novel electrical resistance technique has been developed. A current is passed between two electrodes, and the potential over a fixed distance is measured with two other electrodes. Experiments were carried out in an aluminum foundry alloy(A356) containing up to 30 volume percent 88 μm silicon carbide particles. The particles' behaviour was compared with sedimentation patterns in aqueous systems. The implications for fabrication and remelting of metal matrix composite material are discussed.

ACKNOWLEDGMENTS

The author wishes to express his sincere gratitude to Professor G.A. Irons for his guidance during the course of this project, and his efforts which led to the succesful completion of this project.

A special note of appreciation is given to Mr. O. Kelly for his help with the experimental work. The donations of silicon carbide by Norton Advanced Ceramics of Canada, and aluminum by Alcan are also gratefully acknowledged. The project was financially supported by NSERC.

I would also like to thank Hanu, Karen and Gilles who helped me during the research and in the production of the thesis.

Finally, the thesis is dedicated to my parents who have provided continuing support throughout.

TABLE OF CONTENTS

TABLE OF CONTENTS

LIST OF SYMBOLS

A	area of the particle projected in the direction of motion (m^2)
C_d	drag coefficient
d_p	diameter of particle (m)
E_{surf}	surface energy (N/m)
E_{pot}	potential energy (N/m)
E_{buoy}	buoyancy energy (N/m)
ΔE_t	total change in energy (N/m)
ΔE_i	contribution of changes in energy (N/m)
E_f	fractional strain
F_d	drag force (N)
g	gravitational acceleration (m/s^2)
h	height (m)
r	radius of a shere (m)
R	volume fraction of particles
R_{ep}	Reynolds number based on dispersed phase properties
S	number of particles crossing a horizontal section per unit of time
t	time (s)
V	velocity of propagation of a particular value of a concentration of particles (m/s)

LIST OF SYMBOLS

V_{ab}	discontinuity velocity between regions A and B (m/s)
V_{cp}	characteristic velocity of the particles (m/s)
V_g	terminal settling velocity under gravity (m/s)
V_p	velocity of the particles (m/s)
V_d	velocity of a shock (m/s)
W_a^{slv}	energy changes due to adhesional wetting (N/m)
W_s^{slv}	energy changes due to spreading wetting (N/m)
W_w^{slv}	energy changes due to immersional wetting (N/m)
x	level above the bottom of the crucible (m)
γ	interfacial free energy (N/m)
γ^{lv}	liquid-vapour interfacial energy (N/m)
γ^{sl}	solid-liquid interfacial energy (N/m)
γ^{sv}	solid-vapour interfacial energy (N/m)
μ	viscosity (kg/m s)
ρ	density (kg/m^3)
σ_y	stress (N/m^2)
θ	wetting contact angle
ω	semi-apical angle

LIST OF FIGURES

LIST OF TABLES

CHAPTER 1

INTRODUCTION

With the development of industries such as aeronautics and aerospace, and with the need to decrease the weight of cars, the drive to improve the specific properties of materials (ratio of mechanical properties to density) is very strong. To satisfy this demand, some very ingenious processes have been developed, one of which is the embedding of a light ceramic reinforcement in a metallic matrix. For the remainder of this thesis, this kind of material will be referred as a Metal Matrix Composite or MMC.

The mechanical and physical properties of MMC's are a strong function of the ceramic-matrix interactions [1], and of the volume fraction [2], distribution, and orientation [3] of the ceramic reinforcements (eg. better tensile properties are obtained in the longitudinal direction of the fibers).

There are three general methods to make metal matrix composites:

(1) Sintering of metal and ceramic powders,

(2) Infiltration of liquid metal into preforms of ceramic fibers, and,

(3) Mixing ceramic particles into liquid metals.

Although it is impossible to fabricate MMC's with aligned fibers by the third method, the low processing cost makes this method commercially attractive (Alcan has commercialized a process based on this method [4]). There are four major fundamental problems associated with mixing ceramic particles into liquid metals:

(1) most ceramics are not easily wet,

(2) the particles either sink or float in the melt, depending on the ratio of particle-to-liquid density,

(3) the viscosities of the mixtures are very high, and are shear-rate dependent (thixotropic).

(4) the liquid metal reacts with the particles.

This work is to investigate the second problem. In order to incorporate the SiC particles into the aluminum melt, a novel vortex ring mixer, developed by Dr. Latto (McMaster University, mechanical engineering), was tested. After many tests, it was concluded that this mixer was not functional for the fabrication of MMC's. A marine type mixer, developed by Dr. Hanumanth (McMaster University, Material Science), was tested and the results showed that it was possible to incorporate a fraction of the 10 μm SiC particles with this technology.

Since the goal of this work was to study the relationship between the sedimentation patterns and the concentration of particles, it was decided to use particles with a diameter

of 88 μm instead of 10 μm. This decision was made because it was relatively easy to incorporate the larger sized particles with the marine type mixer without changing the wetting characteristics of the system (i.e. by adding Mg). The effect of wetting on the fabrication of MMC's is under study by other members of the research group.

In order to study the effects of a variation of the concentration of particles on the sedimentation patterns in an aluminum-SiC melt, a novel electrical resistance technique was developed. A current is passed between two electrodes, and the potential over a fixed distance is measured with two other electrodes.

With this apparatus, the sedimentation patterns in MMC's were analyzed with settling theory developed for aqueous systems, and some relationships were developed to describe the settling behaviour and the formation of layers where the concentration of particles suddenly changes (shock). The settling phenomenon is referred to as hindered settling and can be empirically described by the Richardson and Zaki equation [5], among others :

$$V_p = V_g(1 - R)^{4.65} \qquad (1)$$

where $\mathbf{V_p}$ is the velocity of the particles, $\mathbf{V_g}$ is the terminal settling velocity under gravity and **R** is the volume fraction of particles.

However, when severe particle interaction occurs such as flocculation, there are often system-specific deviations from Equation 1. There may be clustering or agglomeration due to the surface effects in these systems.

CHAPTER 2

LITERATURE REVIEW

The first part of the literature review consists of a description of mechanical properties of MMC's, followed by a discussion of different fabrication methods. In order to analyze the distribution of particles during the processing of MMC's, the second part deals with a review of the theory of two-component vertical flow relevant to sedimentation.

2.1 METAL MATRIX COMPOSITES

Metal matrix composites (MMC) have immense potential as structural materials in the aerospace, aeronautic, and car industries, especially in elevated temperature applications, due to their high temperature stability over conventional alloys systems and fiber reinforced plastics [6]. Earlier R&D activity in MMC's was generally restricted to continuous fiber reinforced systems. In recent years, the focus has shifted to particulate which are available at lower cost. By choosing the proper processing techniques, these composites can improve the specific properties; as well, they possess their own special properties, such as good wear/abrasion resistance [6].

2.1.1 MECHANICAL PROPERTIES

To demonstrate the general mechanical property trends with different volumetric fraction and size of particles, an Al-7%Si alloy reinforced with SiC particles may be considered. Figure 2.1 shows the effect of the volume fraction of SiC particles on the proof stress taken at 0.2% strain (σ_Y)of Al-Si/SiC composites for different particles sizes. It can be seen that σ_Y increases as the volume fraction of SiC particles increases. This effect however depends on the particle size. The results of Figure 2.1 demonstrate that both the volume fraction and the particle size control the proof stress of the composites. This means that the degree of hardening is a function of the interparticle spacing, which is controlled by the distribution of the particles. As the volume fraction is increased, small SiC particles tend to agglomerate (a consequence of the fabrication process), resulting in lower strength than expected for a homogeneous distribution. For larger particles, such agglomeration does not occur, and, thus, the composite shows an important increase of the proof stress compared to the matrix alloy [2].

The effect of the volume fraction of SiC particles on ductility (fractional strain, E_f, measured at fracture) of the composite alloys is shown in Figure 2.2. It can be seen that E_f strongly decreases with increasing volume fraction of SiC particles, and this decrease is more pronounced for the smaller size particles. From these results, it is concluded that the addition of SiC particles leads to embrittlement of the matrix alloy. The particles,

which are irregularly shaped, act as areas of local stress concentration. This aids crack initiation and propagation, especially when agglomeration takes place, as in the case of a large volume fraction of small particles [2].

Figure 2.3 compares the wear resistance of SiC-whiskers/AA 6061 alloy composite with various wear-resistant alloys such as Duralumin. As shown in this figure, very good wear resistance results can be obtained by the addition of SiC ceramics [7].

The matrix/fiber, or matrix/particle interface is partially responsible for the mechanical properties of the composite. The stresses on the composite must be transmitted through the interface to the reinforcing material. If the interface is not strong, the matrix must support all of the stress. This means that the addition of reinforcing elements will have no beneficial effect. The characteristics of an good interface are:

- sufficient cohesion forces to transmit the stress from the matrix to the reinforcement elements,
- stability with respect to time and temperature, and
- matched thermal dilatation coefficients of the matrix and the reinforcement to diminish the effect of the internal stresses, especially at high temperature [3].

Since the reinforcement material must sustain the principal stresses, we need fibers or particles with very good mechanical properties such as:

- high tensile strength (this depends essentially on chemical composition, fiber diameter and morphology),

- high modulus of elasticity to tolerate applied high stresses with small deformation, and

- stability of mechanical properties at high temperatures, and compatibility with the matrix (chemical stability at the fiber-matrix interface, and similar thermal expansion coefficients) [3].

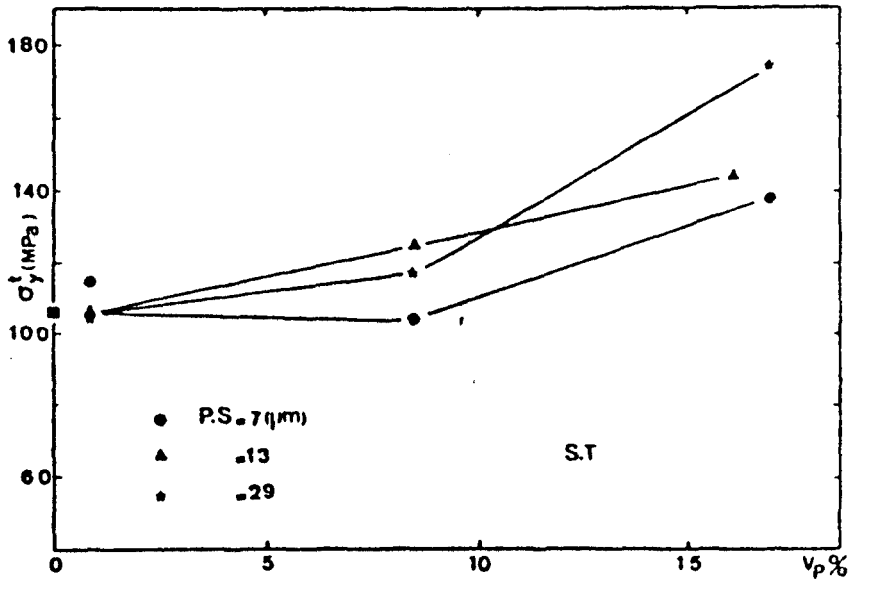

Figure 2.1: Effect of SiC content on tensile proof stress for solution-treated composites of different particle sizes.

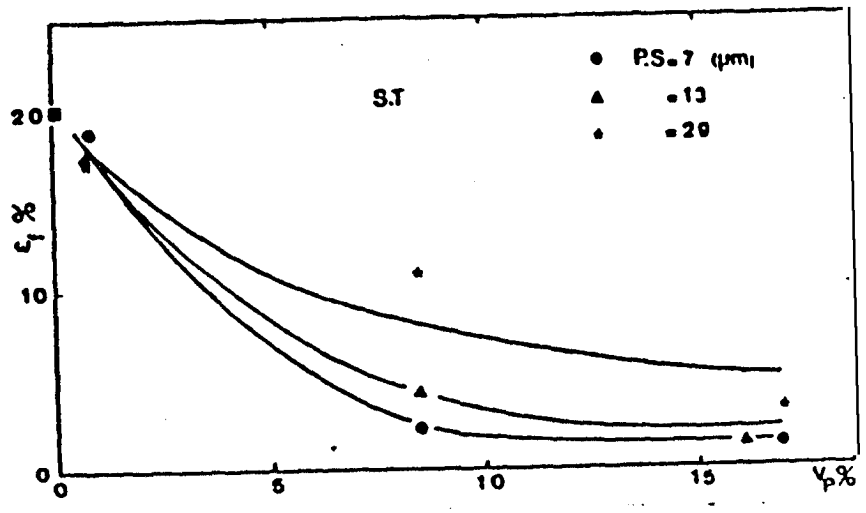

Figure 2.2: Effect of SiC content on failure strain for solution-treated composites of different particle sizes.

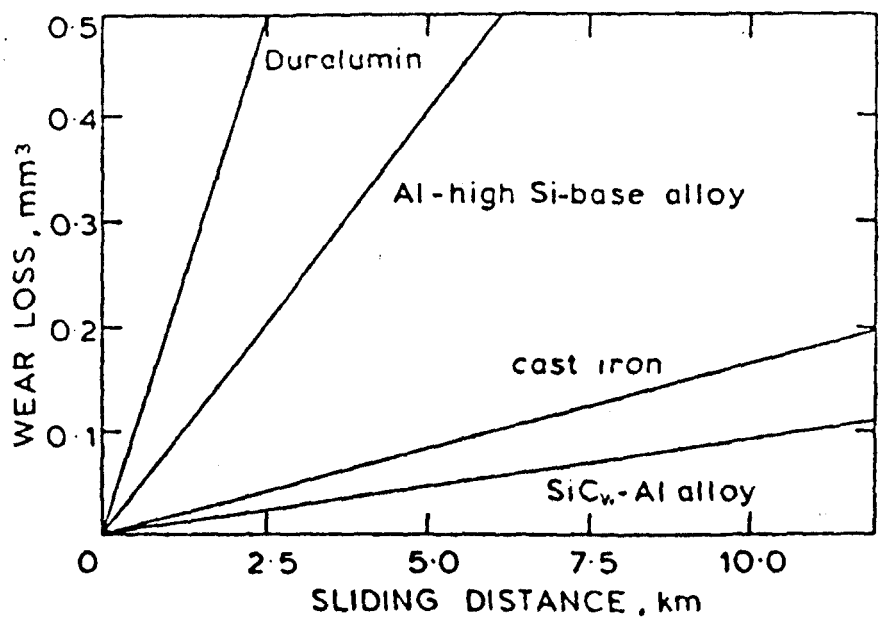

Figure 2.3: Wear resistance of SiC-Al metal matrix composites and various alloys.

2.1.2 PROCESSING MODES USED FOR FABRICATION

The modes of fabrication of metal matrix composites are different depending on whether fibers or particles are used as the reinforcing element.

The following methods of fabrication can be used on particles or short fibers (whiskers): infiltration, sintering and mixing.

Infiltration with liquid aluminum is relatively simple. A preform is first made to the desired shape, usually using a binder, preheated up to ~700 ^{0}C and is then placed in a die preheated to ~300 ^{0}C. Molten aluminum alloy heated to ~ 800 ^{0}C is added and the preform is infiltrated. Infiltration is either achieved by evacuating the die, or by applying a pressure as in squeeze casting. In squeeze casting, a pressure of ~100 MPa is applied directly through a plunger during the solidification of MMC's [7]. The fabrication procedure is shown schematically in Figure 2.4. Fabrication costs are relatively high, but a great diversity of shapes can be produced [8].

Hot Isostatic Pressing (HIP) was first intensively studied in the late 1950's, and the 1960's as a technique for the hot consolidation of refractory metal powders, ceramic powders and cermets [9]. In recent years, the HIP technique has been applied extensively to the sintering of metal and ceramic powders like SiC particulate reinforced MMC's.

The apparatus for HIP consists of a large, water-cooled, pressure vessel within which is arranged a resistance-heated furnace, thermally insulated from the pressure vessel. Inert gases such as He, Ar and N_2 are used for applying the pressure [9]. It is important that the metal powder size and the ceramic particle size are arranged so that a uniform mix, without extensive reinforcement clustering, is obtained [8]. The major parameters which affect the strength properties of MMC's fabricated by solid-state diffusion bonding are pressure, temperature, and heating time [9].

The mixing of ceramic particles into liquid metal is potentially the cheapest method in situations where only moderate improvements over the un-reinforced alloy are required. There are four major fundamental problems associated with mixing ceramic particles into liquid metals:

(1)most particles are not easily wet,

(2)the particles either sink or float in the melt, depending on the ratio of particle-to-liquid density,

(3)the viscosity of the mixture is very high, and is also shear-rate dependent (thixotropic), and,

(4)the liquid metal reacts with the particles.

2.1.3 WETTING CONSIDERATION

Compatibility between the matrix and the reinforcement is the most difficult condition to achieve. During the initial step of fabrication, compatibility is required so that the matrix can spread over and wet the surface of the reinforcements [8]. The initial stage of wetting involves both the external surface of particles and the internal surfaces which exist between the particles in the clusters that make up the dry powder. The wetting process is dependent on the nature of the liquid phase, the characteristic of the surface, the dimensions of the interstices in the clusters, and the nature of the mechanical process used to bring together the components of the system [10]. The three definably distinct types of wetting are designated as adhesional wetting, spreading wetting, and immersional wetting, according to the mechanical process taking place. They are readily defined in terms of the changes in the interfacial free energy γ involved. To apply these concepts to the particles problem, it is useful to consider the particles as cubes (A-D in Figure 2.5). The energy changes that take place are given by:

A to B adhesional wetting:

$$W_a^{slv} = \gamma^{sl} - (\gamma^{sv} + \gamma^{lv}) = -\gamma^{lv}(\cos\theta + 1) \qquad (2)$$

B to C immersional wetting:

$$W_w^{slv} = 4\gamma^{sl} - 4\gamma^{sv} = -4\gamma^{lv}\cos\theta \qquad (3)$$

C to D spreading wetting:

$$W_s^{slv} = (\gamma^{sl} + \gamma^{lv}) - \gamma^{sv} = -\gamma^{lv}(\cos\theta - 1) \qquad (4)$$

The angle of contact θ is introduced into these equations through the Young equation:

$$\gamma^{sv} = \gamma^{sl} + \gamma^{lv}\cos\theta \qquad (5)$$

It is useful to consider under which conditions the particles would wet spontaneously. This occurs when W is negative; if W is positive, work must be expended on the system for the process to take place. For the three separate stages, it may be concluded that adhesional wetting is spontaneous if θ is $< 180°$, immersional wetting is only spontaneous if θ is $< 90°$, and spreading wetting is only spontaneous when $\theta = 0°$. For the total process

$$W_t = W_a^{slv} + W_w^{slv} + W_s^{slv} = 6\gamma^{sl} - 6\gamma^{sv} = -6\gamma^{lv}\cos\theta \qquad (6)$$

and for spontaneity, θ must be $< 90°$. However, since one of the separate stages requires zero contact angle, this must be the condition for spontaneous wetting, for without it the particles would tend to float and some work would be required to wet the particles [10].

For practical purposes, we have to consider the total change in energy during the transfer of a particle from the atmosphere to the melt. The total change in energy is:

$$\Delta E_t = \sum_{i=1}^{N} \Delta E_i \qquad (7)$$

where ΔE_i are the contributions of changes in the surface, potential, kinetic, and thermal energies. By neglecting the kinetic and thermal effects, it can be shown that the various energy contributions during the transfer of a shere of radius r, from a semi-apical angle 0 to ω, are given by:

$$E_{surf} = \pi r^2 \gamma_{lg} [2(1 - \cos\omega)\cos\theta + \sin^2 \omega] \qquad (8)$$

$$E_{pot} = -\frac{4}{3}\pi r^4 \rho_p g(1-\cos\omega) \qquad (9)$$

$$E_{buoy} = -\frac{\pi r^4}{48}\rho g(-3\cos 4\omega + 8\cos 3\omega + 12\cos 2\omega - 72\cos \omega + 55) \quad (1)$$

where γ is the surface tension, ρ the density, θ the contact angle, and **g** the acceleration due to gravity [11].

Figure 2.6 shows the overall energy change for two SiC particles, one having a diameter of 10 μm and the other 500 μm. The contact angle used ($\theta = 160°$) corresponds to a non wetting system. The surface tension of liquid aluminum used is 0.006 N/cm.

During the transfer, the total change in energy in the system is $\Delta E_{total} = E_{surf} + E_{pot} + E_{boy}$. If ΔE_{total} is bigger than 0, no tranfer of particles will occur. If ΔE_{total} is smaller than 0, the transfer will occur even if the aluminum doesn't wet the SiC particles ($\theta > 90°$). As is shown in Figure 2.6, the particle of 500 μm is transferred in the melt. The 10 μm particle is not transferred into the melt, meaning that a mixer and/or a modification of the chemistry of the aluminum is needed for the transfer.

The wettability in the Al/SiC system is a major factor characterizing the interface. The wettability is expressed as the angle θ measured through the Al liquid between gas and solid. The θ angle is evaluated by the sessile-drop method with the apparatus shown in

Figure 2.7.

"Previous studies showed that the Al/SiC system exhibits a non-wetting (contact angle $\theta > 90^0$) behaviour up to 1223 K, where a sharp transition to wetting ($\theta < 90^0$) of SiC by liquid aluminum occurs. It has been attributed to the disappearance of the effect of the oxide layer on liquid Al at about 1223 K under high vacuum. At lower temperatures, this layer prevents a true metal/substrate interface from developing" [12]. Figure 2.8 shows the variation of contact angle with time for the Al/SiC system at 973 K.

It should be keep in mind that these results were obtained under high vacuum conditions. Under normal processing conditions, as during the addition of SiC particles in the Al melt, the oxide film that developed on the particles by oxidation in air increases the holding time needed to obtain the wetting condition ($\theta < 90^0$). "The SiC oxidation appears to have an adverse effect on the wetting of SiC by aluminum" [12].

The addition of Si in the Al melt, used to avoid the formation of Al_4C_3, does not significantly affect the wetting properties of the system [12].

The addition of Mg to an Al melt promotes wetting by reducing the surface tension of the melt. The addition of 3% Mg to Al reduces the surface tension from 0.760 to 0.620 N m^{-1} at 993 K [13]. The surface tension measurements are difficult to make, explaining

the variability of results shown by different authors.

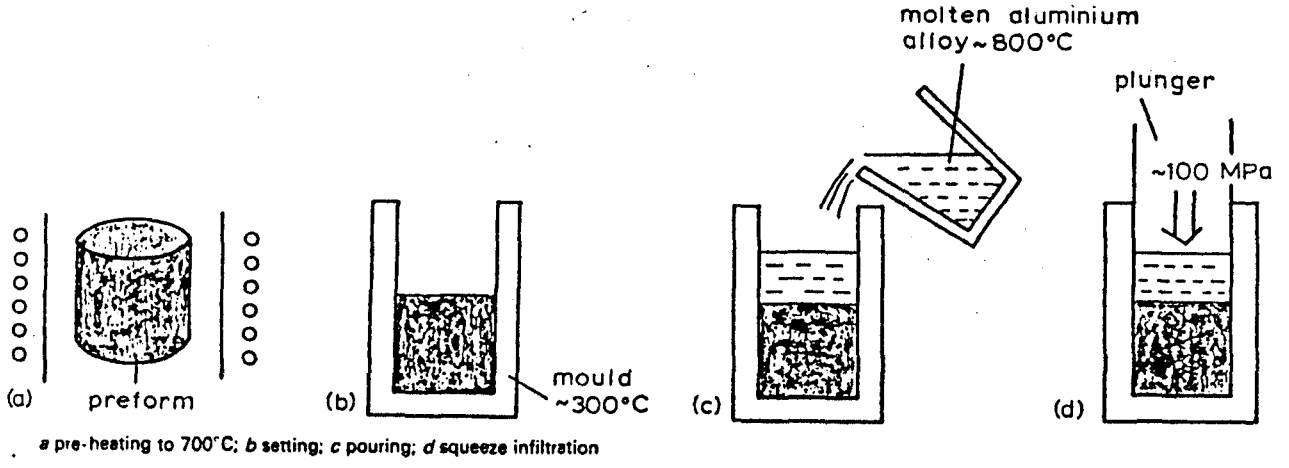

Figure 2.4: Fabrication procedure of MMC's using squeeze casting.

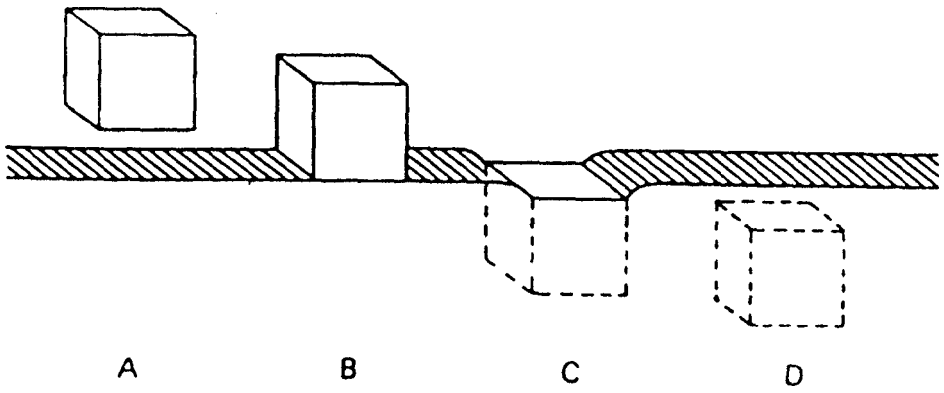

Figure 2.5: The three stages involved in the complete wetting of a solid cube by a liquid: A to B adhesional wetting, B to C immersional wetting, C to D spreading wetting.

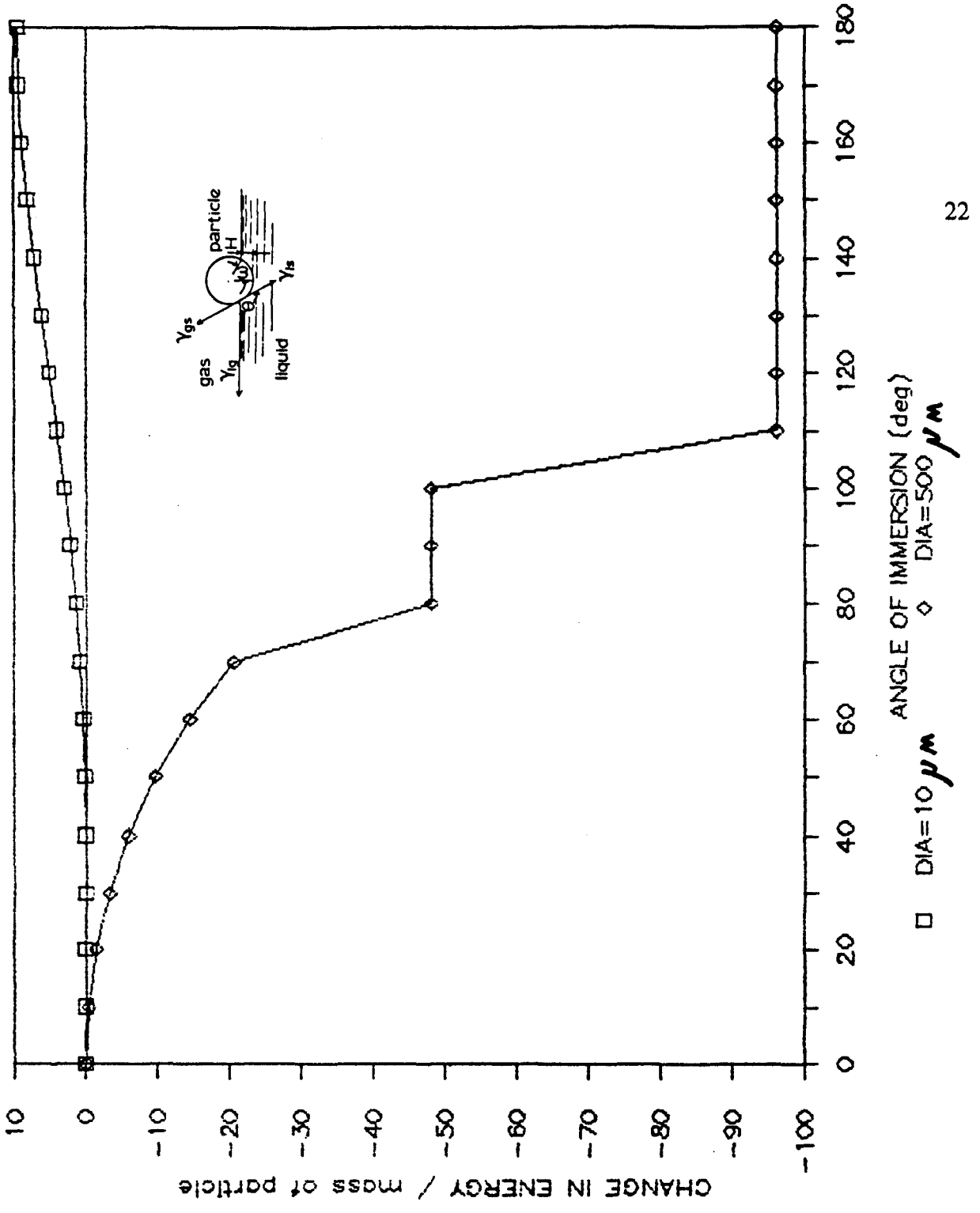

Figure 2.6: Variation of energy vs angle of immersion for 10 and 500 μm SiC particles into aluminum melt.

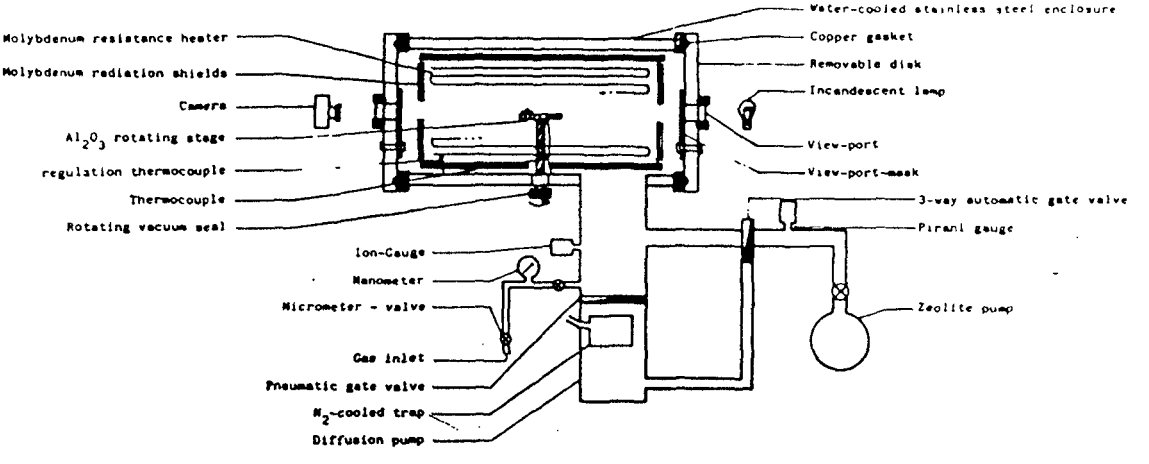

Figure 2.7: Sketch of the sessile-drop apparatus.

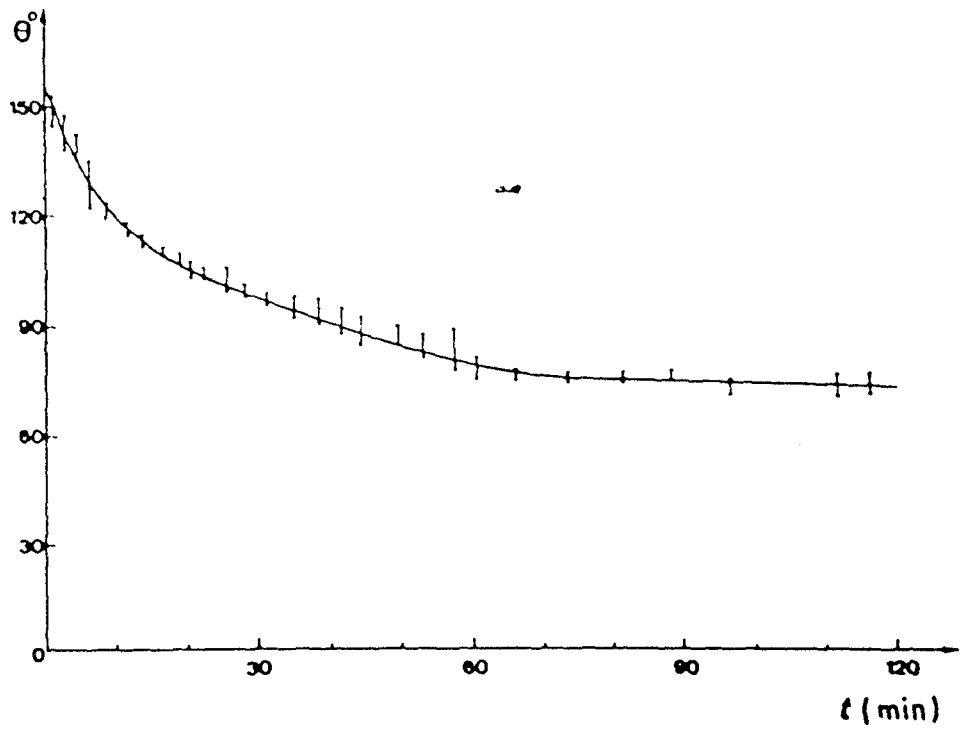

Figure 2.8 : Variation of the contact angle with time for the Al/SiC system at 973 K.
$P = 10^{-4}$ to 5×10^{-5} Pa.

2.1.4 MIXING

The mixing of fluids and particles is of considerable importance to many industries. A great amount of energy is spent in the world in mixing and maintaining homogeneous distribution of particles. There are many types of mixers available often involving the use of oscillating or rotating devices.

A novel ring-vortex mixer developed by Dr. Latto (McMaster Universiy, Mechanical Engineering) was tried in order to mix the SiC particles with the liquid aluminum. A ring-vortex is a rotating torroid of fluid, produces by an oscillating device, which may travel in an approximately linear direction (Figure 2.9). The fluid within a ring vortex is rotating in such a way that the relative velocity of the fluid at its boundary approaches zero, and consequently the shear stress around it is quite small. The displacement of the ring through the fluid is relatively unhindered and it can be used as a device for the efficient transport of material from one location to another, which is the basic requirement for many mixing system [13].

A marine type propeller developed by Dr. Hanumanth (McMaster University, Material Science) was also tried. The marine type propeller eliminates the difference of concentration by inducing turbulence and circulation within the mass of liquid.

Alcan [4] has commercialized a process based on this kind of technique, Figure 2.10, wherein particles and metal are sheared past each other to promote wetting of the particles by the metal. The mixing occurs while minimizing the introduction and retention of gas in the mixture and at the particle-liquid interface. Mixing is done at a maximum temperature where the particles do not chemically degrade substantially in the molten metal during the time required for processing. Mixing is preferably accomplished with a dispersing impeller, or a dispersing impeller used with a sweeping impeller [14].

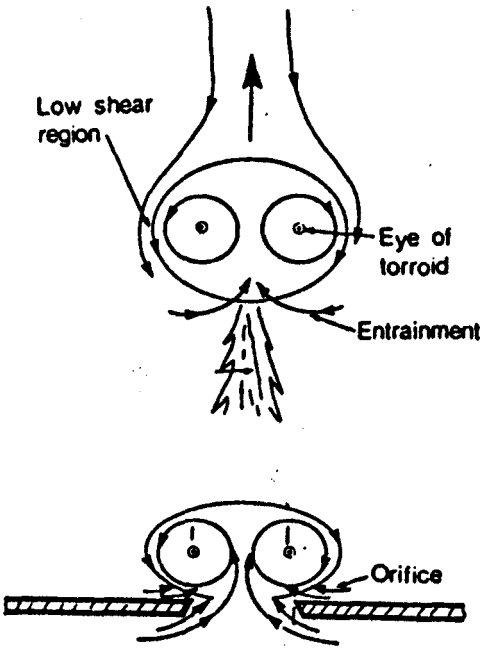

Figure 2.9: Diagram of the formation and progress of a vortex ring.

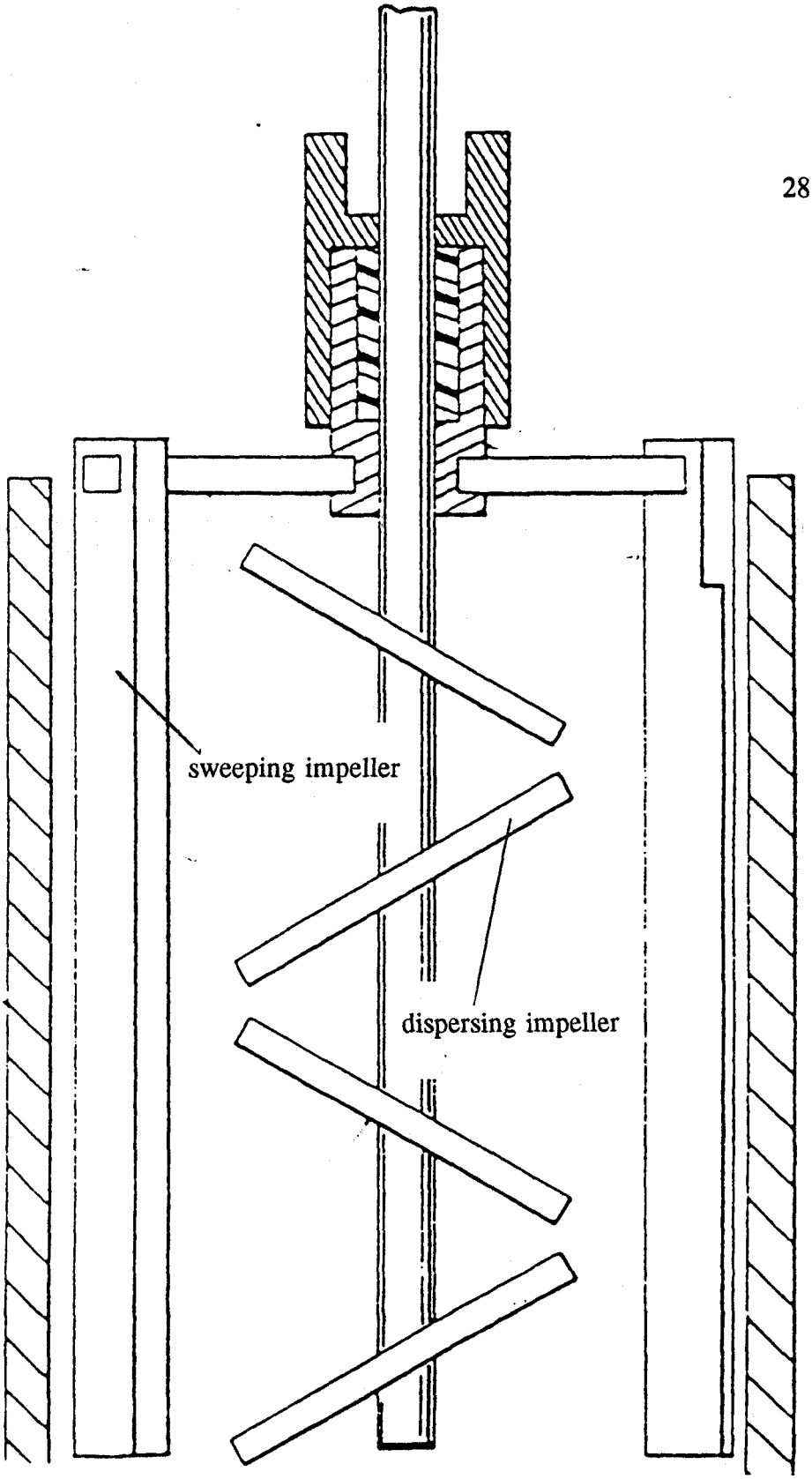

Figure 2.10: Side sectional view of the mixing apparatus commercialized by Alcan.

2.1.5 SiC-Al SYSTEM

The alloys used as matrices are generally light to capitalize on the excellent strength/weight ratios obtained after reinforcement. The alloys generally contain aluminum as the principal element.

The most often studied MMC system is probably the Al-SiC system. SiC particles are often used as reinforcement because of the following advantages [3]:

- the particles are usually chemically inert within the matrix,
- properties are retained at elevated temperatures,
- they have a high modulus of elasticity and do not deform plastically,
- low density,
- relatively low price.

Aluminum is a metallic element in group III of the periodic table. Aluminum has a valence of +3 in all compounds, with the exception of a few high temperature monovalent and divalent gaseous species. High purity aluminum is soft and lacks strength but, with small amounts of other elements, its alloys have high strength-to-weight ratios. The utility of the metal is enhanced by its tendency to form a stable adherent oxide surface (Al_2O_3) that resists corrosion. The surface tension of molten aluminum is 0.86 N/m in the range of 700-750 °C. The viscosity of 99.996% aluminum at these same temperatures is 0.001-

0.0012 Pa.s. The properties of aluminum vary significantly with purity and with alloying. The physical properties reported below are for aluminum of min 99.99% purity [15]:

atomic number:	13
atomic weight	26.9815
density at 25 °C, kg/m^3	2698
melting temperature, °C	660.2
electrical resistivity at 20 °C, Ω-m	2.6548×10^{-8}
Young's modulus, MPa	65,000
tensile strength, MPa	50

Silicon carbide SiC, is a cristalline material, with a color that varies from nearly clear through pale yellow or green to black, depending upon the amount of impurities. The properties of SiC depend upon purity and the method of fabrication. SiC is well known as a hard material occupying a relative position on Mohs scale between alumina at 9 and diamond at 10. The Young modulus of SiC is 410 GPa [16].

It is particularly difficult to achieve good compatibility with an Al matrix, because Al readily reacts to form intermetallics with most ceramics. It is also very difficult to achieve good wetting. SiC is essentially stable below the melting point of Al, but reacts with Al alloys at temperature above the liquidus [8]. The reaction is:

$$4Al + 3SiC = Al_4C_3 + 3Si \qquad (11)$$

The reaction produces aluminum carbide, which degrades the reinforcement, and Si, which changes the composition of the matrix. However, if the Si content of the alloy is sufficiently high (approximately 7%), the reaction will be slowed sufficiently, and the reinforcement will be stable [8]. Metallographic structures of several intermediate compositions of the Al/Si system are shown in Figure 2.11 [17]. The intermediate compositions are mixtures of aluminum containing about 1% Si in solid solution as the continuous phase, with particles of essentially pure silicon. Alloys with less than 12% Si are referred to as hypoeutectic, those with close to 12% Si as eutectic, and those with over 12% Si as hypereutectic.

Despite some processing problems, the MMC's made from SiC particles and aluminum alloys via liquid-metal-process may be the first to achieve large scale production. The goal of this work is to investigate the sedimentation patterns during the fabrication of MMC's. The following theory of two-phase flow will serve as a framework to analyze the experimental results.

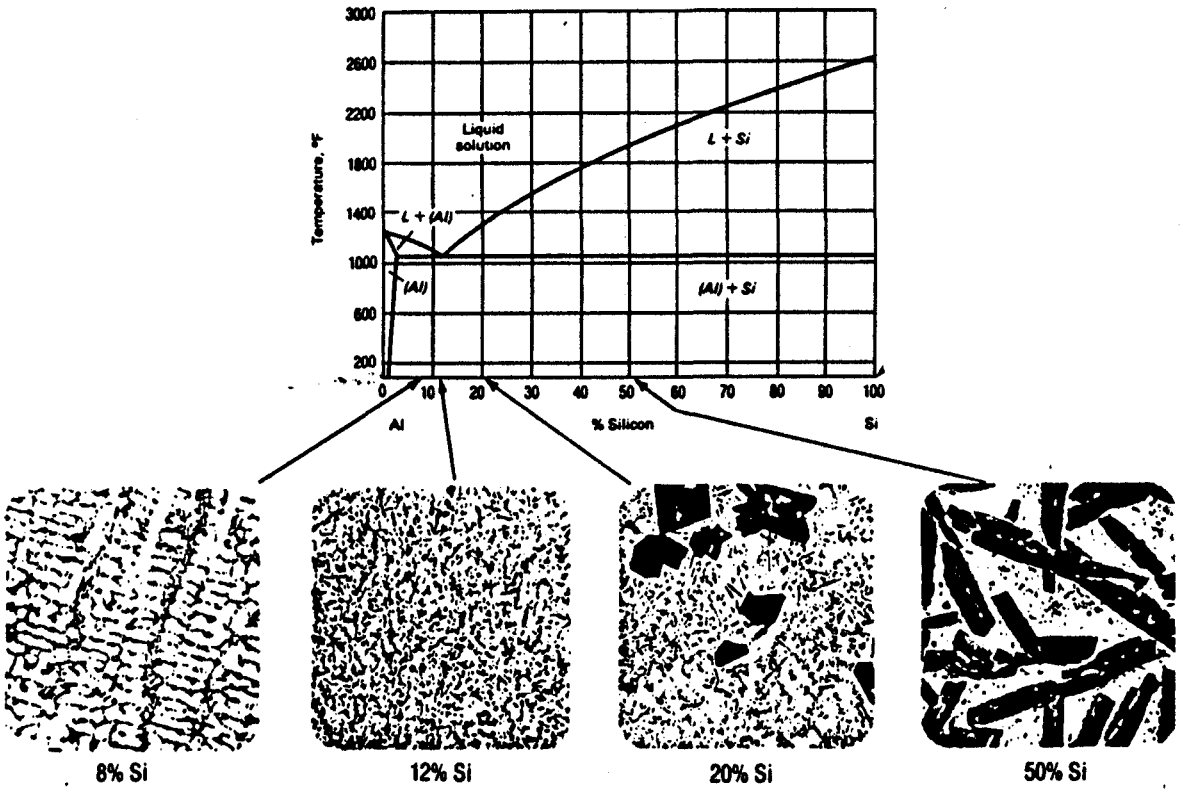

Figure 2.11: Aluminum-silicon phase diagram and cast microstructures of alloys of various composition.

2.2 TWO-COMPONENT VERTICAL FLOW

Under certain circumstances, the particles may be in contact with the molten aluminum alloy for extended periods of time. An example of this may be in foundries where production casting cycles could require the holding of molten composite for many hours [1]. Since SiC and Al have different densities (3300 kg/m^3 vs 2700 kg/m^3), the ceramic particles would settle down to the bottom. The following theory, describing the sedimentation of particles in aqueous systems, will be used to analyze the sedimentation of SiC particles in liquid aluminum.

2.2.1 GRAVITY SETTLING OF A SINGLE PARTICLE

If a particle moves relative to the fluid in which it is suspended, the force opposing the motion is known as drag force. Knowledge of the magnitude of this force is essential if the particle motion is to be studied [18]. Conventionally, the drag F_d is expressed according to Newton:

$$F_d = \frac{C_d A \rho V_s^2}{2} \qquad (12)$$

Generally C_d, is a function of the particle Reynolds number:

$$Re_p = \frac{V_g\, d_p\, \rho}{\mu} \qquad (13)$$

the form of the function depends on the regime of the flow. This relationship for rigid spherical particles is shown in Figure 2.12. At low Reynolds numbers (i.e. under laminar flow conditions when viscous forces prevail), C_d can be determined theoretically by solving the Navier-Stokes equations. The solution is known as Stokes' Law:

$$F_d = 3\,\pi\,\mu\,V_g\,d_p \qquad (14)$$

which applies at low Reynolds Numbers; the upper limit of its validity depends on the error that can be accepted. Elimination of F_d between equation 12, 13, and 14 gives another form of Stokes' Law:

$$C_d = \frac{24}{Re_p} \qquad (Re_p < 0.2) \qquad (15)$$

For Reynolds numbers > 1000, the flow is fully turbulent with inertial forces prevailing, and C_d becomes reasonably constant at approximately 0.44 (the Newtonian region). The region of Reynolds Number between 0.2 and 1000 is known as the transition region; C_d is either described in a graph, or by one or more empirical equations.

A single particle settling at constant velocity in a gravity field is subjected primarily to drag force and buoyancy.

By combining equation 12 and 14, one arrives at Stokes' Law:

$$V_g = \frac{g\, d_p^2\, (\rho_s - \rho)}{18\, \mu} \qquad (16)$$

This is known as the terminal settling velocity under gravity. Equation 16 can also be applied to nonspherical particles if the particle size d_p is the equivalent Stokes diameter as determined by sedimentation particle-size measurement [18].

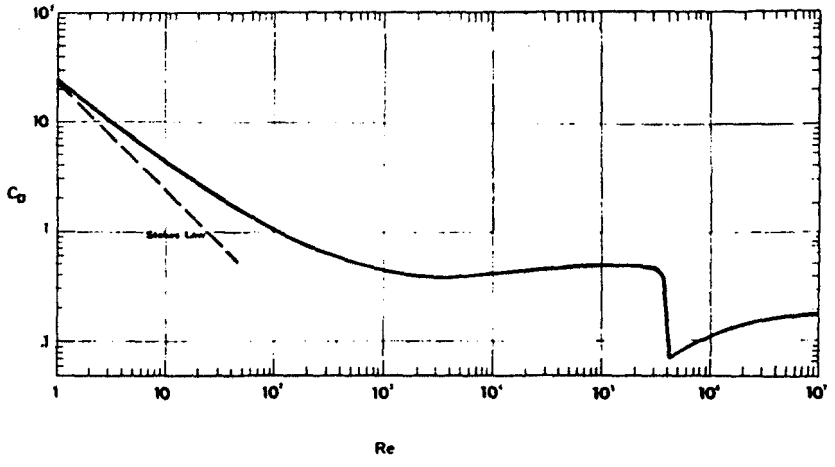

Figure 2.12: Drag coefficient of a sphere as a function of Reynolds number.

2.2.2 SETTLING OF SUSPENSIONS

As the particle concentration in the suspension increases, particles come closer together and interfere with each other. If the particles are not distributed uniformly, the overall effect is a net increase in settling velocity since the return flow caused by volume displacement predominates in particle-sparse regions. This is the well-known effect of cluster formation which is significant only in nearly monosized suspensions. With most practical widely dispersed suspensions, clusters do not survive long enough to affect the settling behaviour and, as the natural flow is more uniformly distributed, the settling rate steadily declines with increasing concentration [18].

This phenomenon is referred to as hindered settling and can be approached from two premises: as a Stokes-Law correction by introduction of a multiplying factor, or by adopting effective fluid properties for the suspension different from those of the pure fluid. These two approaches yield essentially identical results [18]:

$$V_p = V_g (1 - R)^2 f(1 - R) \qquad (17)$$

For Newtonian fluids,f(1 - R) has different forms depending on the approach adopted. The differences between the available expressions for f(1 - R) are not great and are frequently within the experimental accuracy. The most important form is the well-known Richardson and Zaki [5] equation:

$$f(1 - R) = (1 - R)^{2.65} \tag{18}$$

Other possible equations are given by Carman-Kozenny [18]

$$f(1 - R) = \frac{(1 - R)}{10\,R} \tag{19}$$

and by Brinkman [18]

$$f(1 - R) = (1 - R)^{2.5} \tag{20}$$

"The above correlations apply only to the cases where floculation is absent such as with coarse mineral suspensions (> 100 microns). Suspensions of fine particles, because of the very high specific surface of the particles, often floculate and therefore show different behaviour" [18].

2.2.3 SEDIMENTATION

If we are to expand the analysis to cover the flow of many particles in a medium of restricted extent, we must account for the effect of both the motion and the simple presence, even without motion, of all the other particles on the one we wish to consider.

The theory of sedimentation, as proposed by Kynch [19], is based on the assumption that the velocity V_p of any particle is a function only of the local concentration R of particles in the immediate neighbourhood. To simplify the analysis, it is also assumed that the particles have the same size and shape and that the concentration is the same across any horizontal layer.

It is convenient to introduce the particle flux:

$$S = R\ V_p \tag{21}$$

which is the number of particles crossing a horizontal section per unit of time. As R increases from zero to its maximum value R_∞, V_p decreases continuously from V_g to zero. In order to link the particle flux to the geometry of sedimentation, let x be the height of any level above the bottom of the crucible. Consider two layers at x and x+dx. During an interval of time dt, the accumulation of particles between the two is the difference between S(x+dx) in through the upper layer and S(x) out through the lower layer, per unit area:

$$\frac{\partial}{\partial t}(R dx)dt = S(x+dx)dt - S(x)dt \tag{22}$$

Dividing by dxdt, the continuity equation is derived:

$$\frac{\partial R}{\partial t} = \frac{\partial S}{\partial x} \tag{23}$$

This relation can be rewritten as:

$$\frac{\partial R}{\partial t} + V(R)\frac{\partial R}{\partial x} = 0 \tag{24}$$

where

$$V(R) = -\frac{dS}{dR} \tag{25}$$

In order to visualize equation 24, let us project this relation in a graph (Figure 2.13) where position x is plotted against time t for curves having the same value of R. The co-ordinates (x,t) and (x+dx,t+dt) of two adjacent points on such a curve are related by the equation:

$$R(x+dx,t+dt) = R(x,t)$$

i.e.

$$\frac{\partial R}{\partial x}dx + \frac{\partial R}{\partial t}dt = 0 \tag{26}$$

Combining equation 24 and 26, the slope of such a curve is given by:

$$\frac{dx}{dt} = V(R) \tag{27}$$

As R, and therefore V, is a constant along the curve (constant concentration of particles), it must be a straight line. This important result states that a particular value of a concentration is propagated upwards (as being on a straight line), through the dispersion with velocity V.

In order to illustrate the implications of those results, we will use the general case where the initial concentration of particules increases towards the bottom and V_p decreases with increasing R (the case where the initial concentration is homogeneous is a special case). The x against t diagram, together with lines of constant concentration is shown in Figure 2.13. The initial values of the concentration determines R along the x-axis. We know that the line KP of constant concentration has a slope $dx/dt = V_p$ determined by R at the point K where it intersects the x-axis. The equation of any line parallel to KP is:

$$x = x_o + V(R)t \tag{28}$$

At any point P, since the speed of fall of the top of the dispersion is that of the particles in it, then along AB:

$$\frac{dx}{dt} = -V_p(R) \tag{29}$$

The line KP represents the rise through the dispersion with velocity V of a level across which particles of concentration R fall with velocity $V_p(R)$. In time, t, from the start of the sedimentation, the number of particles which have crossed this level is $R(V+V_p)t$ per unit area. The level reaches the surface at the point P when this number equals the total number of particles, n, originally above the level K. Using the initial distribution of particles:

$$n(x_o) = R(V+V_p)t \tag{30}$$

We have now all the tools necessary to find the relationship between V_p and R given the initial concentration of particles and given the position of the surface of sedimentation in function of time. At any point P, the value of V_p is given by the slope of the curve at this point. By combining the equation 28, 29 and 30, we find that:

$$(x - t\frac{dx}{dt})_p = x_o + \frac{n(x_o)}{R} \tag{31}$$

R and n can be expressed as functions of x_o using the initial distribution of particles, and the left-hand side can be determined from the curves. By this manipulation, the value of x_o corresponding to P is determined, and from this, the value of R.

A shock is a sudden finite change of concentration at a certain level. For this phenomenon, the continuity equation no longer applies. It is replaced by an equation stating that the flow of particles into one side of the layer equals the flow out on the other side. If the suffix 1 denotes the layer above the discontinuity and the suffix 2 the layer below, and V_d is the upwards velocity of the discontinuity, we get:

$$R_1(V_{p1}+V_d) = R_2(V_{p2}+V_d) \tag{32}$$

By rearranging the terms, the velocity of the shock is:

$$V_d = \frac{S_1-S_2}{R_2-R_1} \tag{33}$$

where $S = RV_p$. On a S against R diagram the speed V_d is the slope of the line joining the point (R_1,S_1) and (R_2,S_2).

A similar development suggested by Wallis [20], is based on a characteristic velocity (V_{cp}), obtained directly from V_p:

$$V_{cp} = V_p R(1 - R) \tag{34}$$

This characteristic velocity is plotted as a function of R in Figure 2.14. With this representation, if a shock of velocity V_d passes between two regions R_{p1} and R_{p2} (as in sedimentation processes), then the application of conservation of mass implies that the velocities of the dispersed phases must be related by:

$$V_d = \frac{V_{cp1} - V_{cp2}}{R_{p1} - R_{p2}} \tag{35}$$

Graphically, V_d is the slope of a straight line joining the points on V_{cp} for the two solid fractions, R_{p1} and R_{p2}. On Figure 2.14, the slope of the line between R_0 and 0 represents the shock velocity V_{ab}.

A useful characteristic of this development, made by Wallis, is that depending on the shape of the V_{cp} curve, it is possible to determine that particular shocks are not permitted if a straight line cannot be drawn directly between the two volume fractions.

The relationship between V_p and R can be easily determined by plotting the $\log(V_p)$ as a function of log(1-R). Equation 17, $V_p = V_g (1-R)^n$, can be rewritten as:

$$\log(V_p) = \log(V_g) + n \log(1-R) \tag{36}$$

The slope of the line obtained gives the value of n, and the value at 0% SiC gives the value of $\log(V_g)$ which gives V_g.

Typical sedimentation behaviour is shown in Figure 2.15 (a) and (b). Initially, the column contains a uniform mixture, B. A clear liquid region, A, appears by a shock from the initial volume fraction to zero volume fraction. Depending on the initial R_p and shape of the characteristic velocity curve, there may or may not be an intermediate region, C, of variable density between region B and D. Region B eventually disappears, and C, if present, is compressed into D [21]. In aqueous systems, such behaviour can be visually observed, but for metal matrix system, a probe is required to detect the regimes.

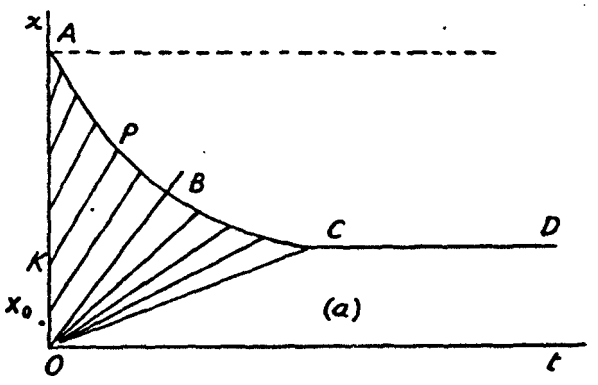

Figure 2.13: Fall of surface of dispersion, showing lines of density propagation.

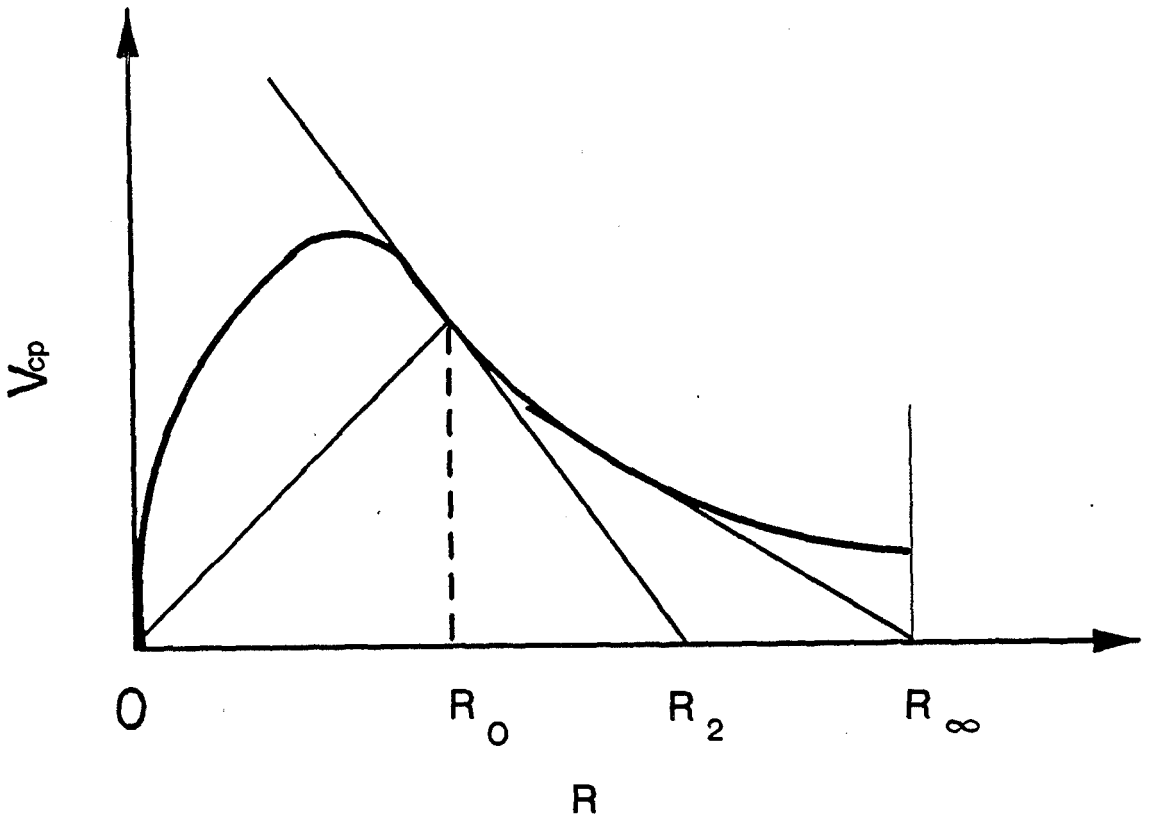

Figure 2.14: The characteristic velocity as a function of particle fraction showing how shocks or discontinuities can propagate in the system.

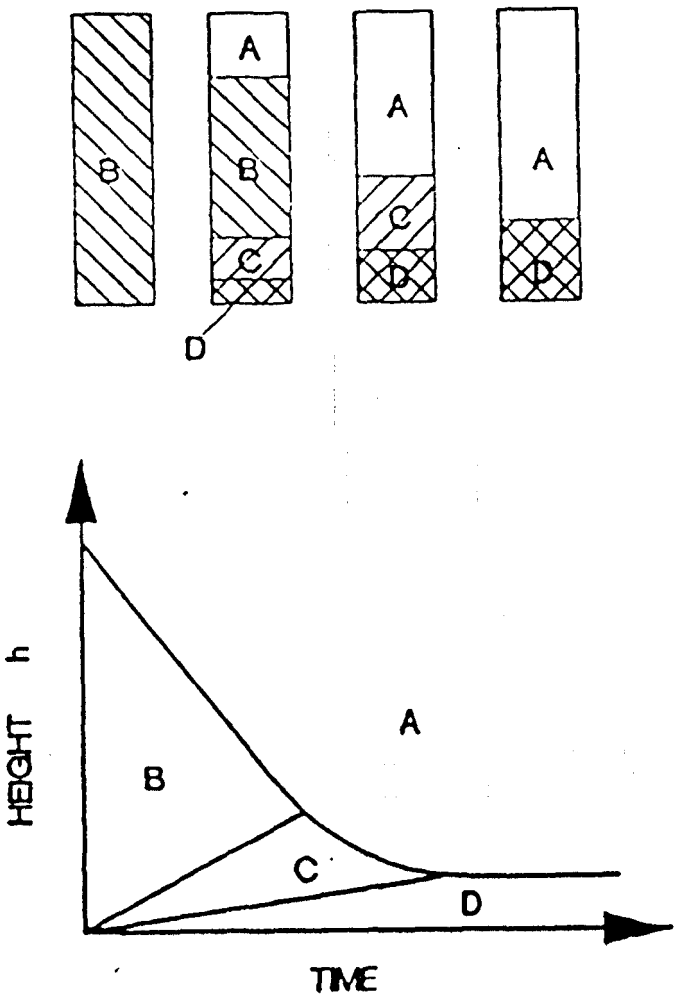

Figure 2.15: (a) Typical history of batch sedimentation from the original density B, to a clarified region, A, and a region of maximum final density, D, after passing through an intermediate region, C. (b) The position of the fronts with time corresponding to (a).

CHAPTER 3

APPARATUS AND MATERIALS

A general schematic diagram of the arrangement of the apparatus is shown in Figure 3.1. The sedimentation experiments were carried out in an alumina crucible (ID: 24.5 cm; Height: 47.5 cm) placed inside a resistance-heated furnace. The melt surface was exposed to air. The crucible was covered with a thermal insulator. The SiC particles were mixed into the melt with a graphite marine-type propeller driven by a variable AC motor.

The resistivity measurements were taken automatically with a commercially-available micro-ohmmeter (TECRAD DMO 350). The DMO 350 is a portable, microprocessor-controlled, high-accuracy, micro-ohmmeter which was designed for the measurement of resistance in solid alloys, such as aluminum.

For the use in liquid aluminum, a 4-point resistivity probe was developed (Figure 3.2). It was constructed from stainless steel, and coated with an alumina paste. The two outer electrodes were used to carry a very brief (30 ms) DC electrical pulse. The micro-resistance across the inner two electrodes was measured simultaneously. The electrodes are made of tungsten soldered to silver wires. Tungsten was chosen because of its resistance to dissolution in liquid aluminum [22]. Silver was chosen because of its

resistance to oxidation at high temperature [23].

The micro-ohmmeter was connected to a micro-computer through a RS 232 port. The micro-computer controlled the micro-ohmmeter, stored the measurements, and performed data analysis.

The green silicon carbide particles used in the experiments (Norton Advanced Ceramics of Canada) were measured by the HORIBA CAPA-700 centrifugal automatic particle size distribution analyzer. The mean particle size was 88 μm with a standard deviation of 19 μm. A commercial foundry alloy, A356 (Alcan), which is often used for metal matrix composites, was used. The major alloying elements are: 7.3% Si and 0.33% Mg.

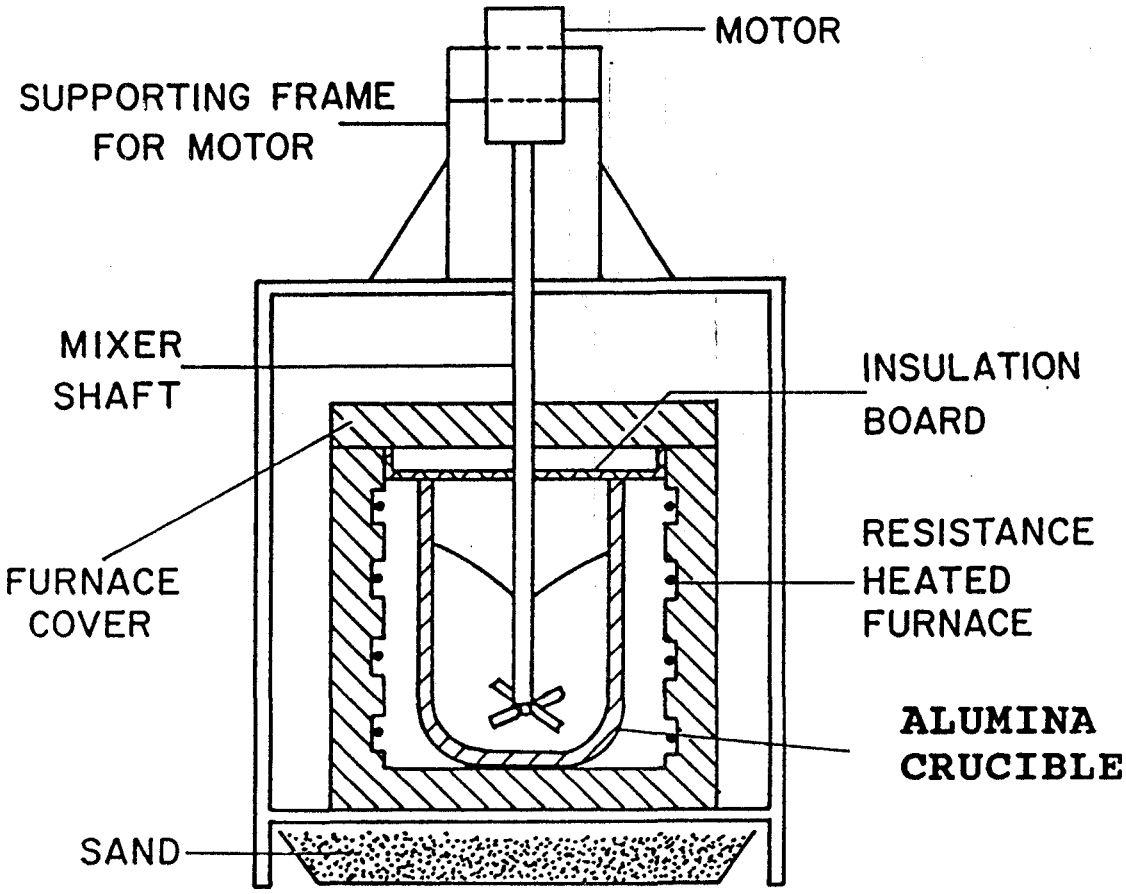

Figure 3.1: Side sectional view of the mixing apparatus.

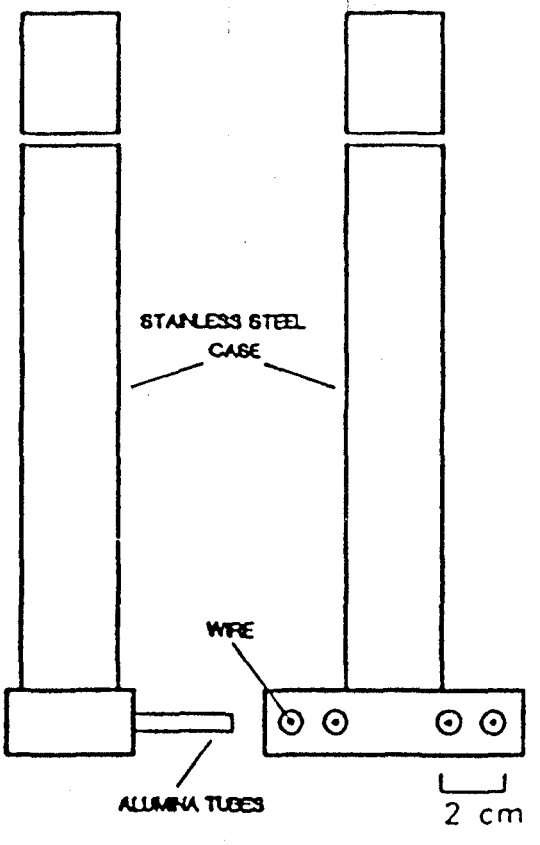

Figure 3.2: Diagram of the 4-point probe, to scale. The two outer electrodes carry the applied current, while the inner two are used for resistance measurement.

CHAPTER 4

EXPERIMENTAL PROCEDURE

Some initial experiments in mercury were done to determine the probe's ability to detect variations in electrical resistance without dealing with high temperatures and the corrosion problems related to liquid aluminum. For these experiments, the probe was immersed in a glass container filled with mercury, and changes in resistivity were created by inserting and moving alumina rods in the region of the probe.

In order to incorporate the SiC particles into the aluminum melt, a novel vortex ring mixer was tested. After many tests with 10 and 88 μm, it was concluded that this mixer was not functional for the fabrication of MMC's. The particles remained floating on the melt surface and it was impossible to incorporate them into the aluminum. The reasons for this failure are explained in the discussion.

For the fabrication of MMC's, 27.2 kg of the alloy were melted initially to produce a melt depth of 210 mm. The melt was maintained at 660° C. Prior to the actual testing, the oxide layer covering the surface of the melt was removed. The mixer was run at a constant speed of 525 rpm for 10 minutes to obtain isothermal conditions inside the melt. With the mixer still running, the probe was then lowered into the

melt, beside the stirrer. Subsequently, SiC particles were added to produce a 5 vol % concentration in the melt, and mixed for a duration of 10 minutes. After shutting off the mixer, the probe was fixed at a depth of 50 mm from the melt surface. After another 10 minutes of mixing, the mixer was stopped and resistivity measurements were started simultaneously. Resistivity was measured every two seconds until sedimentation was complete. This measurement procedure was repeated three times to test the reproducibility of the results.

This procedure was carried out at three different probe locations: 50, 100 and 150 mm below the melt surface. The experiment was then repeated at an increased volume fraction. SiC was added to increase the particle concentration from 5 vol% to 10 vol%, and so on in steps of 5 vol% to a final concentration of 30 vol%.

Table I shows the equivalence relationship between the weight of SiC, and the corresponding volumetric fraction.

TABLE I Relationship between volumetric fraction and weight of SiC in 27.2 kg of Aluminum.

vol %	5	10	15	20	25	30
Weight (g)	1682.3	3551.7	5640.9	7991.3	10655.1	13699.4

For each concentration, samples were sucked into glass tubes from the vicinity of the probe at 100 mm below the melt to ensure an homogeneous distribution of particles.

CHAPTER 5

RESULTS AND ANALYSIS

The basic objective of studying the sedimentation of SiC particles in an aluminum melt is to understand how the sedimentation pattern is related to the volumetric fraction of particles.

In order to interpret the experimental results, the theory of sedimentation in aqueous systems is used in this analysis. As discussed in section 2.2.3, the main assumption of this theory is that at any point in the dispersion the velocity of fall of a particle depends only on the local concentration of particles. This is a very strong assumption that can be justified only if either the speed of propagation is relatively slow or the damping is great [19]. Furthermore, many phenomena specific to the Al/SiC system (i.e. time varying contact angle) can weaken the validity of this assumption. Nevertheless, this theory is useful as a first step in the analysis of experimental data.

In the Al/SiC system, a visual observation is impossible because of the opacity of the components. By using a resistivity probe as described in Chapter 3, it is possible to reconstruct the sedimentation behaviour from the resistivity vs time curves. For

each volumetric fraction of SiC, the sedimentation pattern can be reconstructed by:

(1) splitting the resistivity curves into different sedimentation zones,

(2) identifying each sedimentation zone,

(3) determining the time of occurrence of a transition between the different zones.

In a resistivity vs time curve, the A B and D zones of sedimentation, as described in Section II.2.3, are represented by an interval of constant resistivity. For each curve, the resistivity measured at time zero corresponds to a concentration equivalent to the initial volumetric fraction of particle (ZONE B). After a certain interval of transition, the resistivity is stabilized to a new value. The new resistivity value can be lower or higher than the resistivity at time 0; if it is lower, the probe is in the zone A (clear liquid), if it is higher, the probe is in the zone D (final compaction of particles).

Figures 5.1 to 5.24 show the output of the probe as a function of time, for different volumetric fractions and depths of immersion. Table II indicates the individual graph associated with a volumetric fraction/depth combination.

Table II Relationship between graphs and experimental conditions

	VOLUMETRIC FRACTION (%)					
	5	10	15	20	25	30
DEPTH (mm)						
50	5.1	5.4	5.7	5.10	5.13	5.16
100	5.2	5.5	5.8	5.11	5.14	5.17
150	5.3	5.6	5.9	5.12	5.15	5.18
AVG	5.19	5.20	5.21	5.22	5.23	5.24

The drop in the resistance during settling as a function of the initial nominal SiC volume fraction is shown in Figure 5.25. Below 20% volume fraction, the probe response is quite linear, and it becomes more sensitive, and less reproducible at higher volume fractions.

The data in Figures 5.1 to 5.8, 5.10, 5.11, 5.13, 5.14, 5.16 and 5.17, show resistivity drops as the transition between regions A and B occurs at the probe location. For a particular concentration of particles, the time for the transition takes longer for deeper immersions. As Figures 5.15 and 5.18 show, the melt in the lower portions reaches a final dense packing (region D).

For certain curves corresponding to the lowest initial concentration of SiC (i.e. Figures

5.1, 5.2, 5.4 and 5.7), it is difficult to identify any B zone. This is due to the short period of time in which the probe is in this region, and by the important resistivity disturbance at the beginning of each experiment. This characteristic phenomenon is probably due to the entrapment of gas bubbles inside the melt during the mixing. Another factor that complicates the determination of the B zone for these curves is the thermal noise produced by the high temperature of the system.

It should be noted that in an aqueous system with particles of same size, there is no interval of transition between zone A and B (i.e. a shock occurs between these zones). The addition of this interval of transition in the Al/SiC system come from two factors:

(1) the rate of sedimentation is not the same for all the particles because the SiC particles have a size distribution

(2) the interface is sensed before it reaches the level of the probe because the resistivity measurements characterize the global resistivity of a certain volume around the probe.

To help in the analysis of the Al/SiC system, the transition from zone B to zone A will be denoted as A1 for the cases in which the time needs for the transition is important. In an aqueous system, it is possible to have a zone of transition (zone C) between zone B and D. In the Al/SiC system, a C zone will be difficult to distinguish due to the two factors mentioned above. From the data in Figure 5.9 (15% SiC), the volume fraction first increases at the 150 mm depth, possibly corresponding to a region C, and then

becomes clarified. Similar behaviour occurs in Figure 5.12 (20% SiC); however, the transition to pure aluminum is not as abrupt. In Figure 5.15 and 5.18, the resistance increases at the deeper probe locations due to the growth of the compaction zone. For the 50 and 100 mm immersions of the corresponding initial volumetric fraction, the volume fractions declined, while for 150 mm immersion, it increased as the bed rose to that location.

Each resistivity measurement is a composite of the effects of all the different phenomena affecting the measurements. The resistivity measured by the probe depends on the resistivity of the aluminum alloy and of the distribution, around the probe, of other materials having different resistivities. In the present set up, these other materials are the SiC particles, the crucible, the stirrer, and the surface of the melt. By keeping the probe in exactly the same position inside the crucible, only a change of volumetric fraction of SiC particles in the vicinity of the probe can be responsible for a change of resistivity. A displacement of the probe will change the total resistivity. This phenomenon is shown in Figures 5.1 where a slight displacement of the probe, between the second and third set of measurement, has shifted the last set upward. The important parameters in these curves is the time of occurrence of a transition between different zones. It is for this reason that we can use this probe, although it is impossible with the present apparatus to associate a resistivity measurement to a particular volumetric fraction of particles. However, changes in resistivity can be related to change in volume fraction as Figure 5.25

indicates.

With the data in Figures 5.1 to 5.18, Figures 5.26, 5.27, 5.28 and 5.29 were constructed in the same format as Figure 2.8. For the two lowest volume fractions, 5 and 10% in Figure 5.26, the only transition corresponds to the clarification of the aluminum, that is, from the initial state B, to pure aluminum, A. With 15% SiC, Figure 5.27 shows that it is possible to identify the sedimentation zones A B and C from the resistivity curves. Figure 5.28 (20% SiC) is similar to Figure 5.27 with the addition of a zone A1. It is only in Figure 5.29 (30% SiC) that we can identify a zone D of compaction. The reproducibility of the results is good enough to reconstruct the sedimentation pattern from the resistivity curves for the 5, 10, 15, 20 and 30 % SiC experiments. The measurements made for the 25% SiC experiment contain too much variation to permit reconstruction of the sedimentation behaviour. The most plausible reason is that the position of the probe was not fixed. (It was noted that the stand of the probe moved during the experiment).

In Figure 5.29, the extrapolation of the boundaries A-A1 and C-D to the point of convergence at 130 mm depth at 680 seconds, should correspond to the final state of the melt. The volume fraction in the region D can be estimated in two independent ways:

(1) The change in resistance from the initial 30% to the final state was 1.1 micro-ohm. Using Figure 5.25, this corresponds to 55% SiC.

(2) Applying conservation of silicon carbide volume:

$R_{po}h_o = R_{pf}h_f$

where the o subscript refers to the initial mixture, and f refers to the final mixture. For the final mixture height of 170 mm (300 total depth - 130 mm immersion), this represents an average volume fraction of 53% SiC.

The agreement between these two methods is reasonable, and corresponds to the random close packing of particles observed in packed beds.

The speed of the interface between region A and B, V_{ab}, plotted as a function of (1 - R), according to Equation 17 in Figure 5.30, is consistent up to 15% SiC. According to equation 36, the slope yields a value of n equal to 5.6 and a value for the shock velocity at 0% SiC of 3.35 mm/s. These results can be written as the following relationship between V_p and R: $\mathbf{V_p = 3.35\ (1\text{-}R)^{5.6}}$. As it should be, the velocity at 0% SiC is in reasonable agreement with the Stokesian settling velocity for 88 μm SiC particles of 2.7 mm/s. The sedimentation behaviour of the Al/SiC system is time dependent because the wetting of SiC by Al is time dependent. This wetting phenomenon is possibly responsible for the inconsistencies observed in experiments containing more than 15% SiC. Since it took three consecutive days to complete the experiments (Day 1: 5 and 10 vol%; Day 2: 15, 20 and 25 vol%; Day 3: 30 vol%), we can hypothesize that for the second and third day, the system was composed of SiC particles with varying degrees of wetting, and thus, exhibiting different sedimentation behaviour.

The characteristic velocity from Equation 34 is plotted in Figure 5.31 which can, according to the theory, summarize the settling behaviour of the Al/SiC (88 μm particles) system. (It should be noted that the following analysis will be valid only if the inconsistencies are dependent on the different degrees of wetting of the particles. Moreover, the results produced from the characteristic velocity are only valid for particles having a degree of wetting similar to the particles used to make the linear relationship in Figure 5.30). The front velocities between regions A and B are the slopes of the lines between the origin, and point on the curve at the initial volume fraction. From Figure 5.31, it can be seen that a direct shock to the final volume fraction(53-55% SiC) is only possible for volume fractions below 5% or above 45% SiC. In all other cases, a region of variable density, C, will form at intermediate times.

To ensure an homogeneous distribution of particles, samples were sucked into glass tubes from the vicinity of the probe. The samples were metallographically prepared, and analyzed quantitatively for the area fraction of SiC. However, the analysis shown that too much sedimentation occurs in the tube before solidification to permit this kind of analysis.

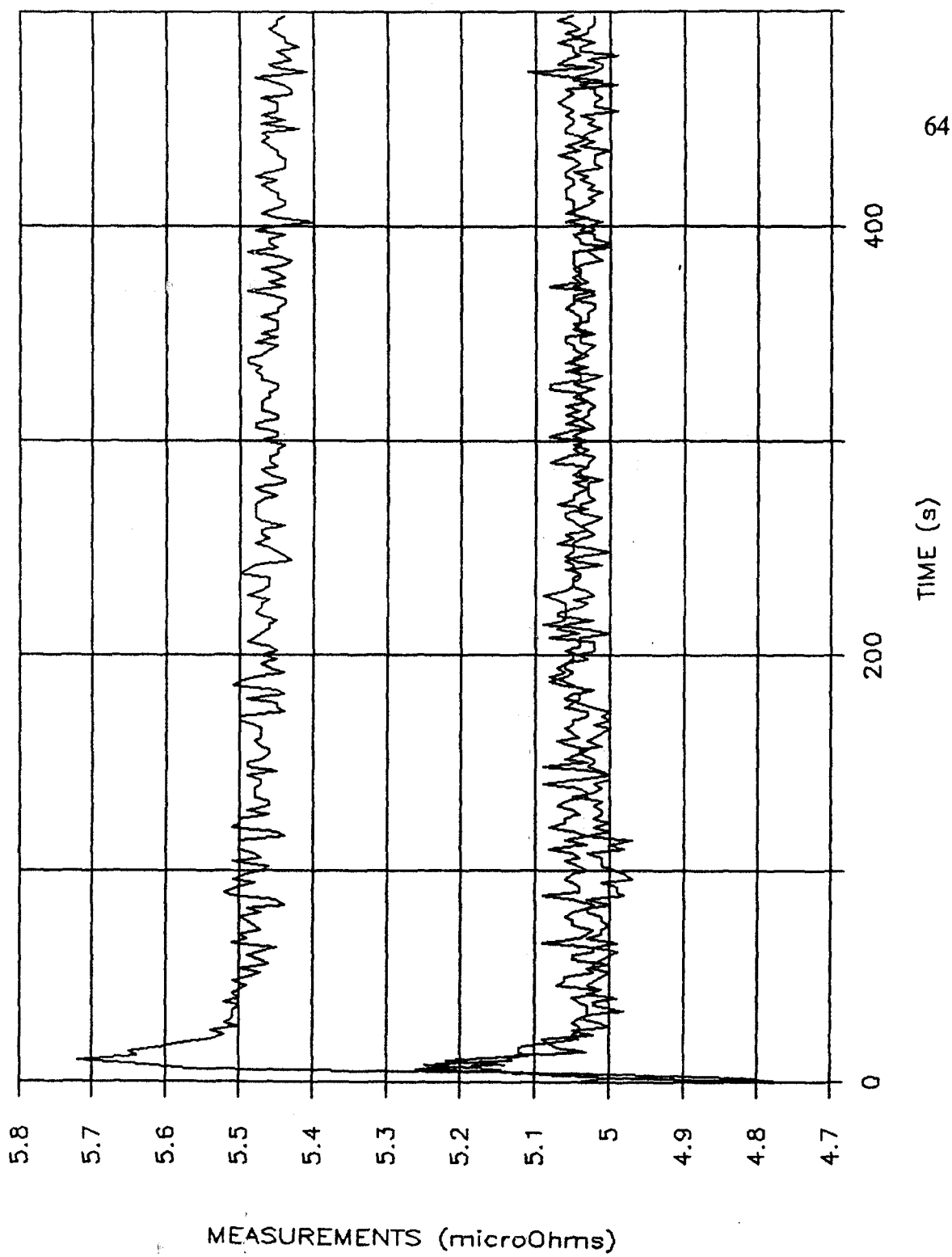

Figure 5.1: The resistivity as a function of time at 50 mm below the melt surface, after the stirrer was turned off, for the 5% SiC MMC.

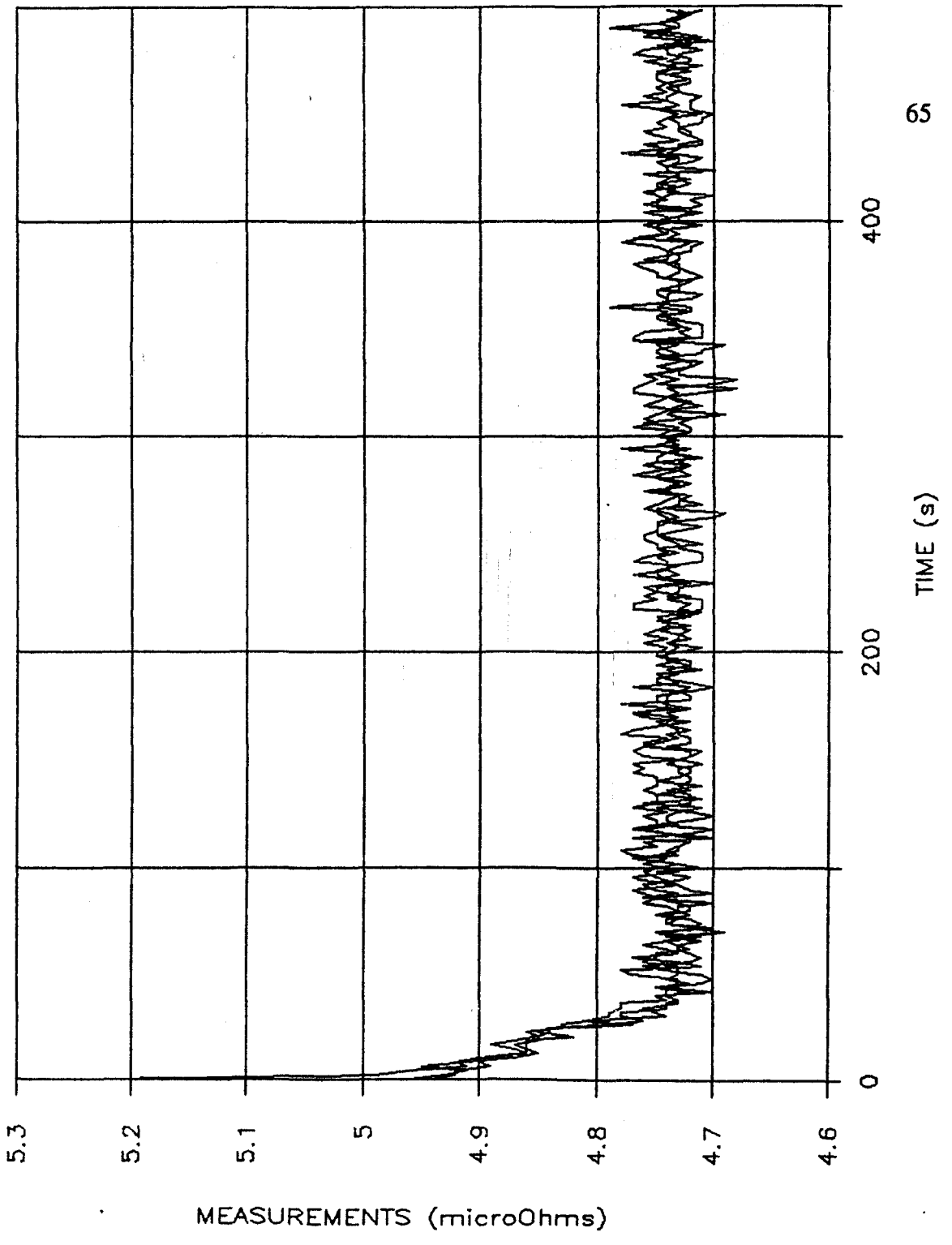

Figure 5.2: The resistivity as a function of time at 100 mm below the melt surface, after the stirrer was turned off, for the 5% SiC MMC.

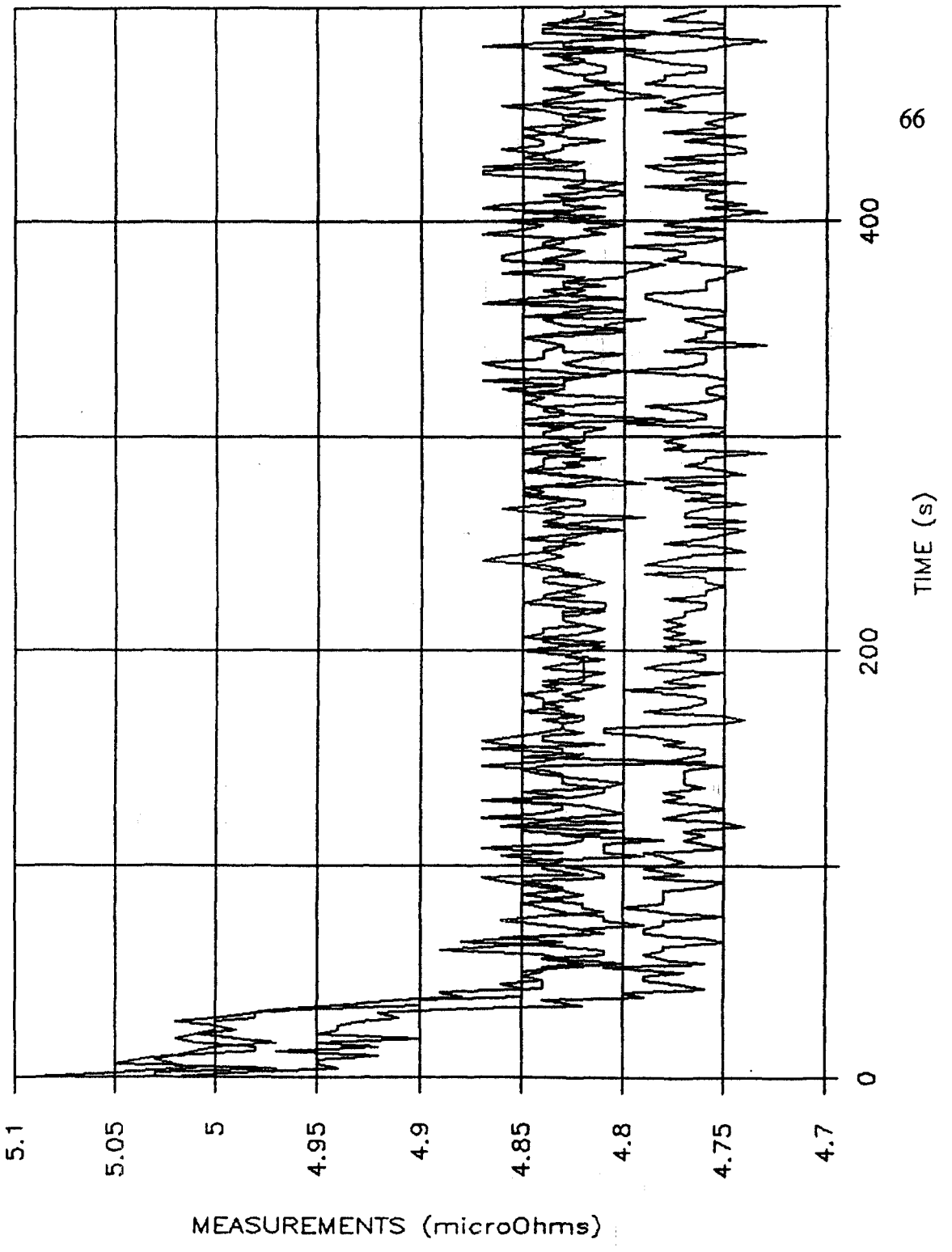

Figure 5.3: The resistivity as a function of time at 150 mm below the melt surface, after the stirrer was turned off, for the 5% SiC MMC.

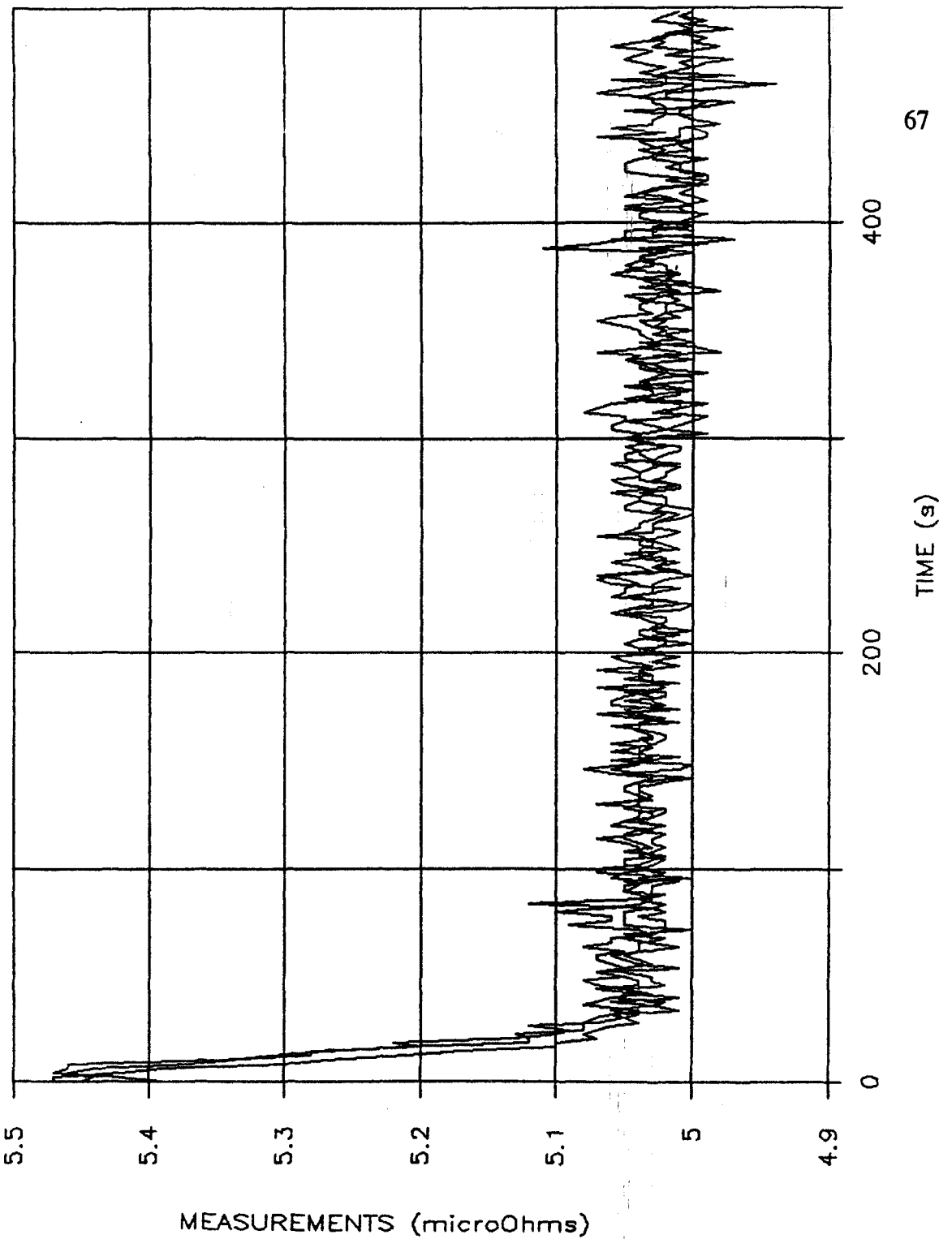

Figure 5.4: The resistivity as a function of time at 50 mm below the melt surface, after the stirrer was turned off, for the 10% SiC MMC.

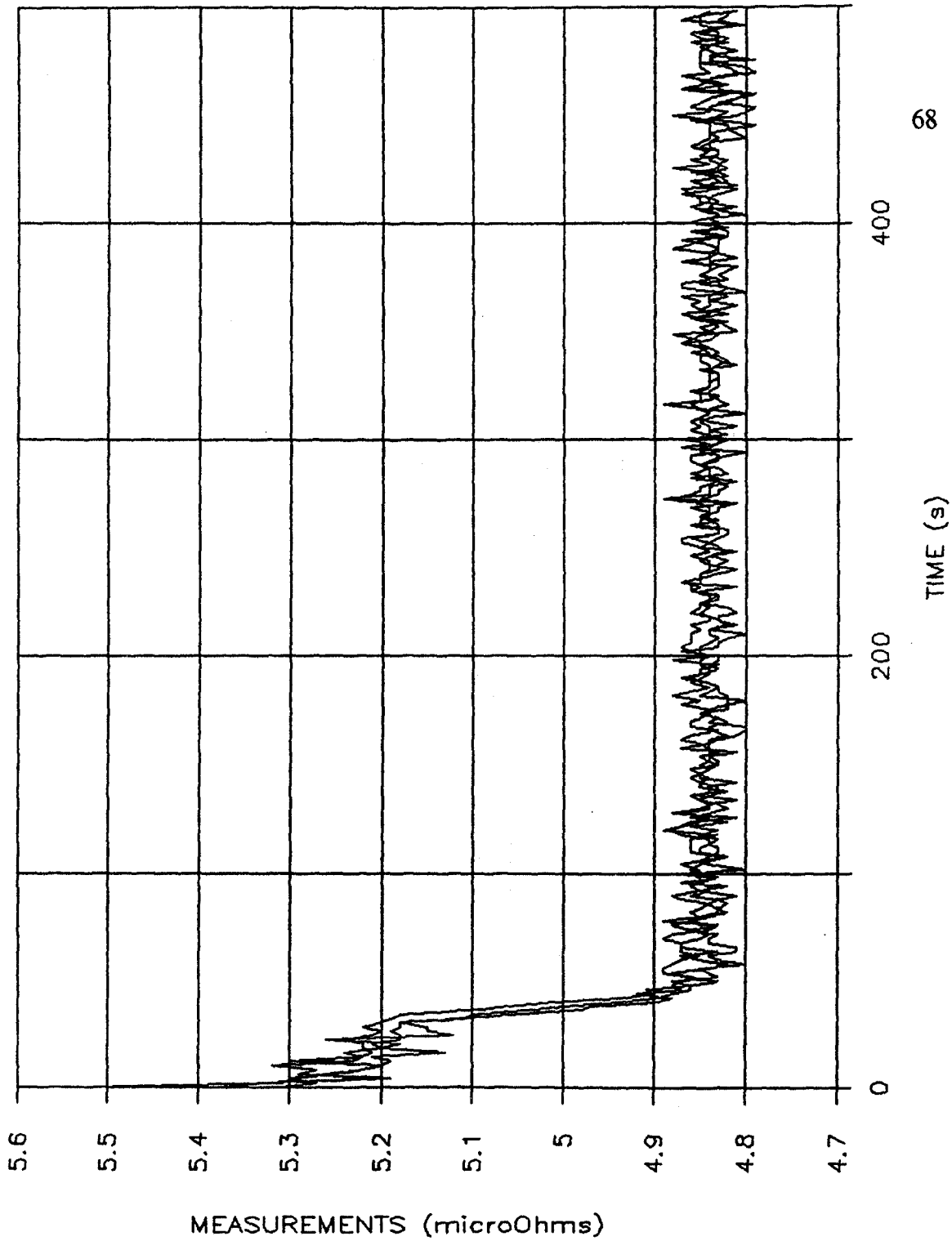

Figure 5.5: The resistivity as a function of time at 100 mm below the melt surface, after the stirrer was turned off, for the 10% SiC MMC.

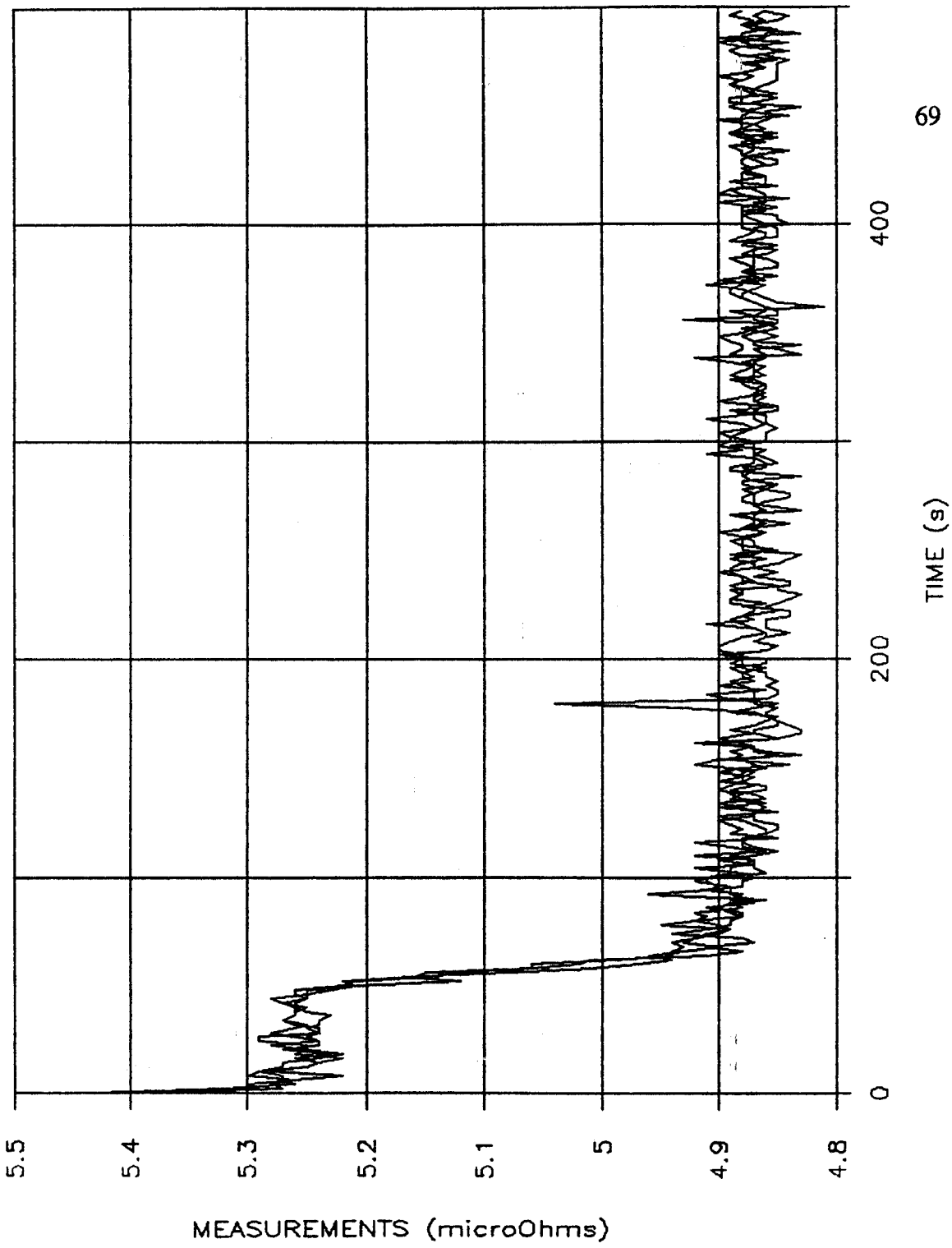

Figure 5.6: The resistivity as a function of time at 150 mm below the melt surface, after the stirrer was turned off, for the 10% SiC MMC.

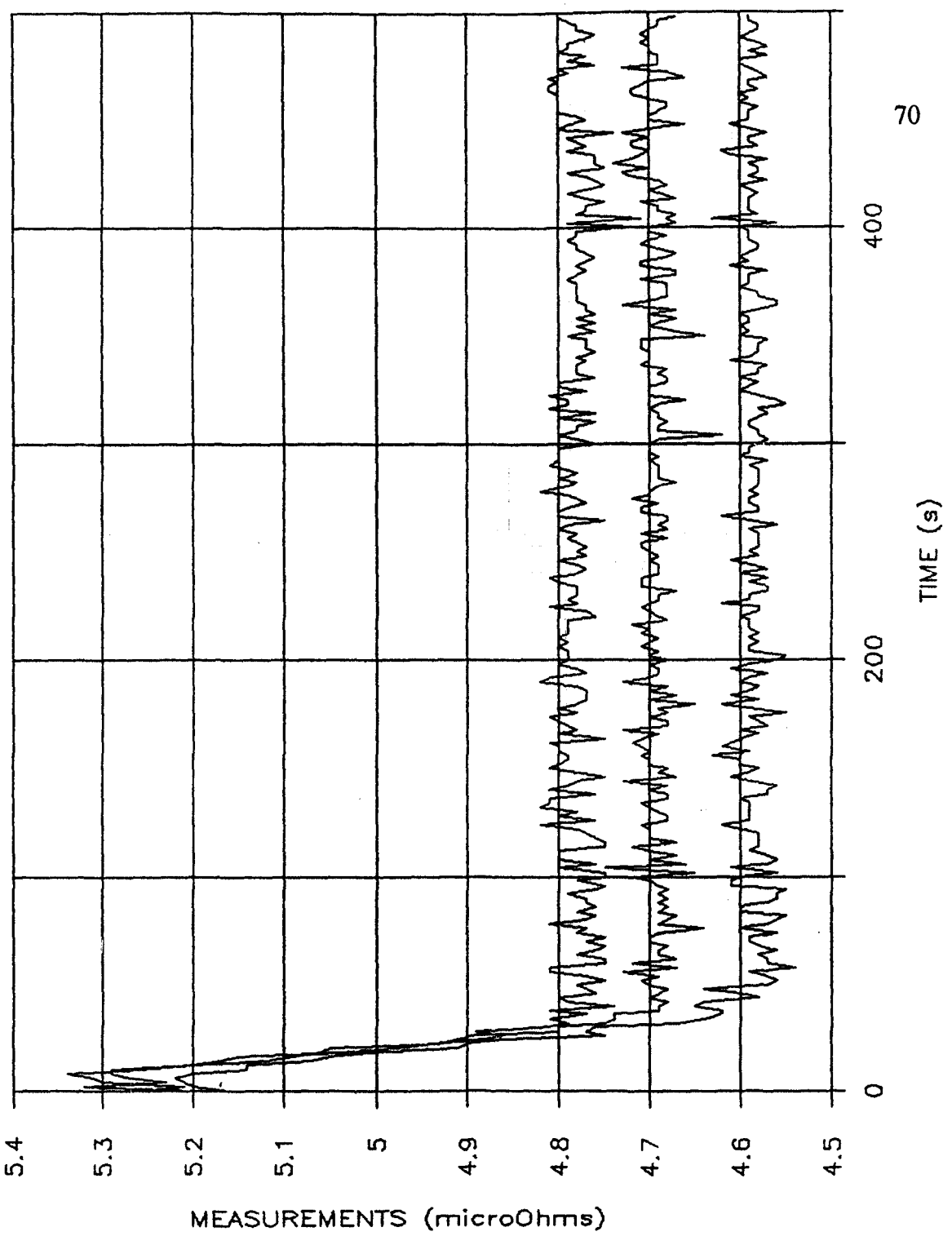

Figure 5.7: The resistivity as a function of time at 50 mm below the melt surface, after the stirrer was turned off, for the 15% SiC MMC.

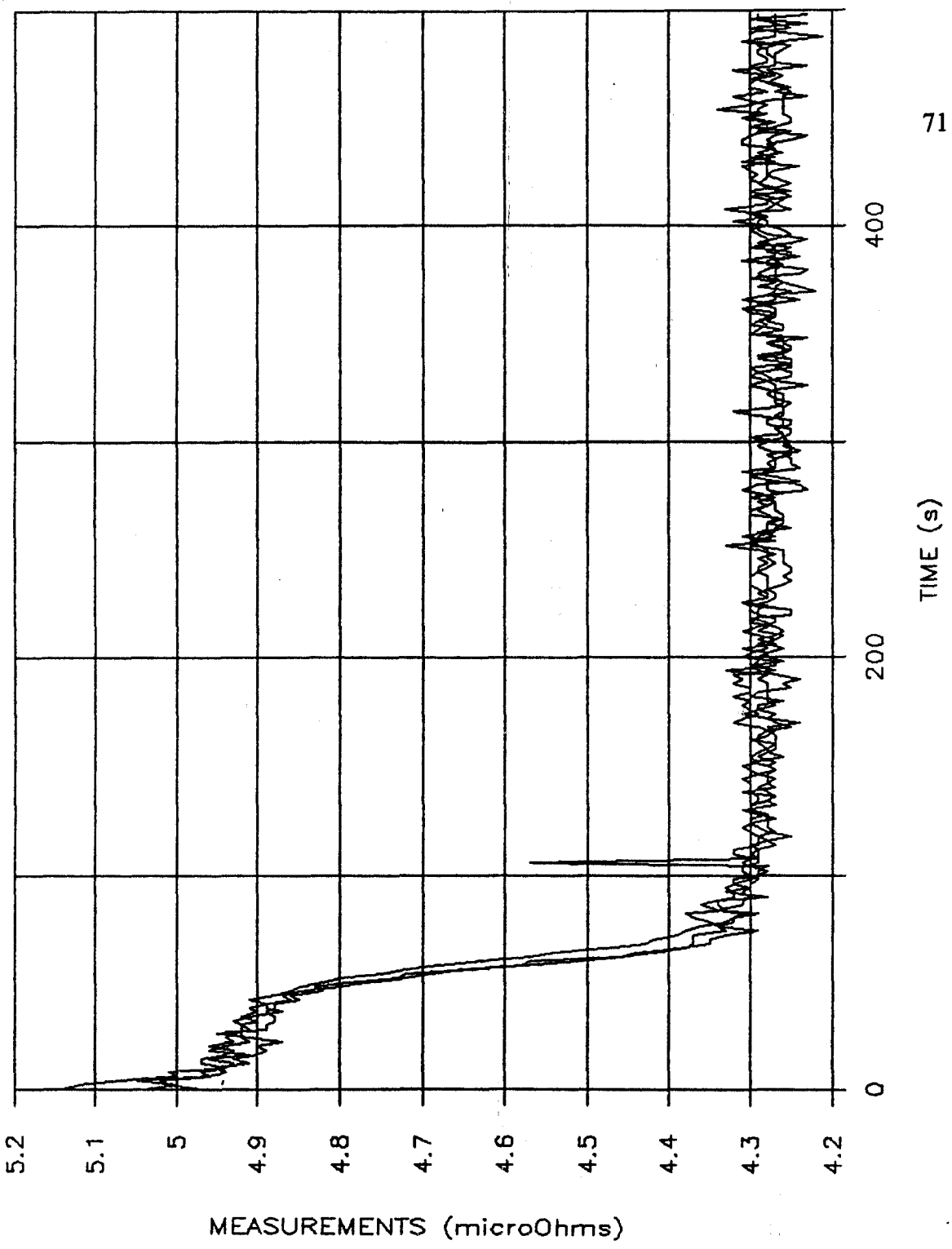

Figure 5.8: The resistivity as a function of time at 100 mm below the melt surface, after the stirrer was turned off, for the 15% SiC MMC.

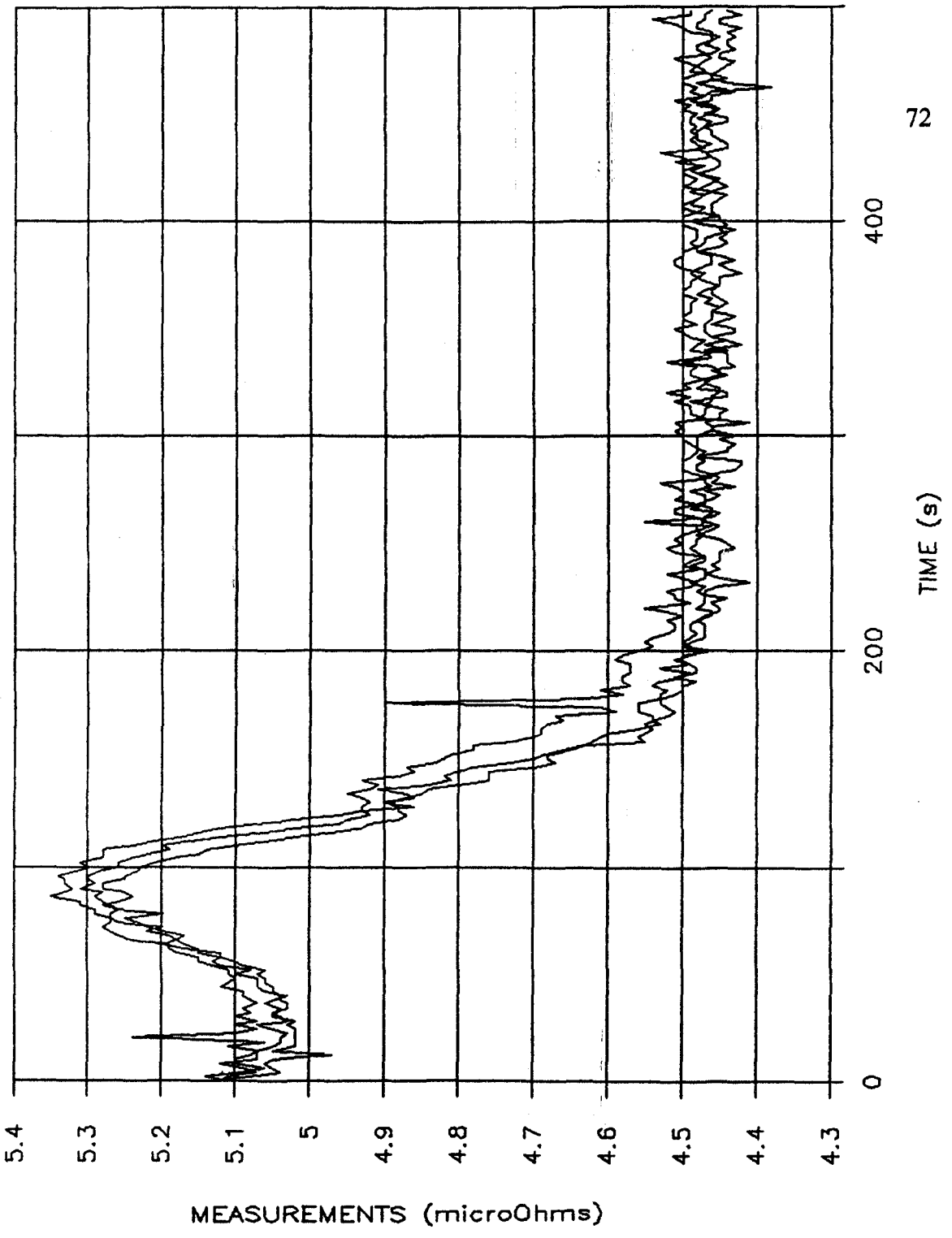

Figure 5.9: The resistivity as a function of time at 150 mm below the melt surface, after the stirrer was turned off, for the 15% SiC MMC.

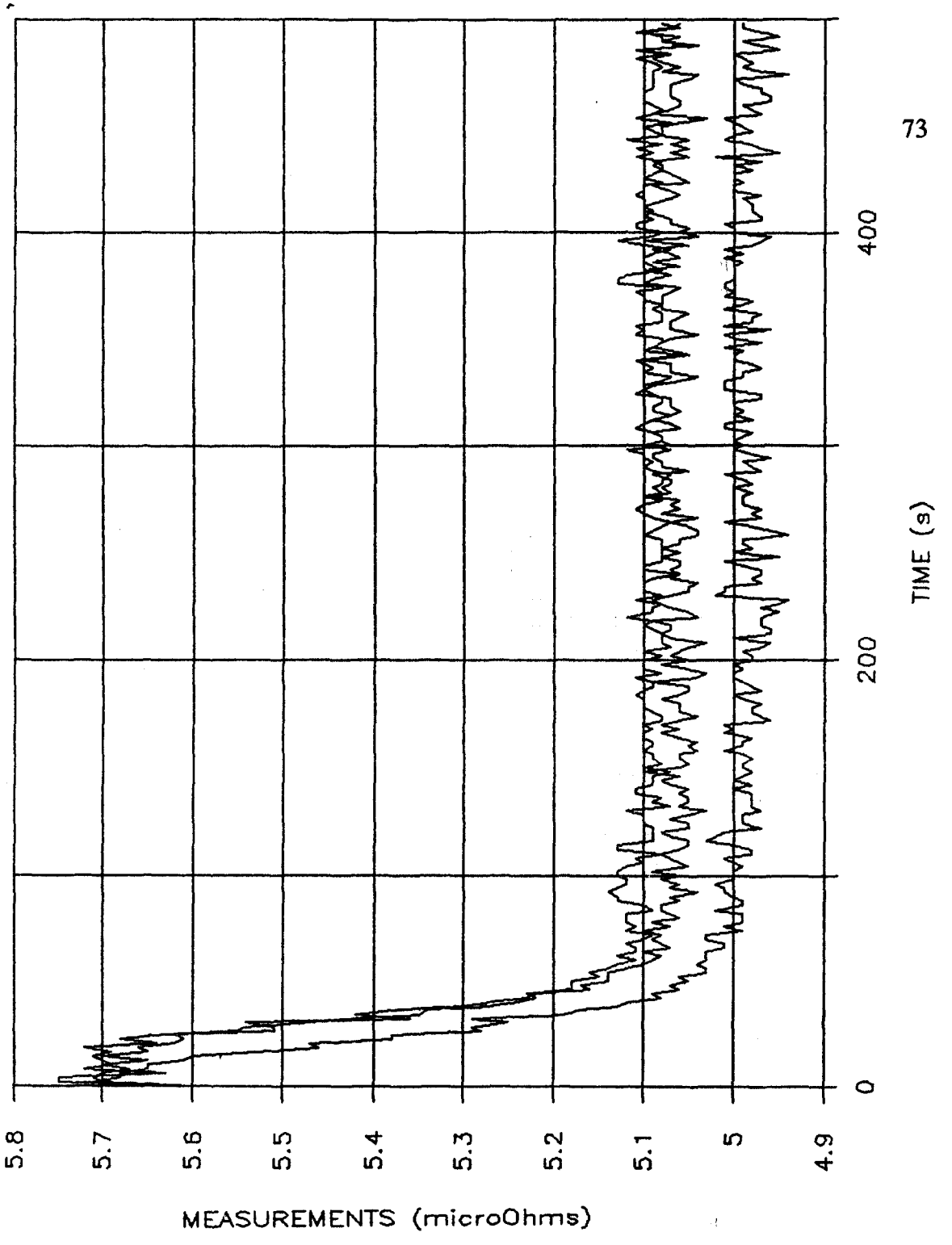

Figure 5.10: The resistivity as a function of time at 50 mm below the melt surface, after the stirrer was turned off, for the 20% SiC MMC.

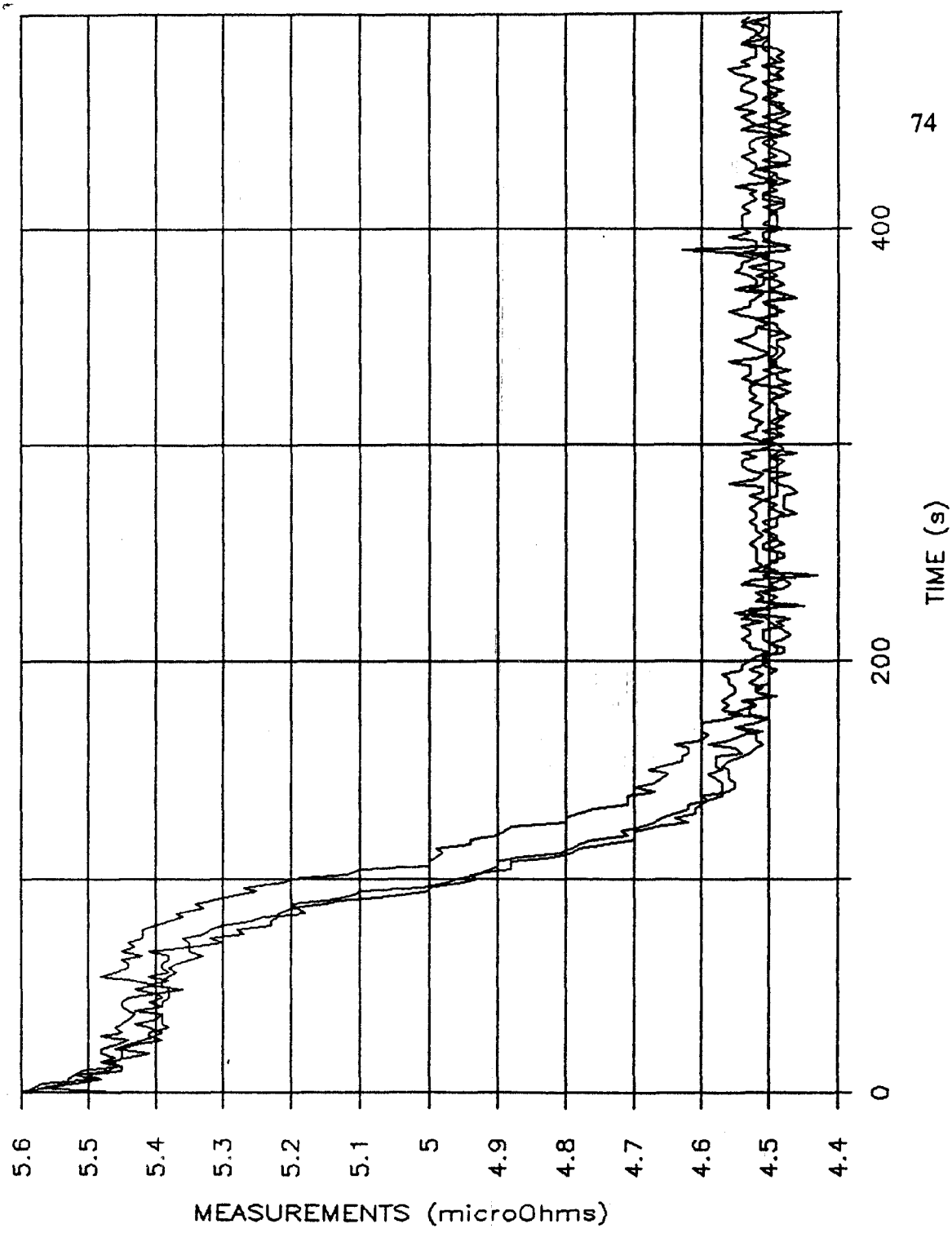

Figure 5.11: The resistivity as a function of time at 100 mm below the melt surface, after the stirrer was turned off, for the 20% SiC MMC.

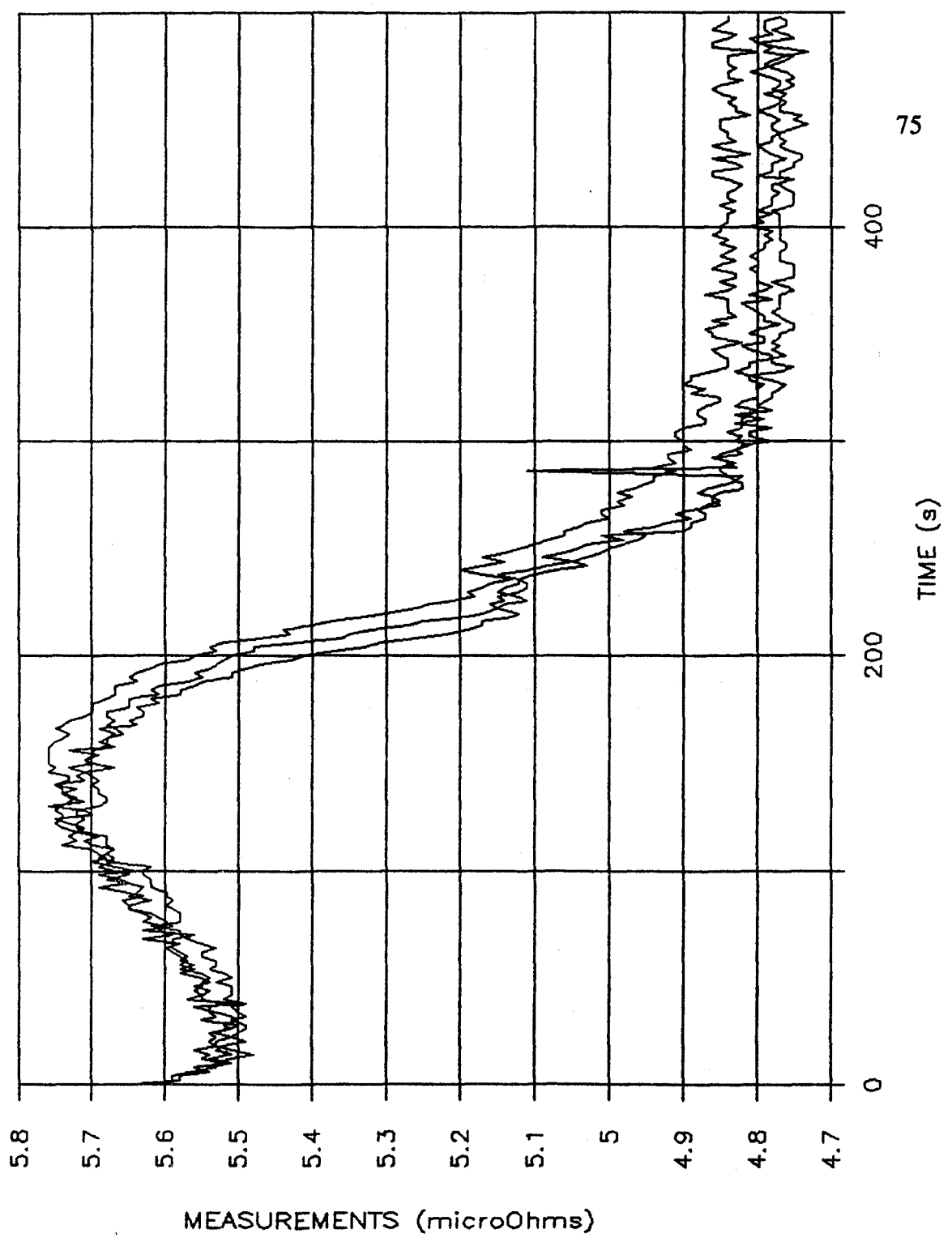

Figure 5.12: The resistivity as a function of time at 150 mm below the melt surface, after the stirrer was turned off, for the 20% SiC MMC.

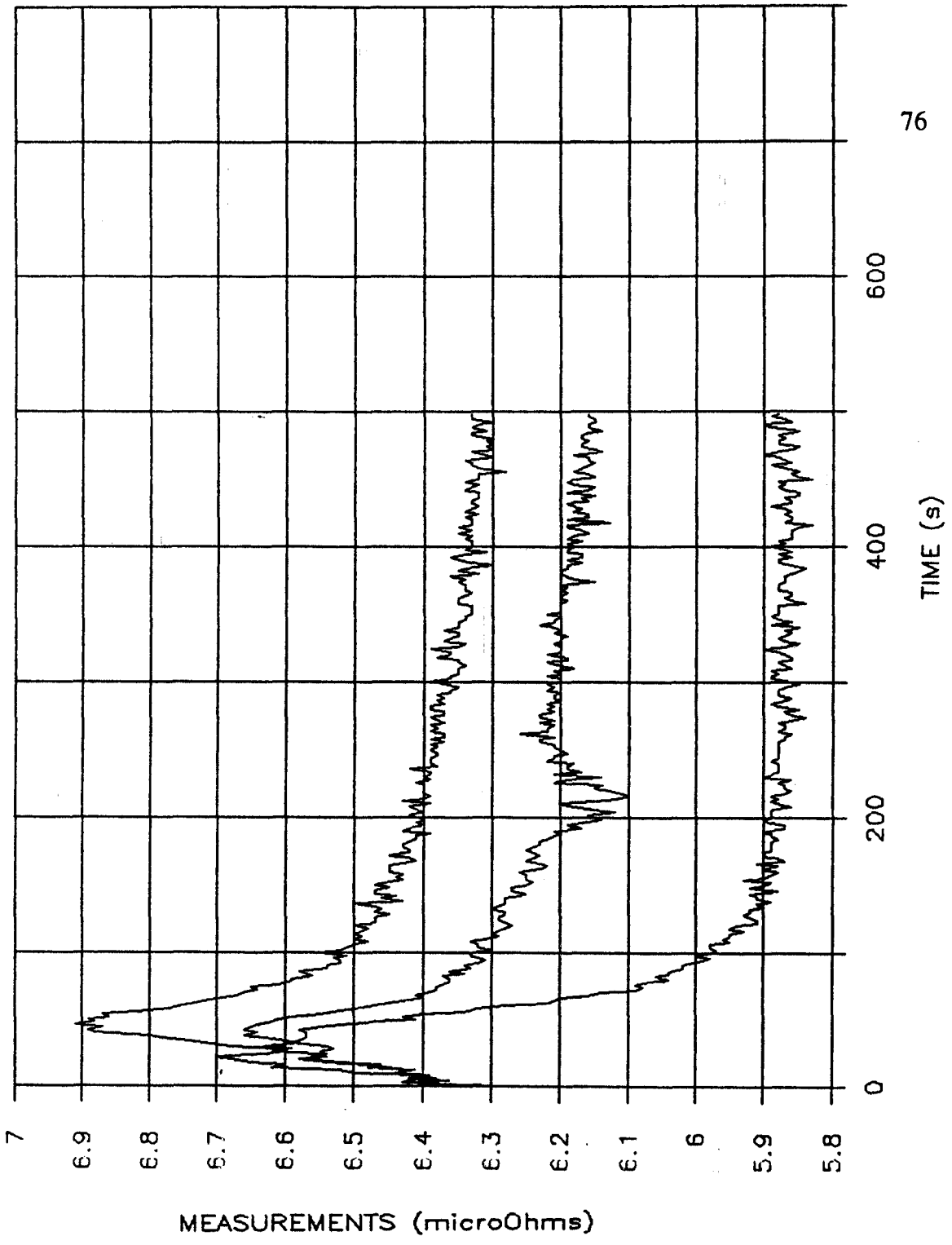

Figure 5.13: The resistivity as a function of time at 50 mm below the melt surface, after the stirrer was turned off, for the 25% SiC MMC.

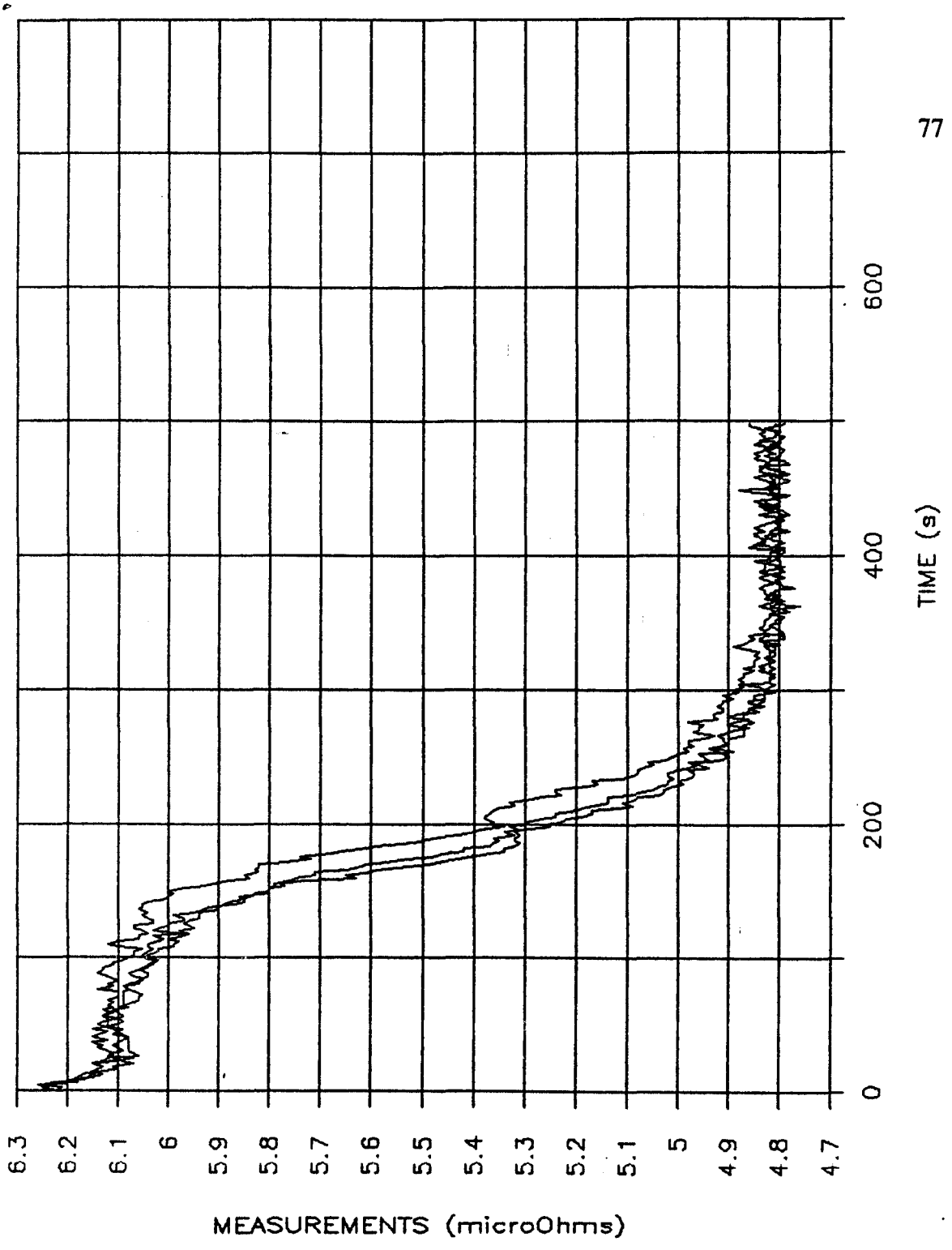

Figure 5.14: The resistivity as a function of time at 100 mm below the melt surface, after the stirrer was turned off, for the 25% SiC MMC.

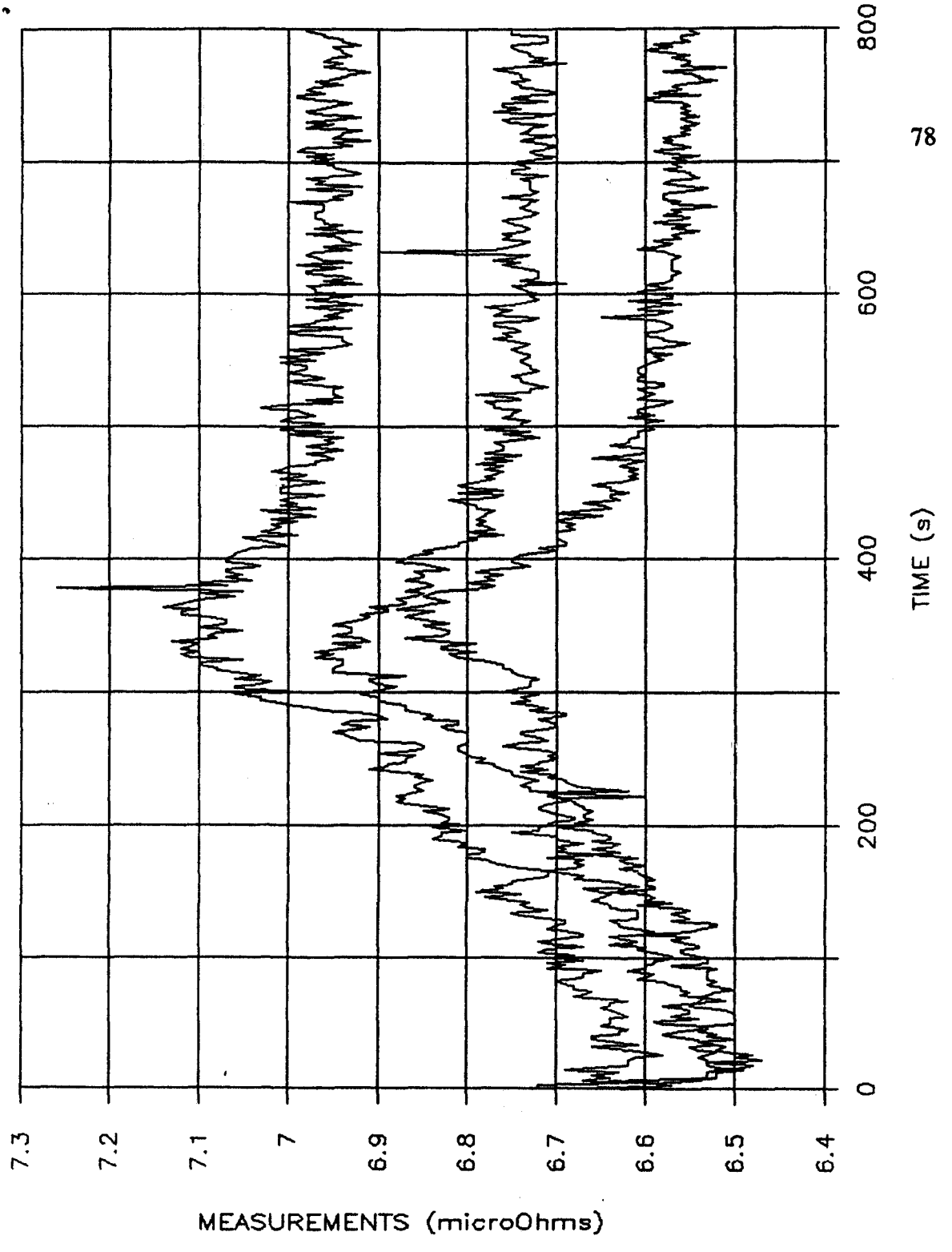

Figure 5.15: The resistivity as a function of time at 150 mm below the melt surface, after the stirrer was turned off, for the 25% SiC MMC.

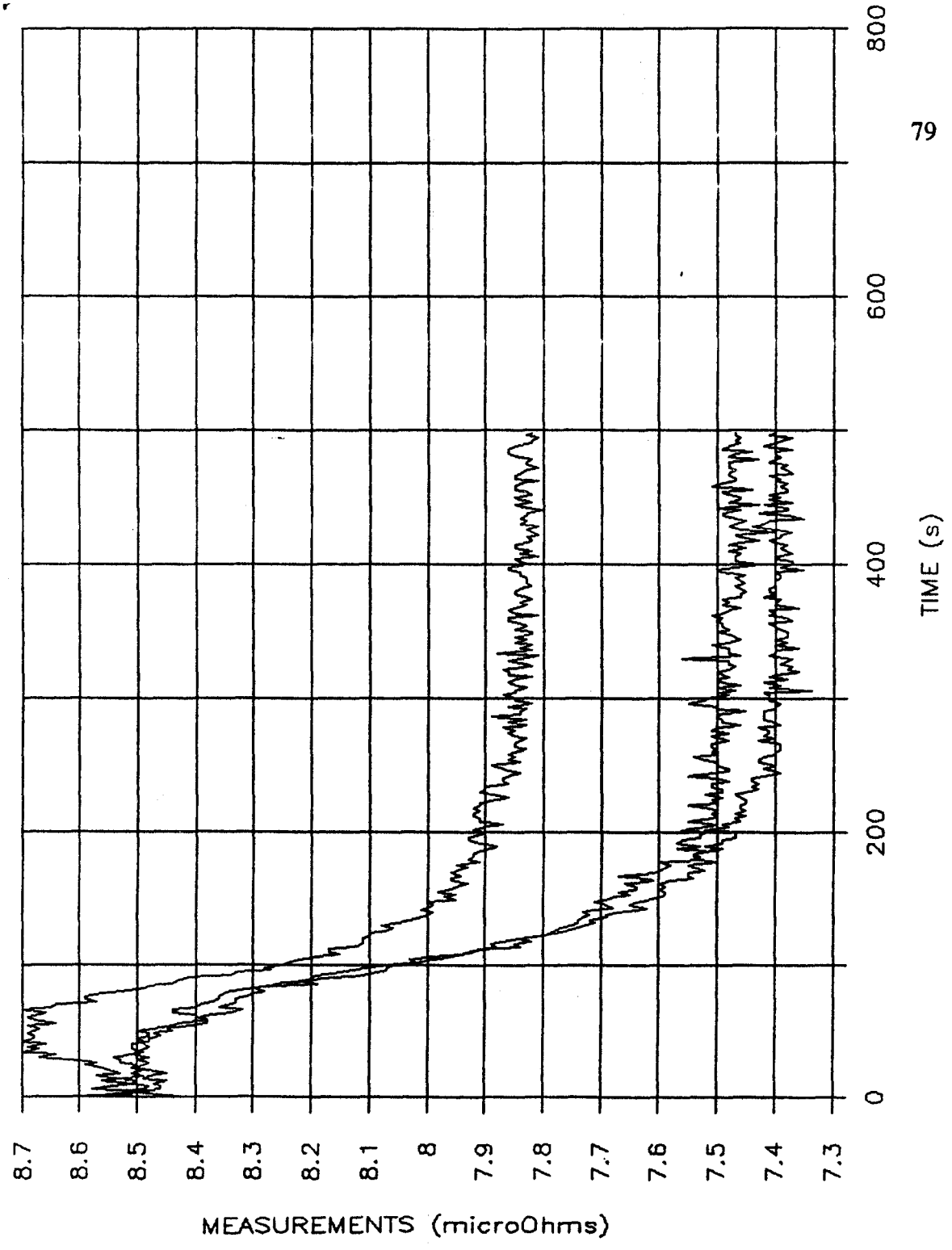

Figure 5.16: The resistivity as a function of time at 50 mm below the melt surface, after the stirrer was turned off, for the 30% SiC MMC.

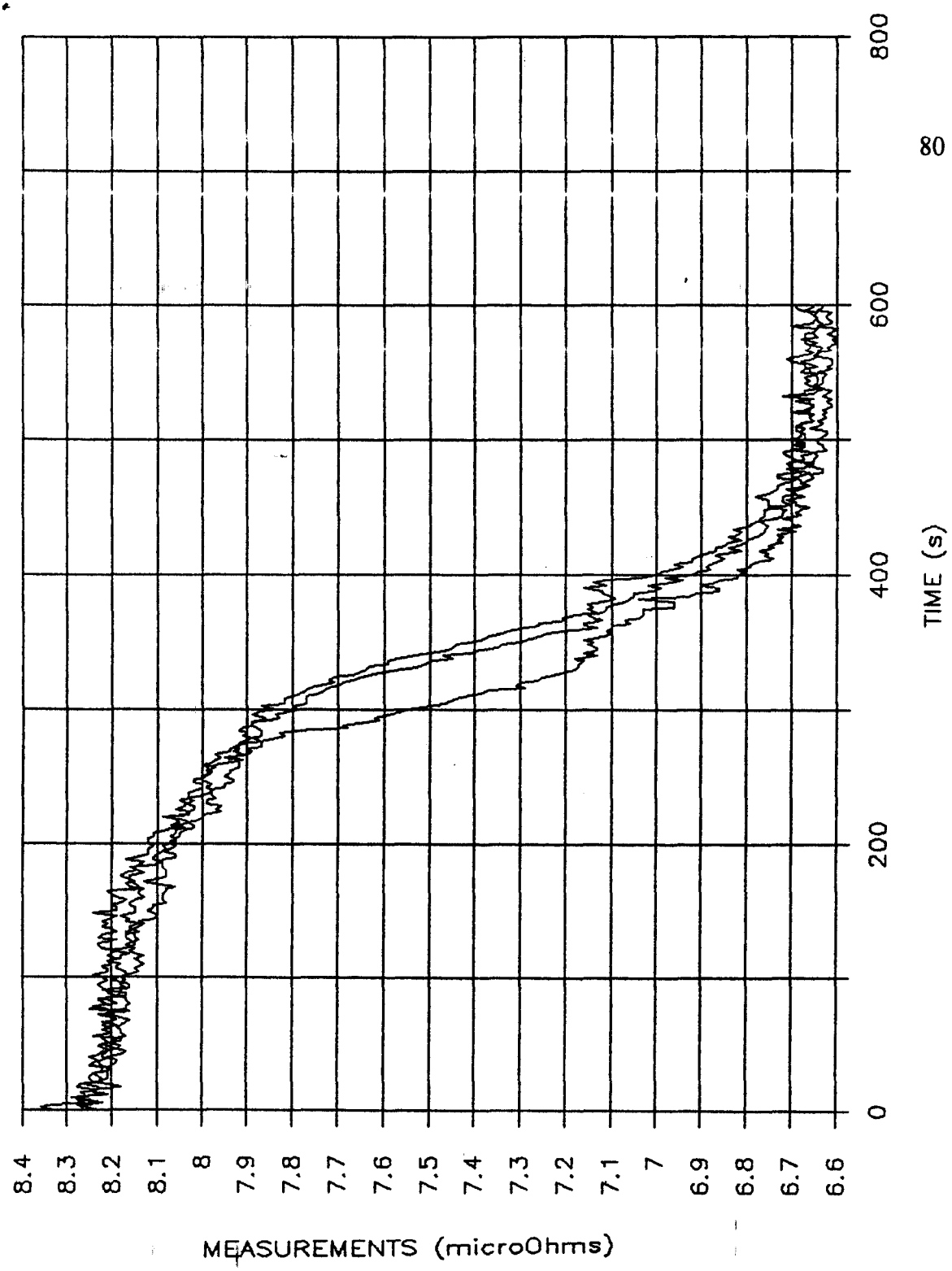

Figure 5.17: The resistivity as a function of time at 100 mm below the melt surface, after the stirrer was turned off, for the 30% SiC MMC.

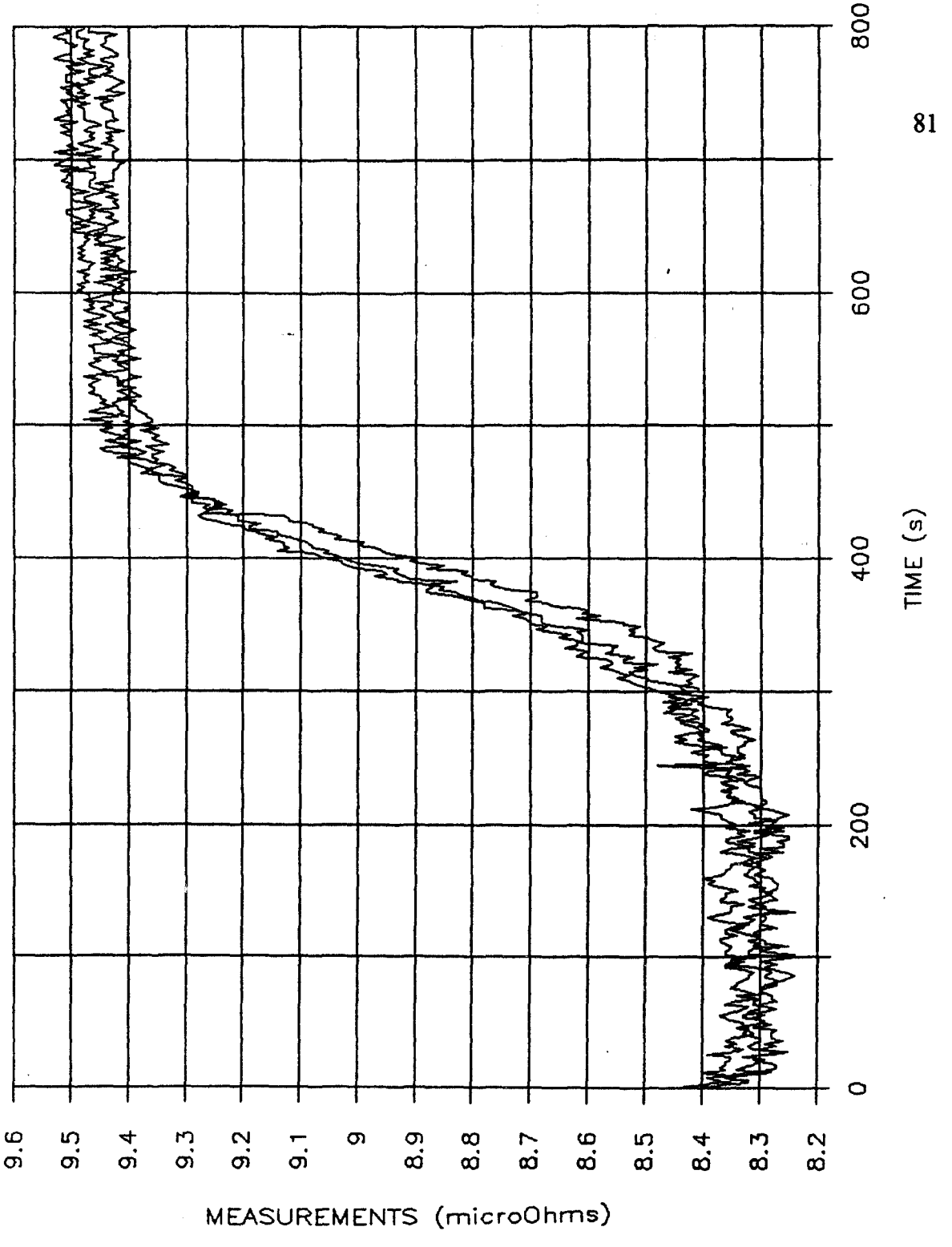

Figure 5.18: The resistivity as a function of time at 150 mm below the melt surface, after the stirrer was turned off, for the 30% SiC MMC.

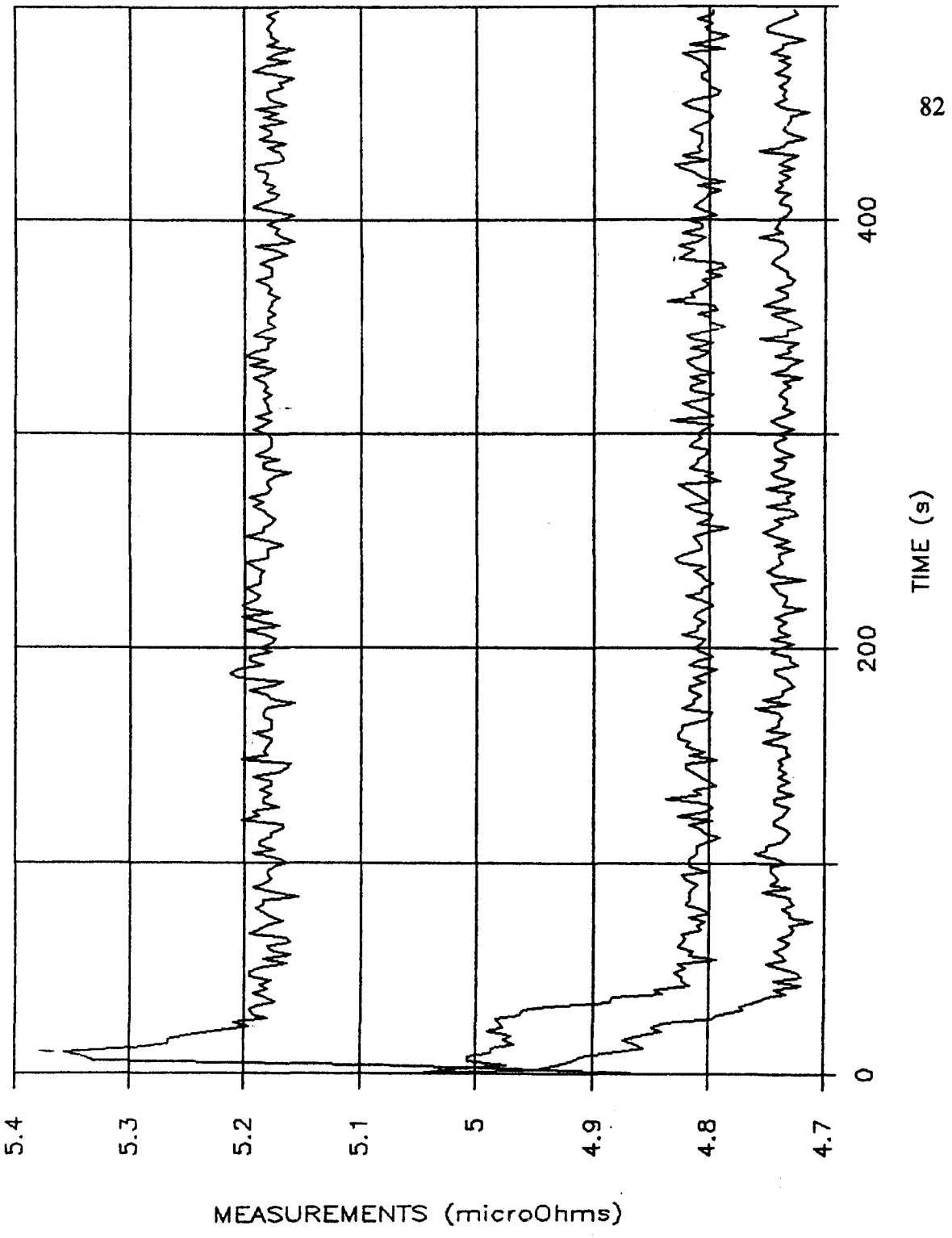

Figure 5.19: The average resistivity as a function of time at 50, 100 and 150 mm below the melt surface, after the stirrer was turned off, for the 5% SiC MMC.

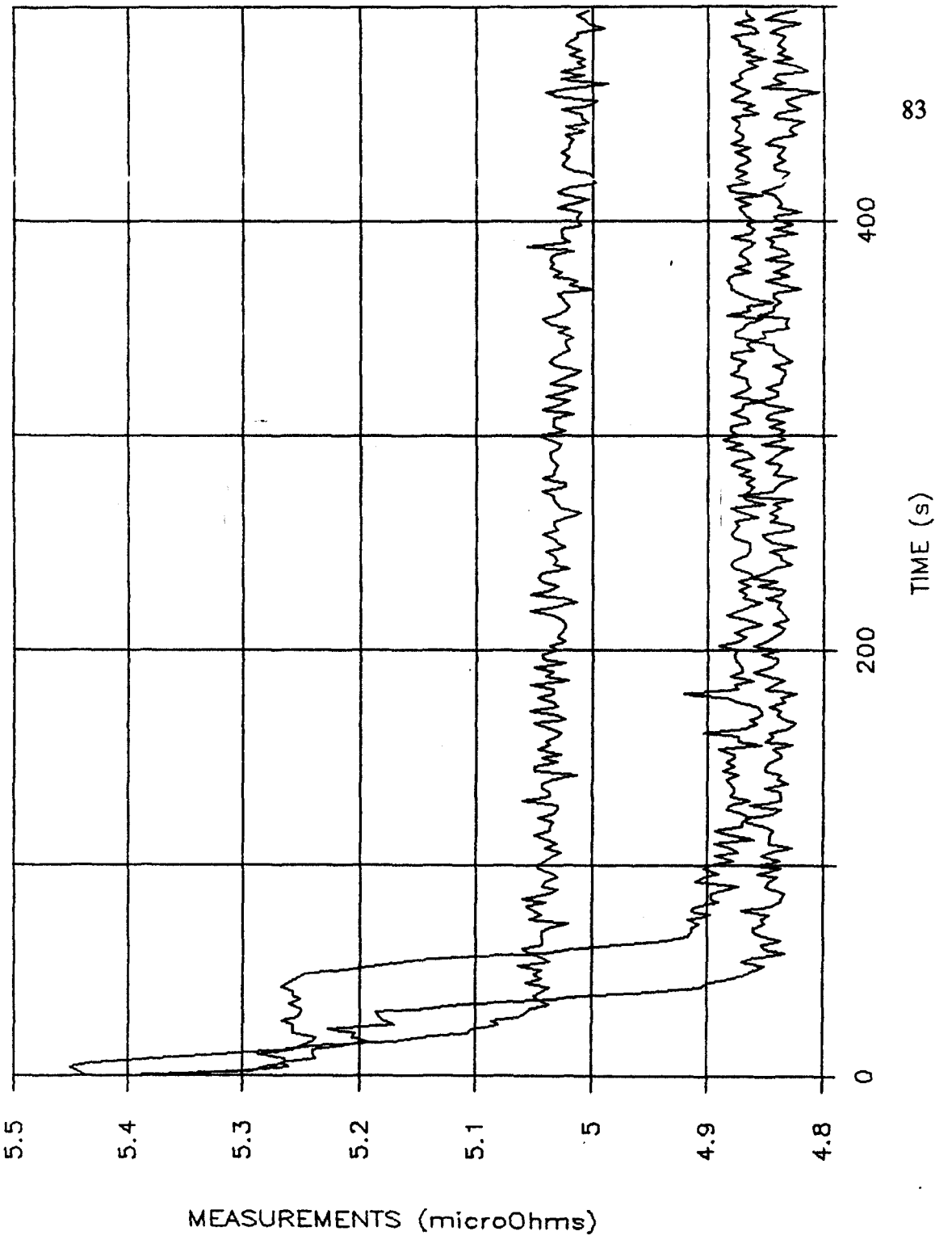

Figure 5.20: The average resistivity as a function of time at 50, 100 and 150 mm below the melt surface, after the stirrer was turned off, for the 10% SiC MMC.

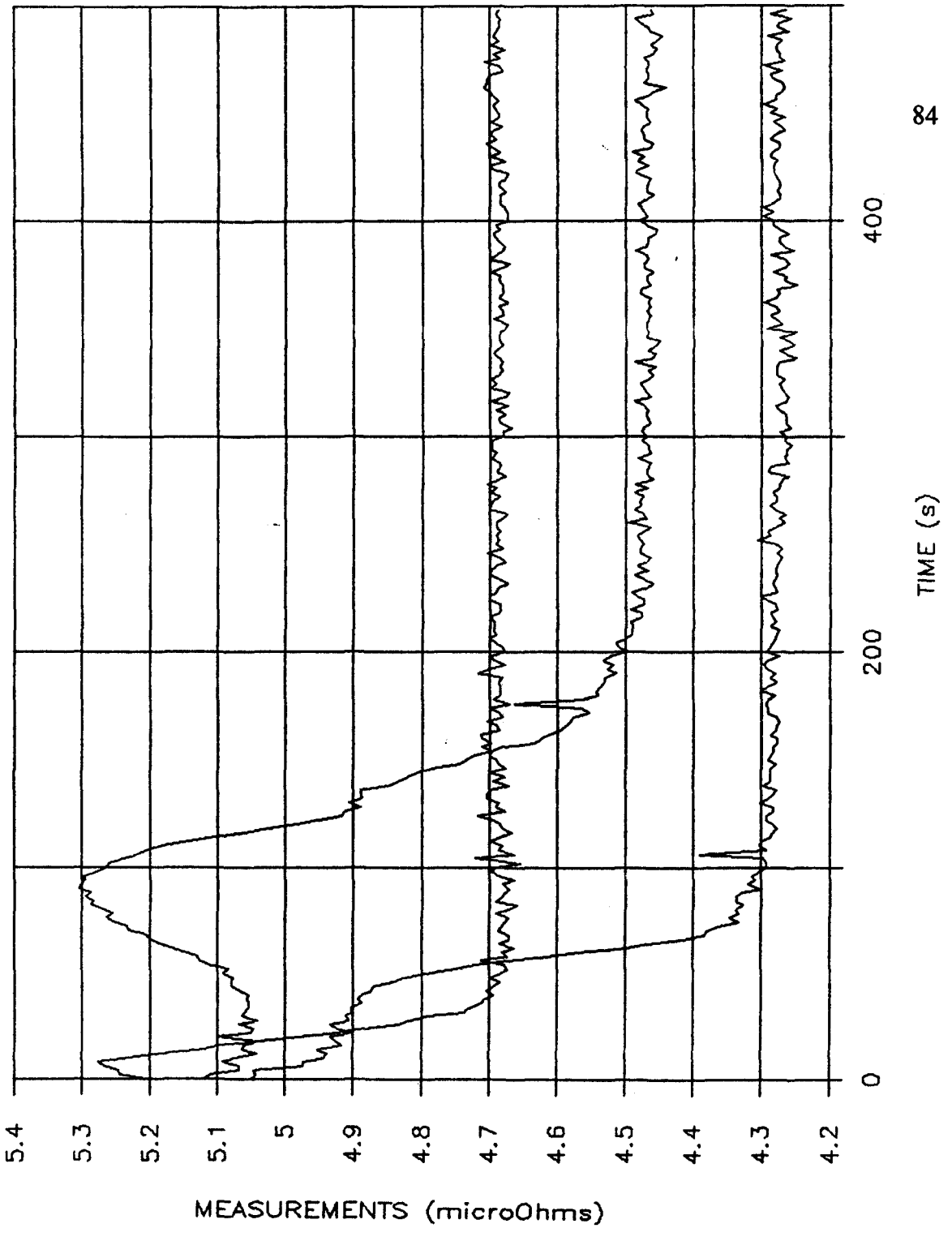

Figure 5.21: The average resistivity as a function of time at 50, 100 and 150 mm below the melt surface, after the stirrer was turned off, for the 15% SiC MMC.

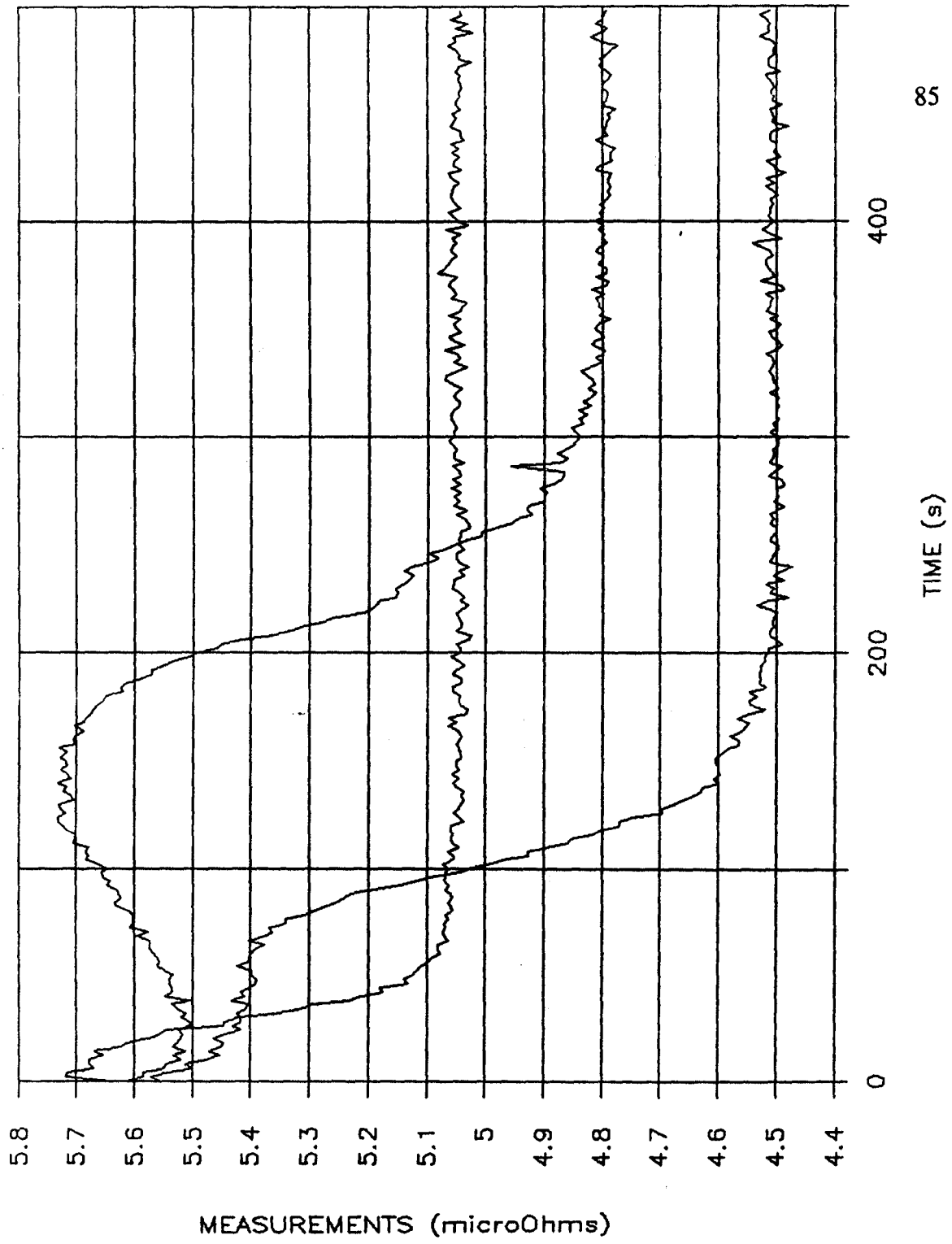

Figure 5.22: The average resistivity as a function of time at 50, 100 and 150 mm below the melt surface, after the stirrer was turned off, for the 20% SiC MMC.

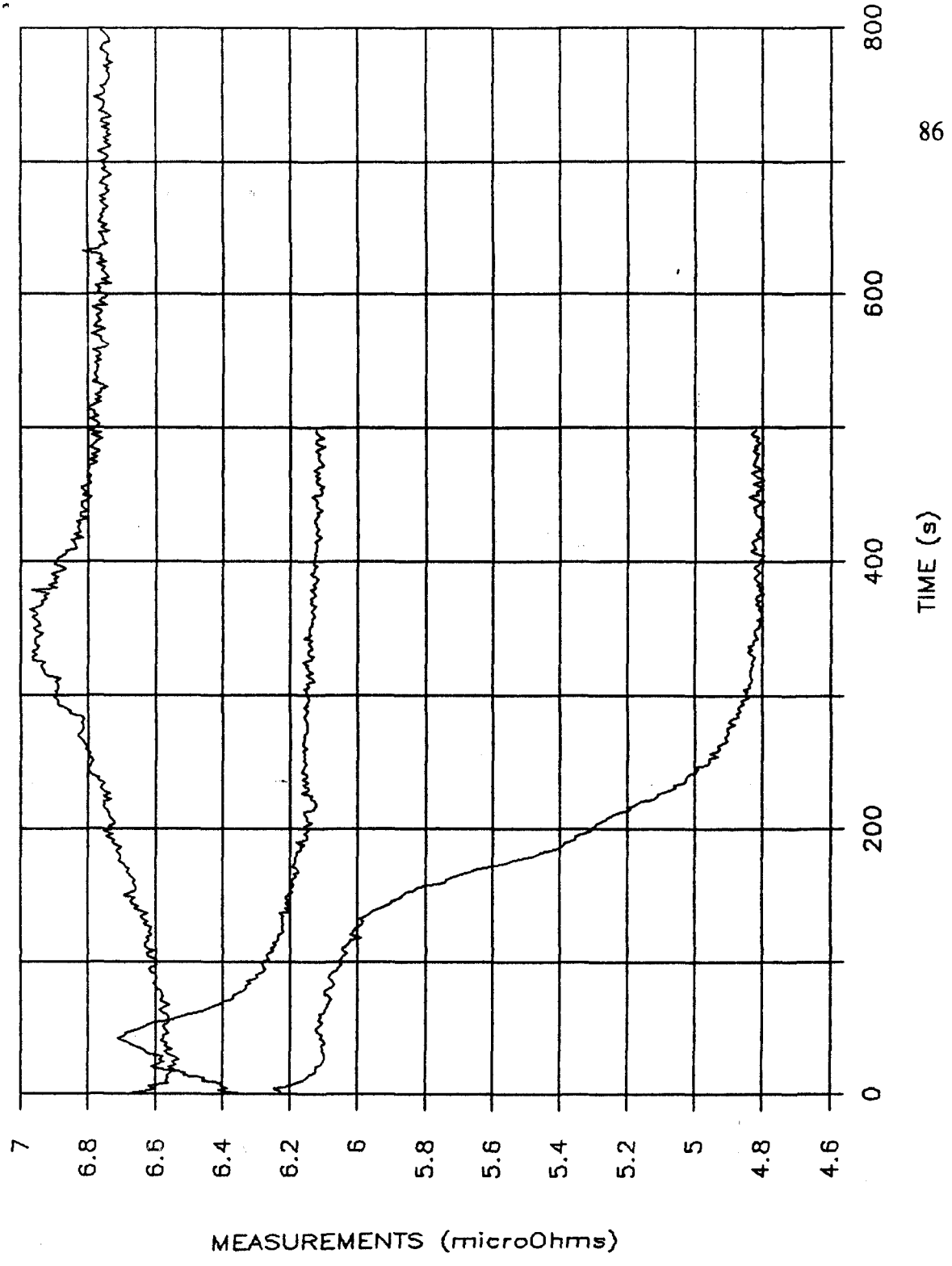

Figure 5.23: The average resistivity as a function of time at 50, 100 and 150 mm below the melt surface, after the stirrer was turned off, for the 25% SiC MMC.

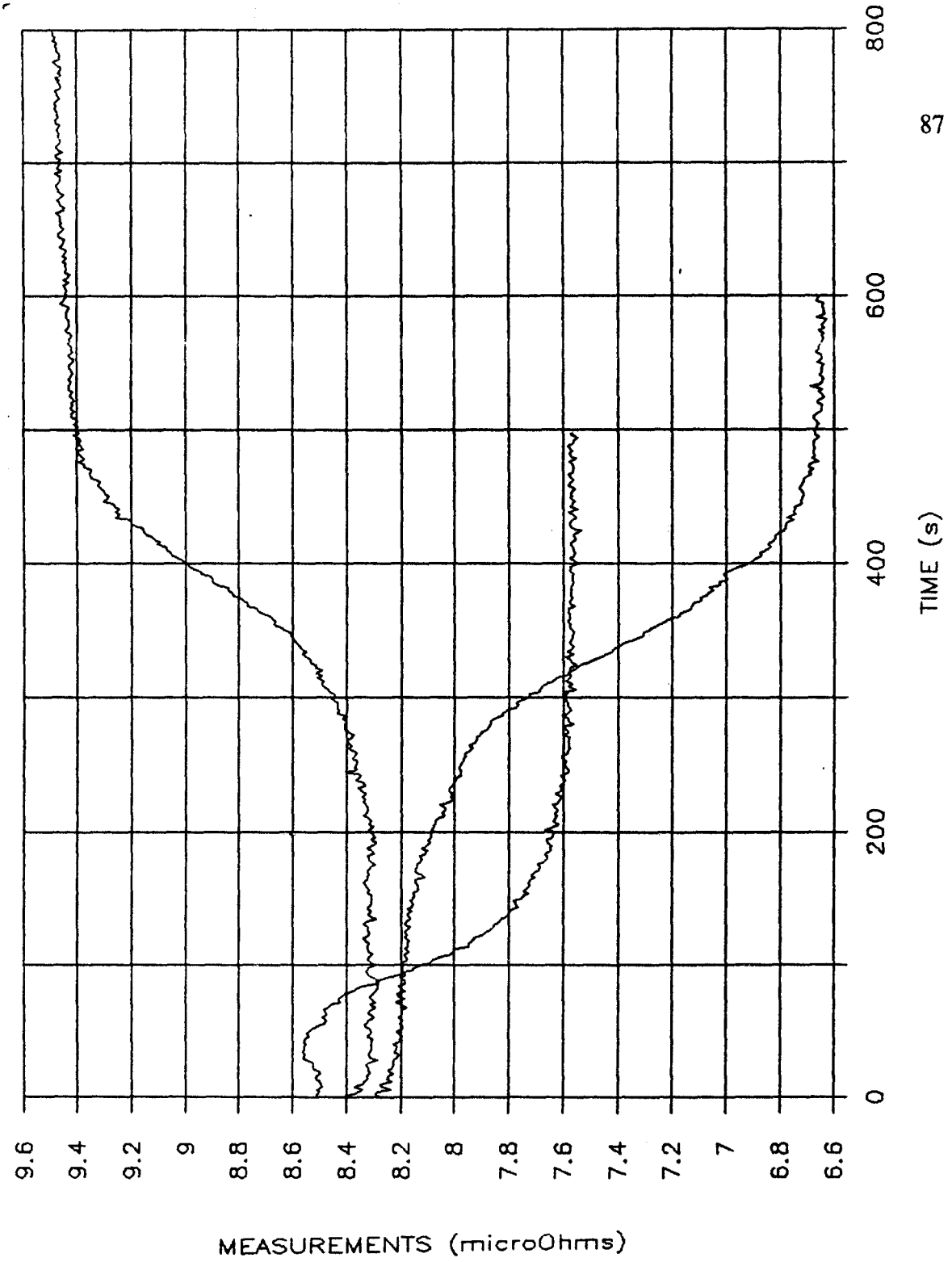

Figure 5.24: The average resistivity as a function of time at 50, 100 and 150 mm below the melt surface, after the stirrer was turned off, for the 30% SiC MMC.

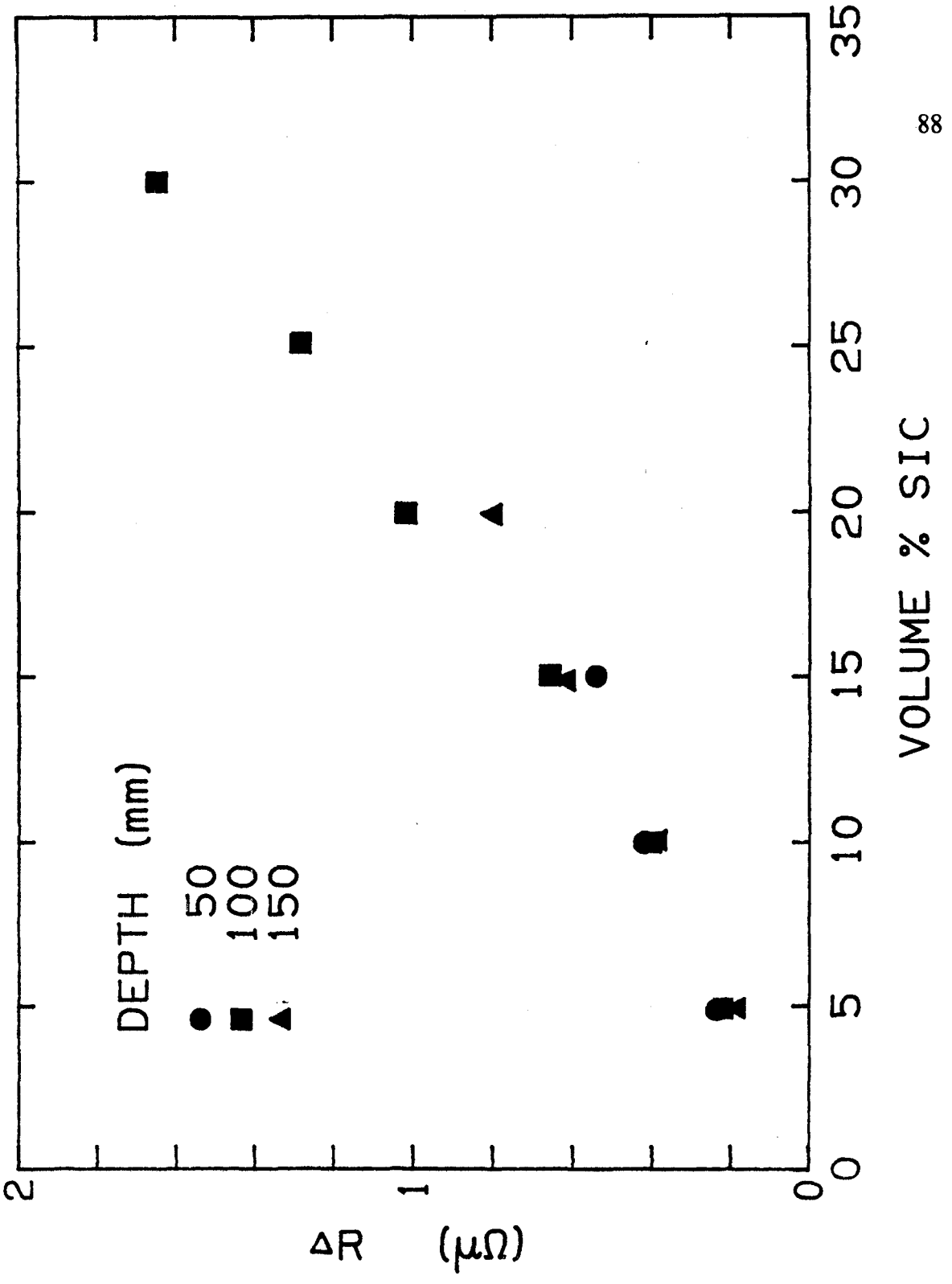

Figure 5.25: The change in resistivity during settling for the different initial volume fractions of particles at different depths of probe immersion.

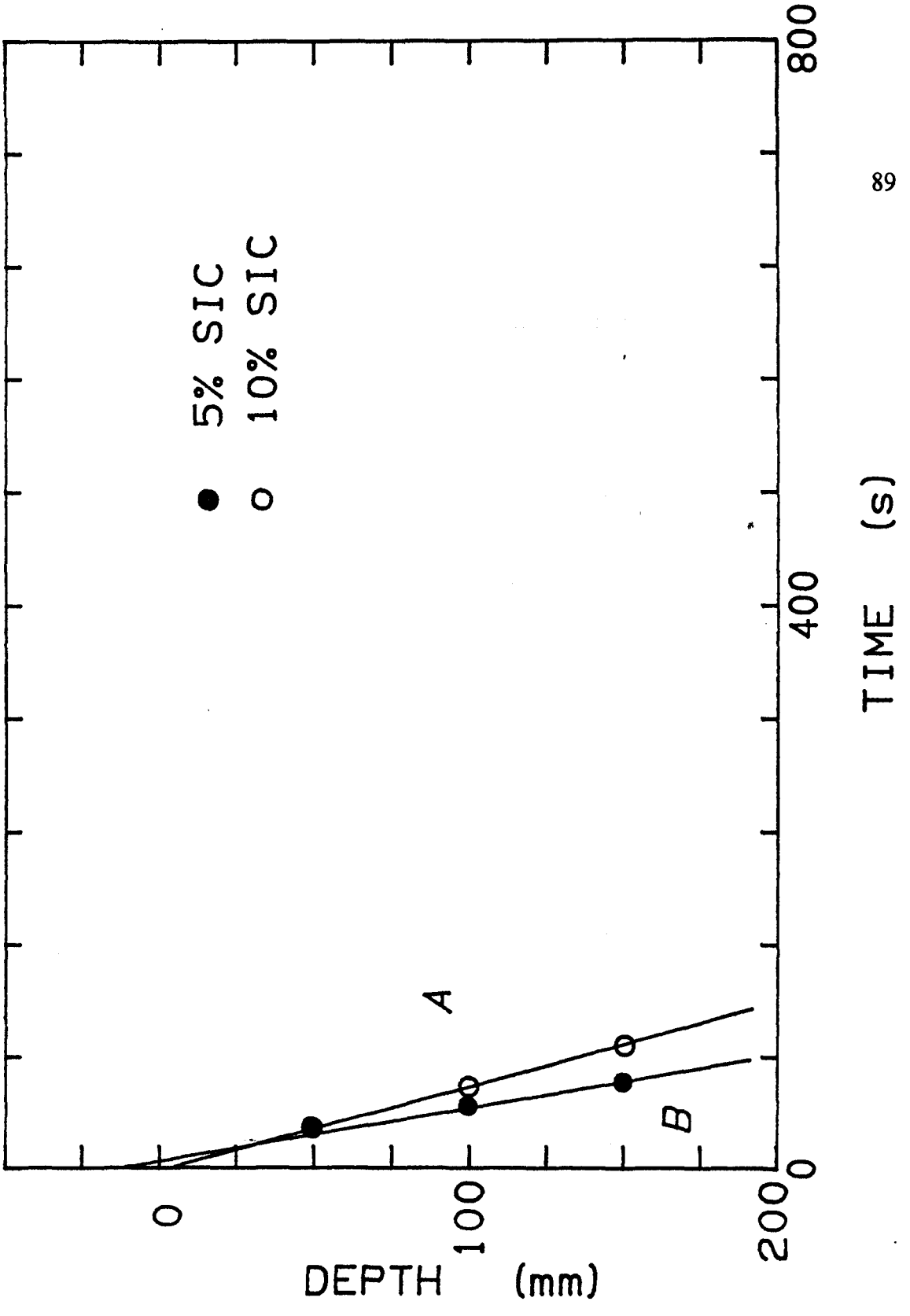

Figure 5.26: The time to pass from the initial volume fraction region B, to a clarified region, A for the 5 and 10% volume fractions at the different heights.

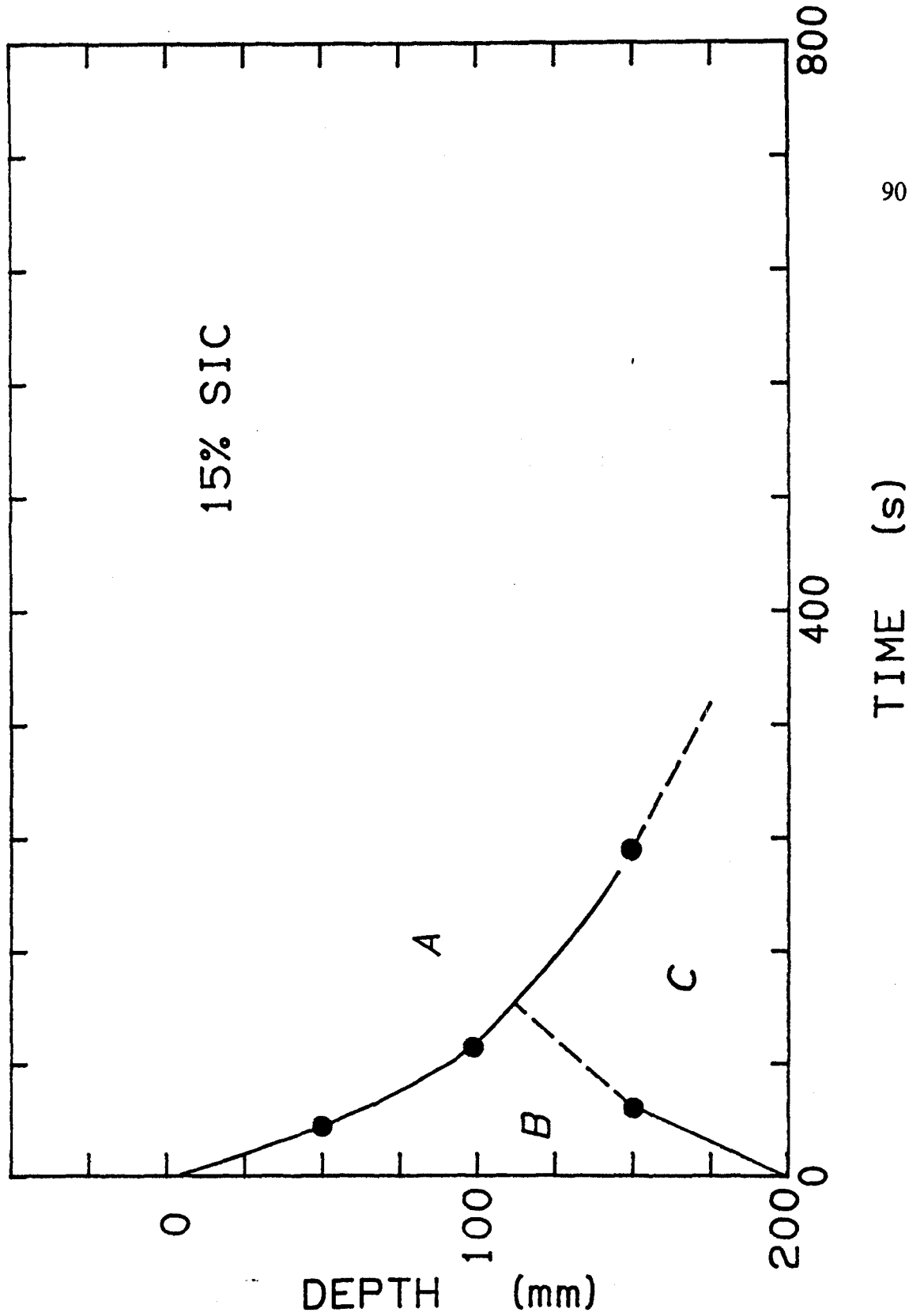

Figure 5.27: The time to pass from the initial volume fraction region B, to a clarified region, A for the 15% volume fractions at the different heights. A region of higher volume fraction, C, was also observed.

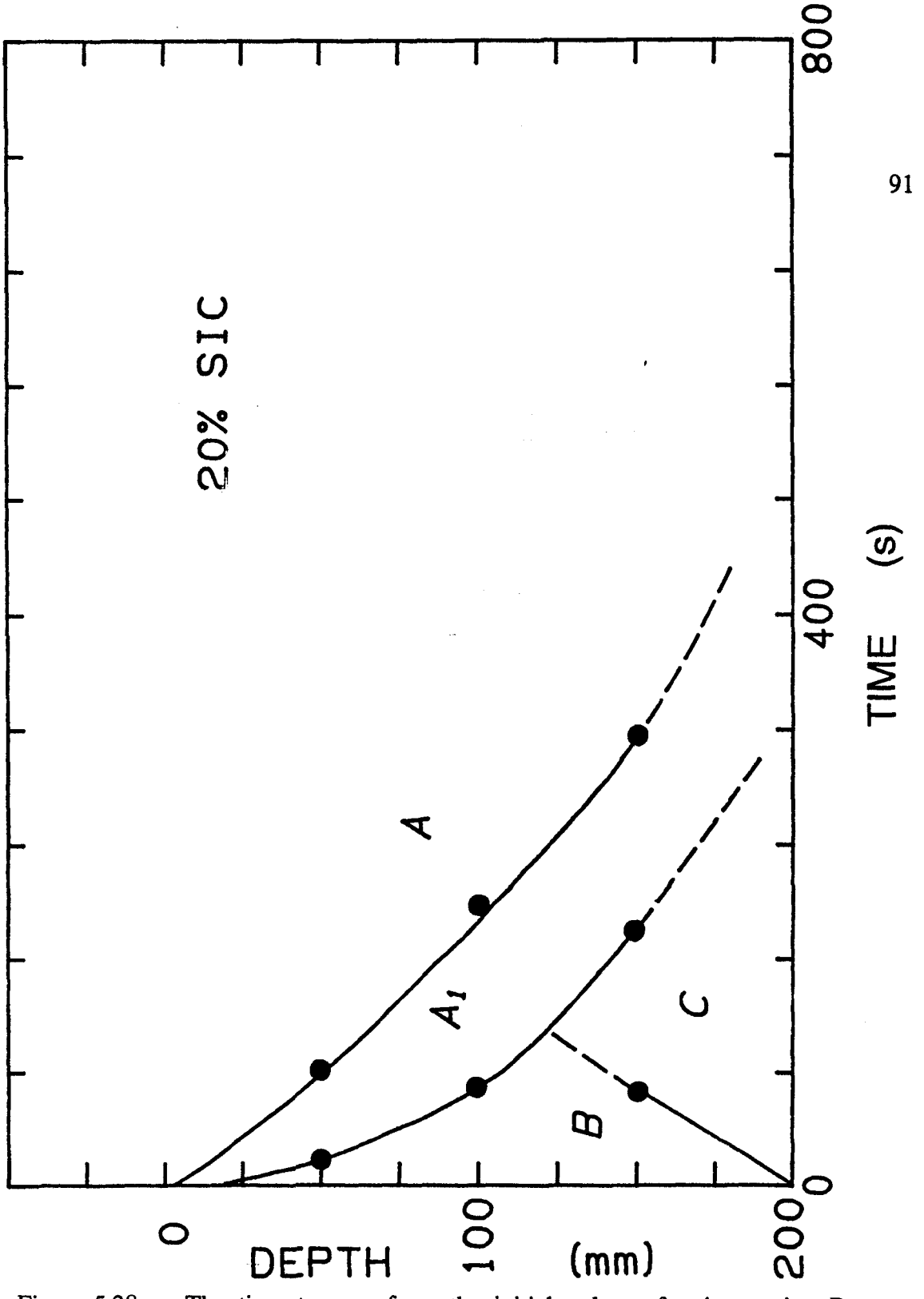

Figure 5.28: The time to pass from the initial volume fraction region B, to a clarified region, A for the 20% volume fractions at the different heights. A transition region, A1, of the intermediate density was noted. A region of higher volume fraction, C, was also observed.

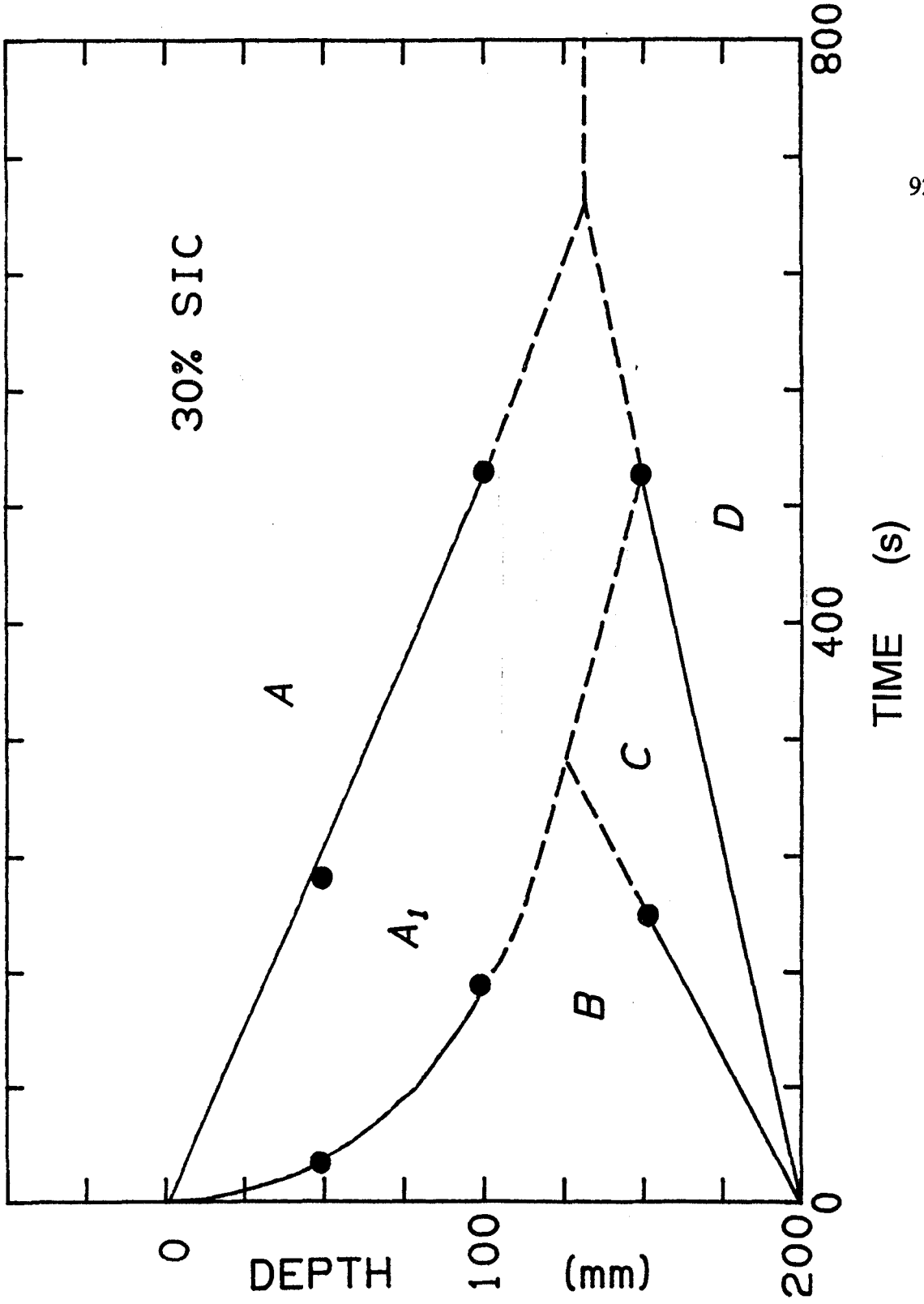

Figure 5.29: The time to pass from the initial volume fraction region B, to a clarified region, A for the 30% volume fractions at the different heights. A transition region, A1, of the intermediate density was noted. A region of higher volume fraction, C, was also observed before a final densification to region D.

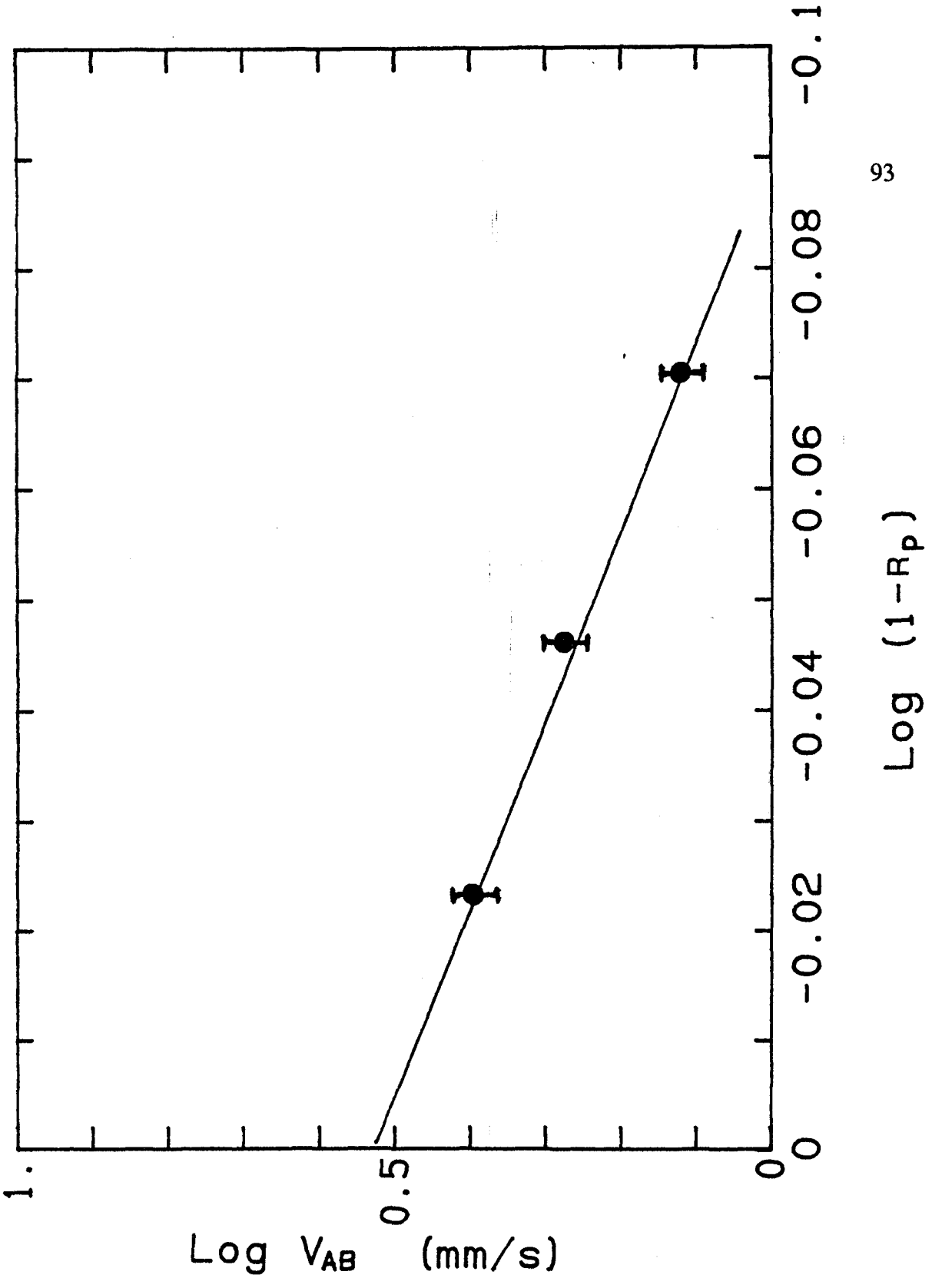

Figure 5.30: The velocity of the shock between region A and B plotted as a function of the aluminum volume fraction.

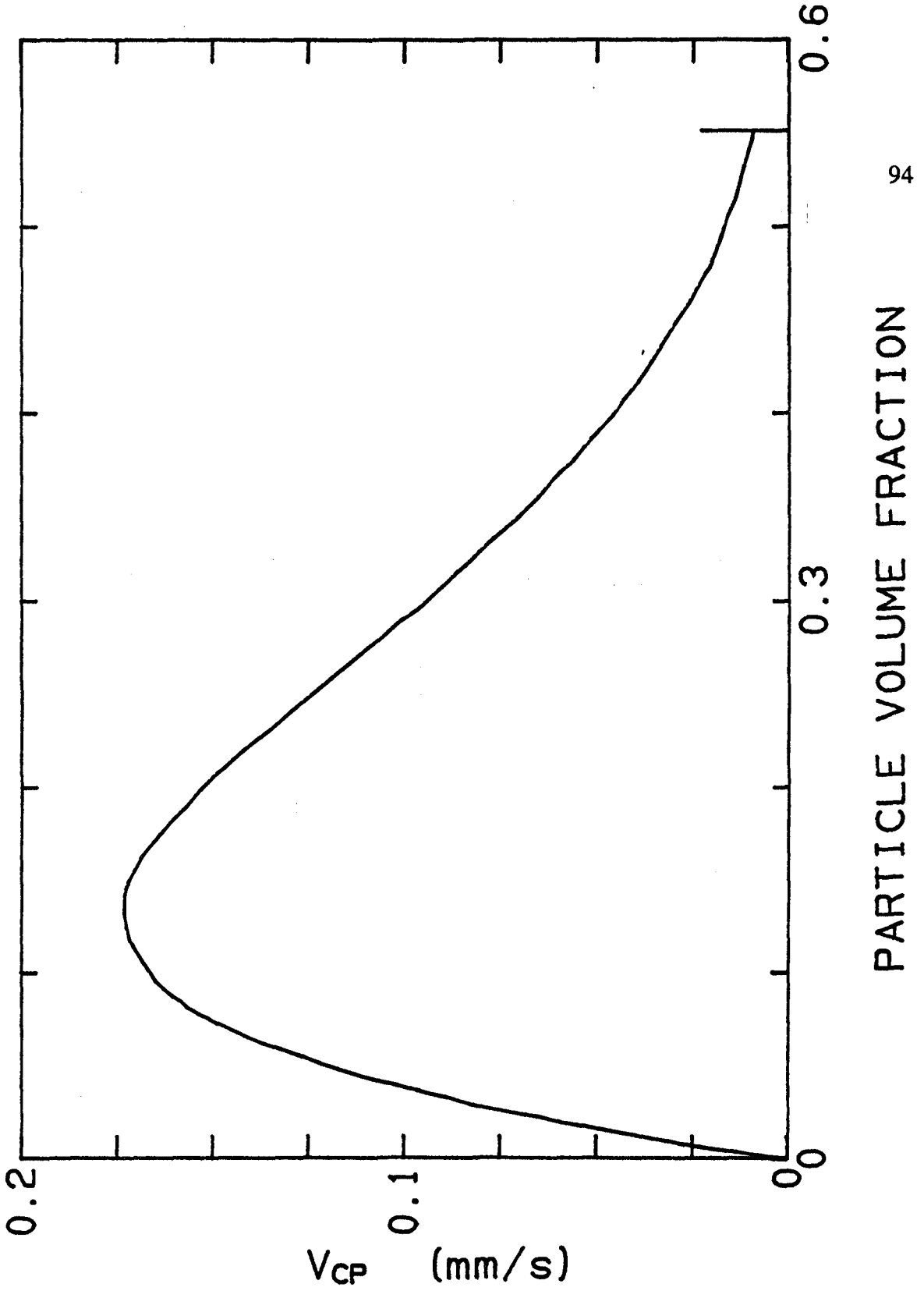

Figure 5.31: The characteristic velocity, V_{cp}, for 88 μm silicon carbide in A356 alloy as a function of volume fraction.

CHAPTER 6

DISCUSSION

The first type of mixing aparatus tested was a ring-vortex mixer. It was tried because of the excellent homogeneous dispersion obtained with slurries [13]. This mixer was unsuccesful with the aluminum/SiC (10 or 88 μm) system because it was impossible to mix the particles into the melt. This can be explained by the fact that the characteristic of the vortex ring mixer is to produce small shear stress into the melt. According to Alcan [4], particles and metal has to be sheared past each other to maintain them in the melt by promoting wetting in the system. The second type of mixer tested was a marine-type propeller driven by a variable AC motor. With this mixer it was relatively easy to mix in the SiC particles having a mean diameter of 88 μm. It was however impossible with this aparatus to mix in all the 10 μm particles because of their bigger ΔE_{total}.

In this work, the effects caused by the wetting phenomenon were avoided when possible. That is why the 88 μm particles were used instead of the commercially used 10 μm. As discussed in section 2.1.3, the objective of this decision was to reduce the contribution of interfacial effects (i.e. wetting) on the global behaviour of the particles. Two practical problems were solved by this decision: the inability to mix all the particles in the melt without modifying the chemistry, and the flocculation of SiC particles (fine particles, because of their very high specific surface, flocculate more than larger particles

[5]). From Figure 5.30, n was determined to be 5.6. The value of n is a measure of the degree of flocculation in the system; values over 10 are characteristic of significant flocculation or network formation of the solid in aqueous systems. Large n values lower the characteristic velocity, particularly at high volume fractions due to the structure formation. The facts that:

(1) the observed value of n was only 5.6, and

(2) a random closed-packed volume fraction was achieved

indicate that flocculation or network formation was not a significant problem. These factors determine the maximum volume fraction of second phase particles which can be incorporated into the melts. Flocculation or network formation may preclude high volume fractions if the particles are poorly wetted. However the contribution of the wetting phenomenon on the sedimentation pattern is probably non-negligable even with the 88 μm particules. Different ways of increasing the wetting between the SiC and the aluminum alloy are under study by other members of the research group. A better comprehension of this phenomenon is necessary for the fabrication of MMC's with the 10 μm SiC particles.

Since this work was the first experimental attempt at McMaster University to study the processing problems associated with the Al/SiC system, it was decided to investigate the possibility of developing a probe able to track the settling of the 88 μm SiC particles. For this purpose, a novel electical resistance technique has been

developed. Some initial experiments in mercury were done to show the possibility of detecting a variation of electrical resistance with the probe without dealing with the high temperature and corrosion problems related with liquid aluminum. It should be kept in mind that the type of experiments involving the in-situ observation of the sedimentation pattern in the Al/SiC system are difficult. Experiences with the Mercury/SiC system showed that the ceramic particles tend to stick to the probe, modifying the resistivity measurements.

The theory of sedimentation uses as the single main assumption that at any point in a dispersion, the velocity of fall of the particles depends only on the local concentration of particles. This is a very strong assumption that can be justified only if either the speed of propagation is relatively slow or the damping is great [19]. The quality of the results deduced from this theory depends on the applicability of the main assumption to the Al/SiC system. Many causes can weaken the validity of this hypothesis:

1) size distribution of particles

2) wall effects

3) time varying wetting effects.

The size distribution of the SiC particles will certainly affect the settling behaviour. When the concentration of particles is small, the small particles fall more slowly than

the big ones, so that the V_p has no definite meaning. However, when the concentration of particles is high, it is probable that all the particles fall with the same V_p vs R relationship whatever their size because of the close packing.

The wall effects are difficult to estimate. It is possible that the greater stress near the wall results in a local decrease of particle concentration but this is likely to be effective at small distances. The same effect probably happens close to the probe as well.

Many other phenomena specific to the Al/SiC system (i.e. time varying contact angle) can weaken the validity of the main assumption. These effects are probably responsible for the following observations.

The inconsistent interfacial speed between region A and B for 20, 25 and 30% v.o. SiC is possibly due to different residence times in the melt. The wetting of SiC by Al is time dependent, thus particles having different residence times will show different settling behaviour because the sedimentation is influenced by the degree of wetting of the particles. Another possible cause for these inconsistencies is the entrapment of gas bubbles during the mixing.

The main objective of this work was to study the relationship between the

sedimentation patterns and the concentration of particles. In an aqueous system, it is possible to determine with some luminous apparatus [5] the relationship between the speed of sedimentation and the concentration of particles. Despite the opacity of the Al/SiC system and the impossibility to calibrate the probe (to associate a resistivity measurement to a particular volumetric fraction of particles), it was possible to reconstruct the relation between the sedimentation patterns and R (Figure 5.26 to 5.29) by using the resistivity vs time curves, and the initial distribution of particles. Until the details of the forces on the particles can be specified, it is impossible to qualify the validity of the main hypothesis of the theory of sedimentation, even for a dispersion of identical particles. However, the fact that the relationship $V_p = 3.35\ (1\text{-}R)^{5.6}$ is only valid to up to 15% SiC, the analysis of the sedimentation patterns in MMC's with this theory should be viewed as a way to describe, qualitatively, the behaviour of the Al/SiC system. Any quantitative results obtained with the help of the theory, especially the V_{cp} vs R curve (Figure 5.31), should be used very carefully. Nevertheless, this theory is useful as a first step in the analysis of experimental data.

Some changes in the apparatus must be done to improve the interpretation of the results. From the previous analysis, three kind of improvements are worthwhile considering:

(1) the reduction of the size distribution of the SiC particles

(2) the reduction of the mobility of the probe inside the crucible

(3) the reduction of the variability of the degree of wetting of the ceramic particles by putting all the particles into the melt at the same time instead of by increments.

During the re-melting of metal-matrix composite stock, there may be significant time between initial and complete melting. In such situations, even small particles can segregate. The present analysis can be used to calculate the changes in volume fraction over increments of time during melting.

This thesis is the first work, as far as I know, showing different sedimentation patterns resulting during the fabrication of MMC's. These results were made possible by the development of a resistivity probe able to resist the high temperature and corrosive environment of liquid aluminum. These sedimentation patterns are very useful for the fabrication of MMC's because they show the evolution of the region of uniform concentration (B) in function of time. The results and the apparatus developed for this work combined with the future results showing the effect of certain parameters on the wetting phenomenon in Al/SiC system will make it possible to study the problems related to the fabrication of the 10 μm Al/SiC system.

CHAPTER 7

SUMMARY AND CONCLUSIONS

The four point conductivity probe developed can be used to observe, in-situ, the sedimentation pattern of the system SiC(88 μm)/A356 aluminum alloy, for different volumetric fractions of particles.

On the basis of this study, the following conclusions can be drawn:

1) The V_p vs R relationship of this system was determined to follow Equation 17 with V_g of 3.4 mm/s (close to Stokes velocity) and n of 5.6. This latter value is characteristic of those encountered in non-flocculating aqueous systems.

2) The particles settled to a final density of 53-55 vol% SiC, after passing through a region of intermediate density. This correspond to the random close packing of particles observed in packed beds.

REFERENCES

1. M.Skibo, P.L.Morris, D.J.Lloyd, "Structure and Properties of Liquid Metal Processed SiC Reinforced Aluminum", Cast Reinforced Metal Composites, ASM International, Sept. 1988, pp 257-261.

2. M.A.Bayoumi, M.Suery, "Structure and Mechanical Properties of SiC-Particle Reinforced Aluminum-Alloy Composites",(presented at ICCM VI/ECCM 2, London, July 1987.

3. C.Milliere, Elaboration, Structure et Proprietes de Materiaux Composites a Matrice Metallique, PhD Thesis, Institut National Polytechnique de Grenoble, Mai 1986.

4. A.D.McLeod, C.Gabryel, D.J.Lloyd, P.Morris, Processing of Ceramic and Metal Matrix Composites, ed. H.Mostaghaci, CIM Conference of Metallurgists, Pergamon Press, New York, Aug.1989, pp 228-235.

5. J.F.Richardson, W.N.Zaki, "Sedimentation and Fluidization: Part 1", Trans. Instn Chem. Engrs, Vol 32, 1954, pp 35-53.

6. K.G.Satyanarayana, B.C.Pai, M.R.Krishnadev, C.G.Krishnadas Nair, "Aluminium Alloy Metal Matrix Composites for Engineering Applications", Regional Research Laboratory, Trivandrum 19, India.

7. K.Ohori, H.Watanabe, Y.Takeuchi, "Silicon Carbide Whisker Reinforced Aluminium Composites - Fabrication and Properties", Materials Science and

Technology, Vol 3, Jan.1987, pp 57-60.

8. D.J.Lloyd, "Metal Matrix Composites - An Overview", Proc. International Symposium on Advanced Structural Materials, ed. D.S.Wilkinson, Pergammon Press, 1988.

9. T.W.Chou, A.Kelly, A.Okura, "Fiber-Reinforced Metal-Matrix Composites", Composites, Vol 16, Number 3, July 1985.

10. G.D.Parfitt, "Dispersion of Powders in Liquids", Encyclopaedia of Chemical Technology, Supplement - Dispersion of Powders in Liquids, pp 339 - 371.

11. P.K.Rohatgi, R.Asthana, S.Das, "Solidification, structures, and properties of cast metal-ceramic particle composites", The Institute of Metals and the American Society of Metals, 1986.

12. V.Laurent, D.Chatain, N.Eustathopoulos, "Wettability of SiC by aluminium and Al-Si alloys", Journal of Materials Science, 1987.

13. B.Latto, "New Mixer for Slurries and Stratified Fluids", Proceeding of the Twelfth International Conference on Slurry Technology, March 1987, New Orleans, Louisiana, pp 165-173.

14. M.D.Skibo, D.M.Schuster, "Cast Reinforced Composite Material", International Patent Application Publication WO 87/06624, Nov. 1987.

15. "Aluminum and Aluminum Alloys", Encyclopaedia of Chemical Technology, Vol 2, pp 129 - 134.

16. "Silicon Carbide", Encyclopaedia of Chemical Technology, Vol 4, pp 520 - 524.

17. "Aluminum Foundry Products", Metals Handbook, Vol 2, Tenth Edition, pp 124 - 128.

18. L.Svarovsky, "Sedimentation", Encyclopaedia of Chemical Technology, Vol 20, pp 559-575.

19. G.J.Kynch, "A theory of Sedimentation", Trans. Faraday Soc., 1952, 48, 166.

20. G.B.Wallis, "A Simplified One-Dimensional Representation of Two-Component Vertical Flow and Its Application to Batch Sedimentation", Interaction Between Fluids and Particles, London: Institution of Chemical Engineers, pp 9-16.

21. R.S.Brodkey, "Multiphase Phenomena III: Solids-Fluid Flow", The Phenomena of Fluid Motions, Chp 18, Addison-Wesley Publishing Co., Toronto, pp 619-643.

22. J.A.Mullendore, "Tungsten and Tungsten Alloys", Encyclopaedia of Chemical Technology, Vol 23, pp 413-425.

23. G.H.Sistare, "Silver and Silver Alloys", Encyclopaedia of Chemical Technology, Vol 21, pp 1-15.

APPENDIX I

COMPUTER PROGRAM USED TO CONTROL THE MICRO-OHMMETER

```
10   REM mmc_measurement()
20   OPEN"COM1:9600,N,8,1,CS,DS,CD"AS#1
30   DIM ACR$(1000)
100  NBMS%=60
110  NBM%=20
120  INTERV%=1
130  AC$=";AC,?,:"
150  REM
160  I%=1
170  PRINT "WHAT IS THE % V.F. OF SiC"
175  INPUT VF%
180    CLS
190    PRINT "PROBE CALIBRATION FOR",VF%," % V.F. OF SiC"
200    PRINT "WHAT IS THE NAME OF THE FILE TO BE OPEN?"
210    INPUT N$
220    OPEN"O",#2,N$
230    CLS
240    PRINT#2,"PROBE CALIBRATION FOR",VF%," % V.F. OF SiC"
```

```
250     CLOSE#2
260     PRINT "ADD SiC"
270     PRINT "TAKE DEPTH OF MELT"
280     I%=I%+1
290     INPUT X$
300     PRINT "START MIXER AND WAIT 5 min."
310     INPUT X$
320     PRINT "VERIFY THE DISTRIBUTION OF TEMPERATURE"
330     INPUT X$
340     FOR HEIGHT% = 5 TO 15 STEP 5
350       PRINT "PUT PROBE AT h=",HEIGHT%," cm"
360       INPUT X$
370       PRINT "WAIT...THE PROBE TAKE MEASUREMENT"
380   REM MEASUREMENT
390       FOR M%=1 TO NBM%
400         ACR$(M%)=""
410         PRINT#1,AC$
420         COMPT%=0
430   REM
440         COMPT%=COMPT%+1
450         IF (COMPT% > 40) THEN PRINT#1,";LO,-,:;LO,+,:"
```

```
455          IF (COMPT% > 40) ,THEN GOTO 410
460          PRINT "WAITING TO BE READ=",LOC(1)
470          PRINT "FREE SPACE =",LOF(1)
480          IF LOC(1) < 10,THEN GOTO 430
490          WHILE NOT EOF(1)
500            AS$=INPUT$(1,#1)
510            ACR$(M%)=ACR$(M%)+AS$
520            IF AS$<>":",THEN GOTO 500
530              IF LOC(1) <> 0, THEN
ACR$(M%)=ACR$(M%)+INPUT$(LOC(1),#1)
540          WEND
550        NEXT
560  REM TO SEE DATA ON SCREEN
570        CLS
580        PRINT "MEASUREMENT AT h=",HEIGHT%," cm"
590        FOR M%=1 TO NBM%
600          PRINT ACR$(M%)
610        NEXT
620        PRINT "DO YOU WANT TO LOOK AGAIN THE DATA (y)"
630        ANSWER$=INPUT$(1)
640        IF (ANSWER$="y" OR ANSWER$="Y"), THEN GOTO 570
```

```
650       PRINT "DO YOU WANT TO RETAKE MEASUREMENT (y)"
660       ANSWER$=INPUT$(1)
670       IF (ANSWER$="y" OR ANSWER$="Y"), THEN GOTO 370
680  REM SAVE DATA
690       OPEN"A",#2,N$
700       PRINT#2,"MEASUREMENT AT h=",HEIGHT%," cm"
710       FOR M%=1 TO NBM%
720         PRINT#2,ACR$(M%)
730       NEXT
740       CLOSE#2
750       PRINT "SUCK SAMPLE"
760       INPUT X$
770       CLS
780     NEXT
790     FOR LEVEL%=5 TO 15 STEP 5
800       CLS
810       PRINT "SEDIMENTATION TEST FOR",VF%,"% V.F. OF SiC"
820       PRINT "PUT PROBE AT h=",LEVEL%,"cm"
830       INPUT X$
840       IF (X$="n" OR X$="N"),THEN GOTO 1500
850       FOR J%=1 TO 5
```

```
860         PRINT "START MIXER AND WAIT 5 min."
870         INPUT X$
880         PRINT "STOP MIXER"
890         INPUT X$
900         PRINT "WAIT...THE PROBE TAKE MEASUREMENT"
910  REM MEASUREMENT
920         LET START$=TIME$
930         FOR M%=1 TO NBMS%
940           TIMER1$=TIME$
950           ACR$(M%)=""
960           PRINT#1,AC$
970           COMPT%=0
980     REM
990           COMPT%=COMPT%+1
1000          IF (COMPT% > 40), THEN
               PRINT#1,";LO,-,:;LO,+,:"
1005          IF (COMPT% > 40), THEN GOTO 960
1010          PRINT "WAITING TO BE READ=",LOC(1)
1020          PRINT "FREE SPACE =",LOF(1)
1030          IF LOC(1) < 10,THEN GOTO 980
1040          WHILE NOT EOF(1)
```

```
1050            AS$=INPUT$(1,#1)
1060            ACR$(M%)=ACR$(M%)+AS$
1070            IF AS$<>":",THEN GOTO 1050
1080              IF LOC(1) <> 0, THEN
ACR$(M%)=ACR$(M%)+INPUT$(LOC(1),#1)
1090          WEND
1095          PRINT "MEASUREMENT NUMBER =",M%
1096          PRINT "MEASUREMENT =",ACR$(M%)
1100          TIMER1$=MID$(TIMER1$,7,2)
1110          TIMER1%=VAL(TIMER1$)
1120          TIMER2$=TIME$
1130          TIMER2$=MID$(TIMER2$,7,2)
1140          TIMER2%=VAL(TIMER2$)
1150          IF (TIMER1%>TIMER2%),THEN TIMER2%=TIMER2%+60
1160          IF (TIMER1%+INTERV% > TIMER2%),THEN GOTO 1120
1170        NEXT
1180        LET ENDT$=TIME$
1190  REM TO SEE DATA ON SCREEN
1200        CLS
1210        PRINT "MEASUREMENT AT LEVEL h=",LEVEL%,"cm"
1220        PRINT "START TIME = ",START$
```

```
1230        FOR M%=1 TO NBMS%
1240          PRINT ACR$(M%)
1250        NEXT
1260        PRINT "END TIME = ",ENDT$
1270        PRINT "DO YOU WANT TO LOOK AGAIN THE DATA (y)"
1280        ANSWER$=INPUT$(1)
1290        IF (ANSWER$="y" OR ANSWER$="Y"), THEN GOTO 1200
1300        PRINT "DO YOU WANT TO CHANGE THE NUMBER OF
  MEASUREMENT (Y)"
1310        ANSWER$=INPUT$(1)
1320        IF ANSWER$="y",THEN ANSWER$="Y"
1330        IF (ANSWER$<>"Y"), THEN GOTO 1370
1340        PRINT "HOW MANY MEASUREMENT DO YOU WANT TO TAKE
              ?"
1350        INPUT ANSWER%
1360        NBMS%=ANSWER%
1370        PRINT "DO YOU WANT TO RETAKE MEASUREMENT (y)"
1380        ANSWER$=INPUT$(1)
1390        IF (ANSWER$="y" OR ANSWER$="Y"), THEN GOTO 860
1400  REM SAVE DATA
1410        OPEN"A",#2,N$
```

```
1420          PRINT#2,"MEASUREMENT AT LEVEL h=",LEVEL%,"cm"
1430          PRINT#2,"START TIME = ",START$
1440          FOR M%=1 TO NBMS%
1450            PRINT#2,ACR$(M%)
1460          NEXT
1470          PRINT#2,"END TIME = ",ENDT$
1480          CLOSE#2
1490        NEXT
1500 REM
1510     NEXT
1520     PRINT "DO YOU WANT TO TERMINATE THIS PROGRAM? (Y)"
1530     INPUT X$
1540     IF(X$="Y" OR X$="y"), THEN END
1550  GOTO 170
1560  PRINT "TAKE MEASUREMENT IN Al MANUALLY"
```

APPENDIX II

METALLOGRAPHY

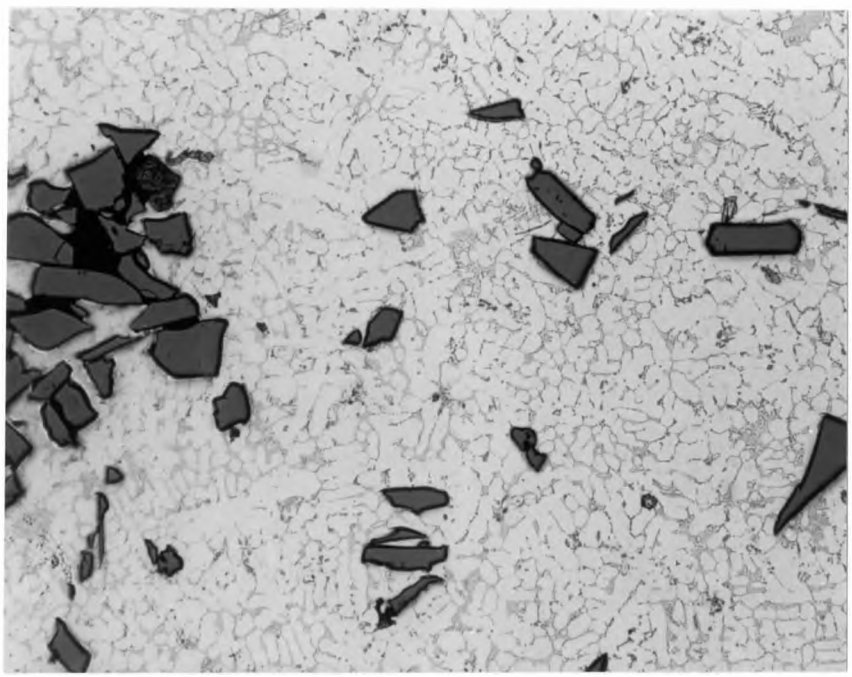

Microstructure of Al-5% SiC (particles)

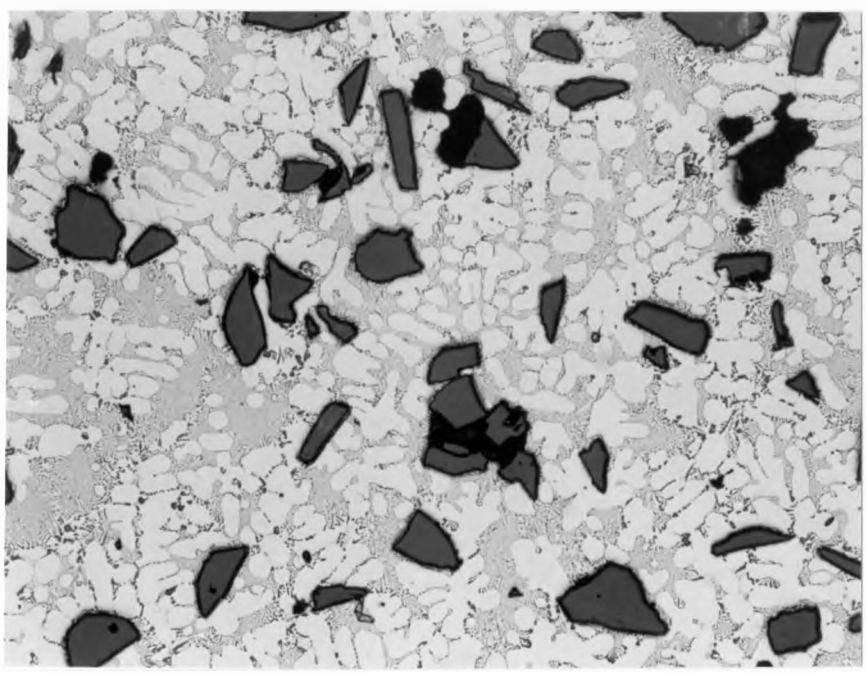

Microstructure of Al-10% SiC (particles)

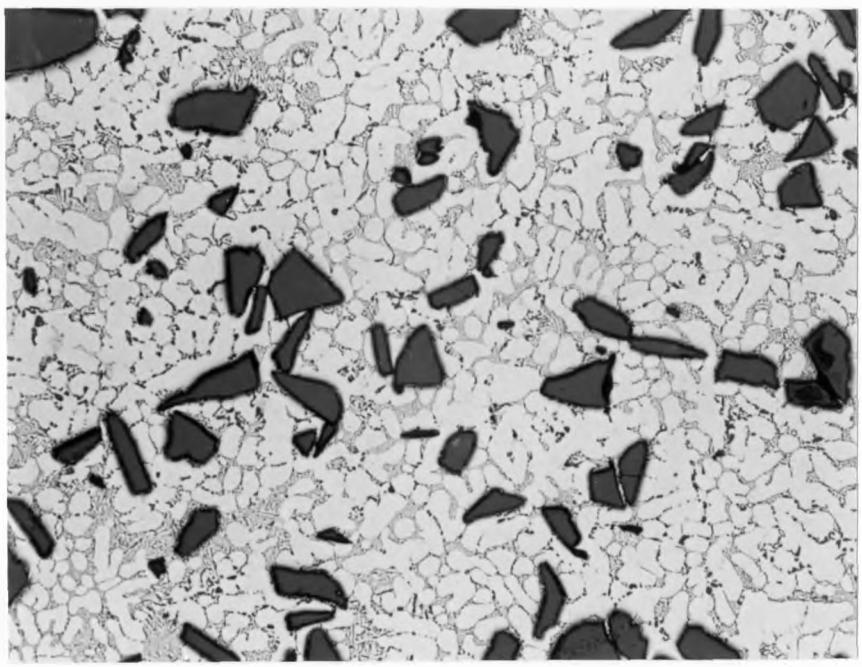

Microstructure of Al-15% SiC (particles)

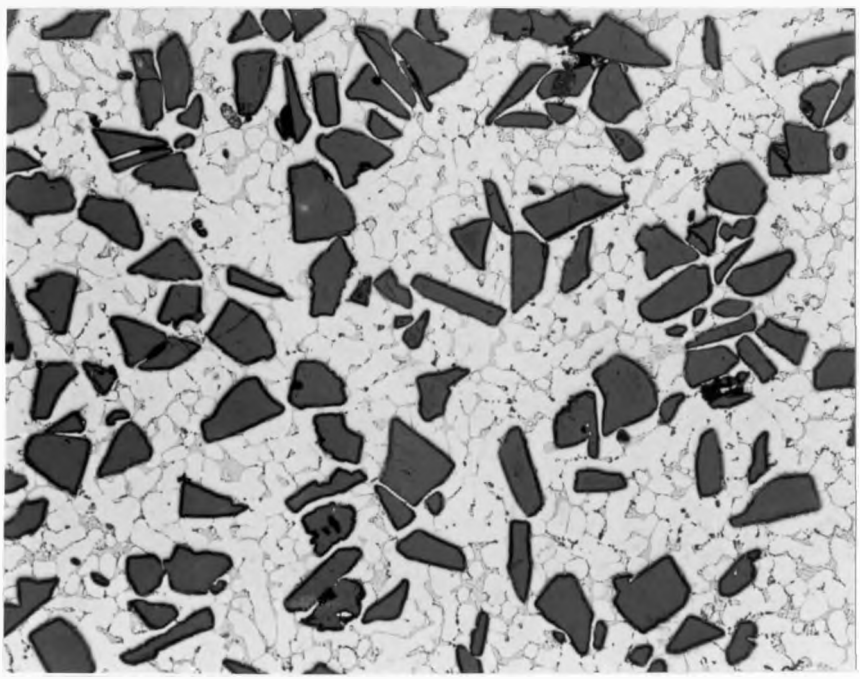

Microstructure of Al-20% SiC (particles)

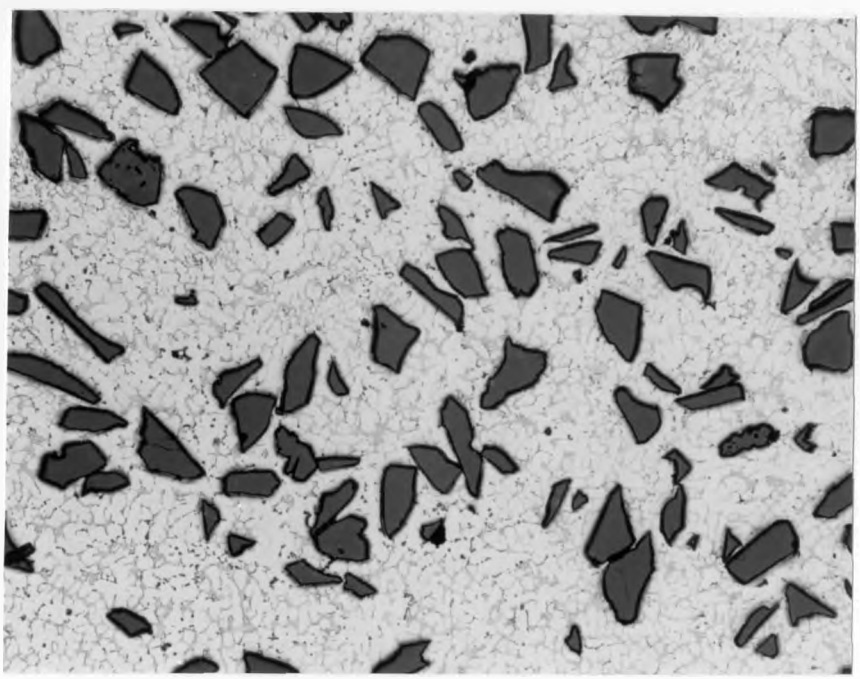

Microstructure of Al-25% SiC (particles)

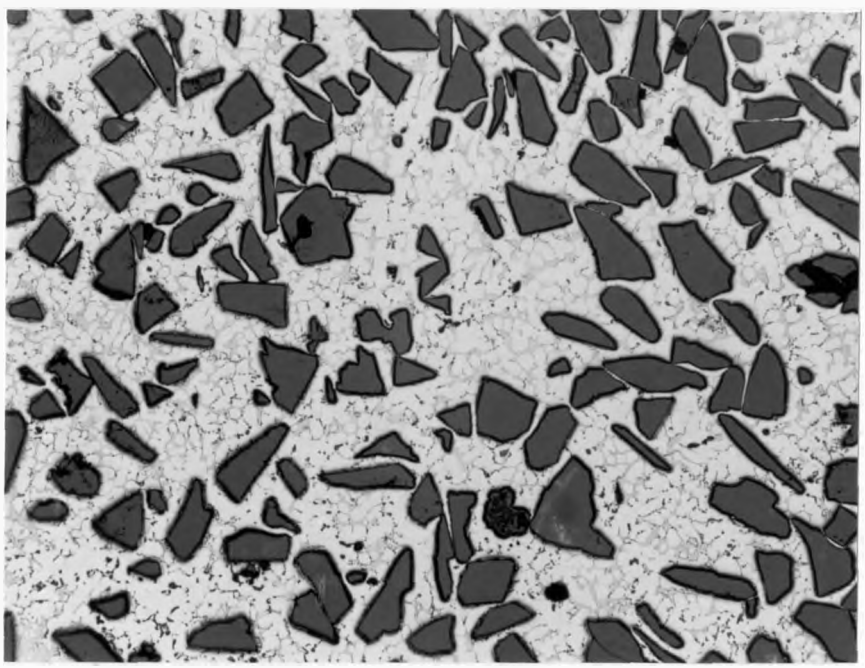

Microstructure of Al-30% SiC (particles)